

## Supplementary Information

### **Redox-Tunable Isoindigos for Electrochemically Mediated Carbon Capture**

Xing Li<sup>1</sup>, Xunhua Zhao<sup>2,3</sup>, Lingyu Zhang<sup>1</sup>, Anmol Mathur<sup>1</sup>, Yu Xu<sup>1</sup>, Zhiwei Fang<sup>4</sup>, Luo Gu<sup>4</sup>, Yuanyue Liu<sup>2</sup>, Yayuan Liu<sup>1\*</sup>

<sup>1</sup> Department of Chemical and Biomolecular Engineering, Johns Hopkins University, Baltimore, Maryland, 21218, United States

<sup>2</sup> Department of Mechanical Engineering & Texas Materials Institute, The University of Texas at Austin, Austin, Texas, 78712, United States

<sup>3</sup> Macao Institute of Materials Science and Engineering (MIMSE), Faculty of Innovation Engineering, Macau University of Science and Technology, Taipa, Macau, 999078, China

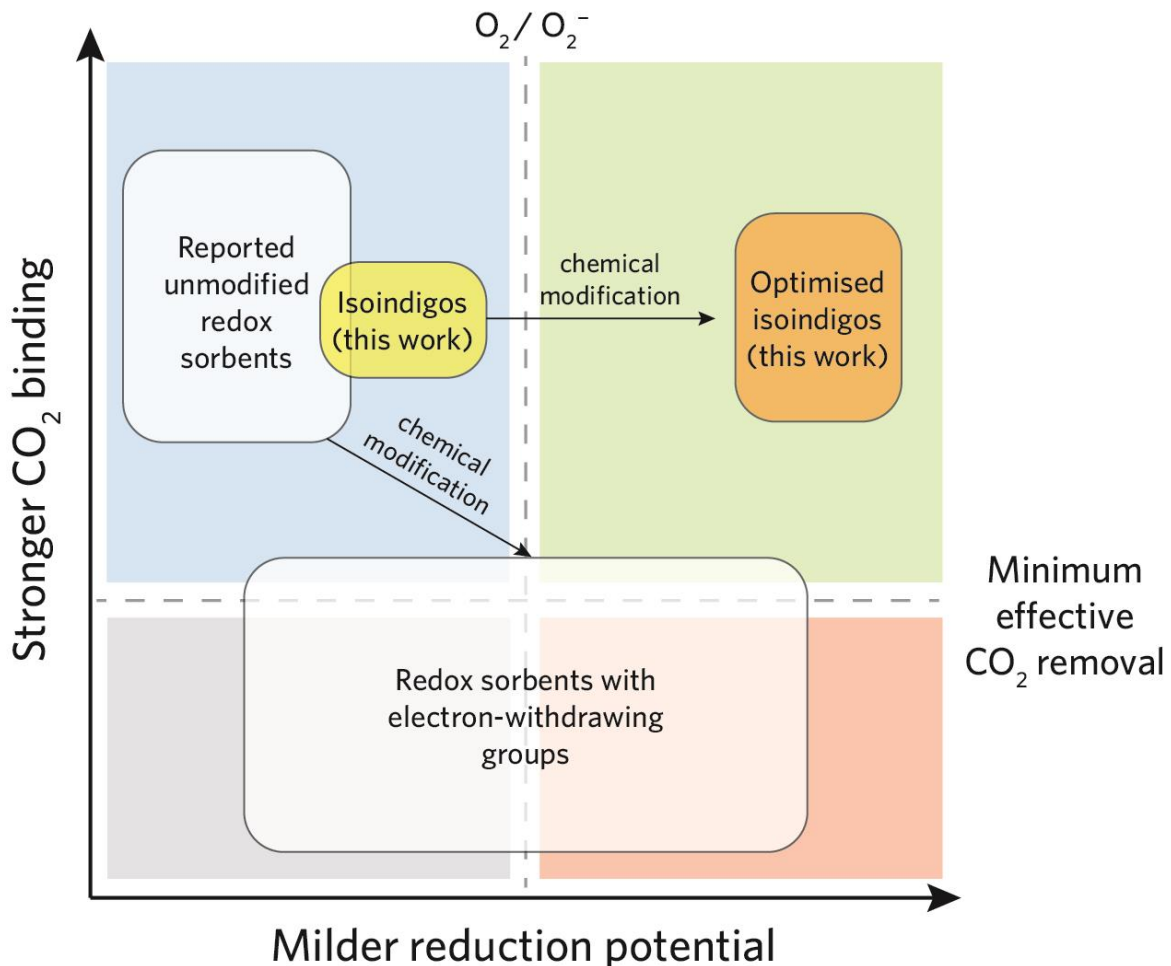
<sup>4</sup> Department of Materials Science and Engineering, Johns Hopkins University, Baltimore, Maryland, 21218, United States

\*Correspondence to: yayuanliu@jhu.edu

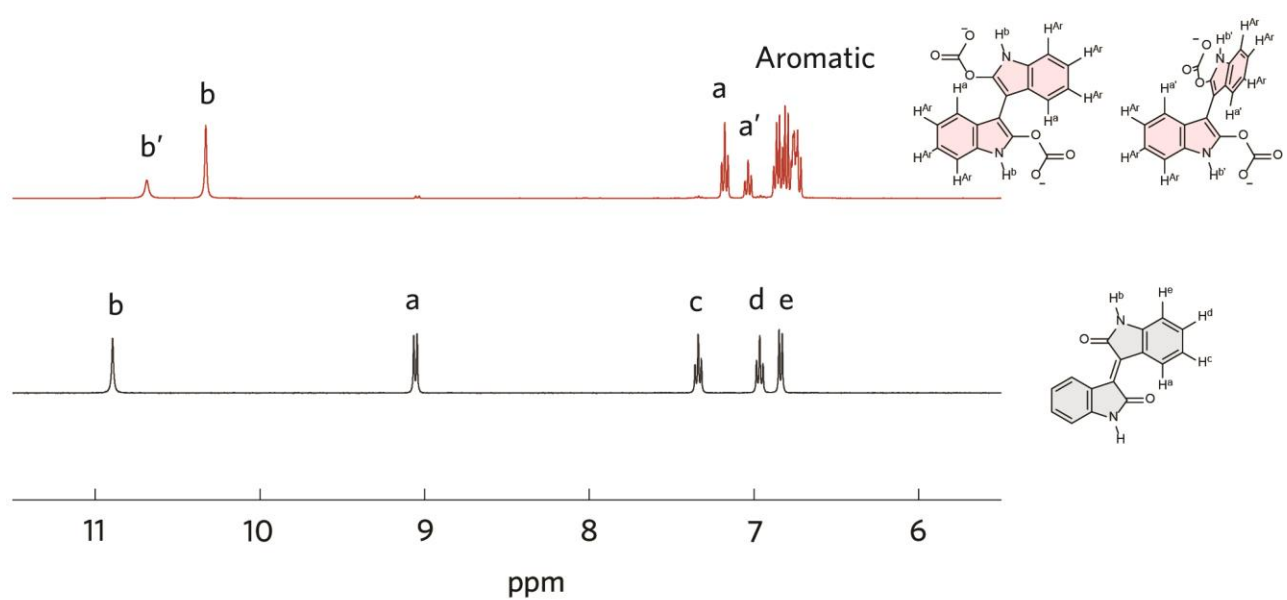
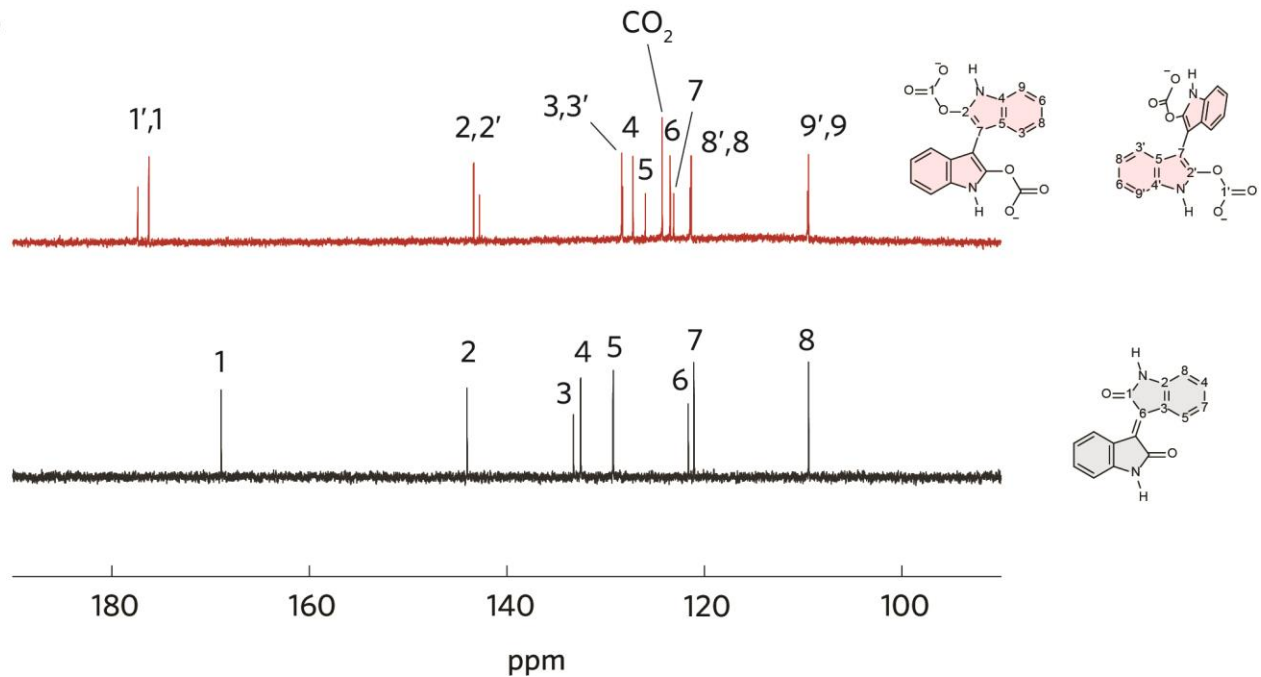
## Table of Contents

Supplementary Figures .....	3
Supplementary Tables.....	43
Supplementary Methods .....	49
Synthesis of isoindigos.....	50
Bulk electrolysis.....	86
Nafion membrane pretreatment.....	88
DFT calculations .....	88
Cell culture .....	88
Cytotoxicity assay and cell morphology .....	88
Supplementary Notes .....	90
Supplementary References.....	97

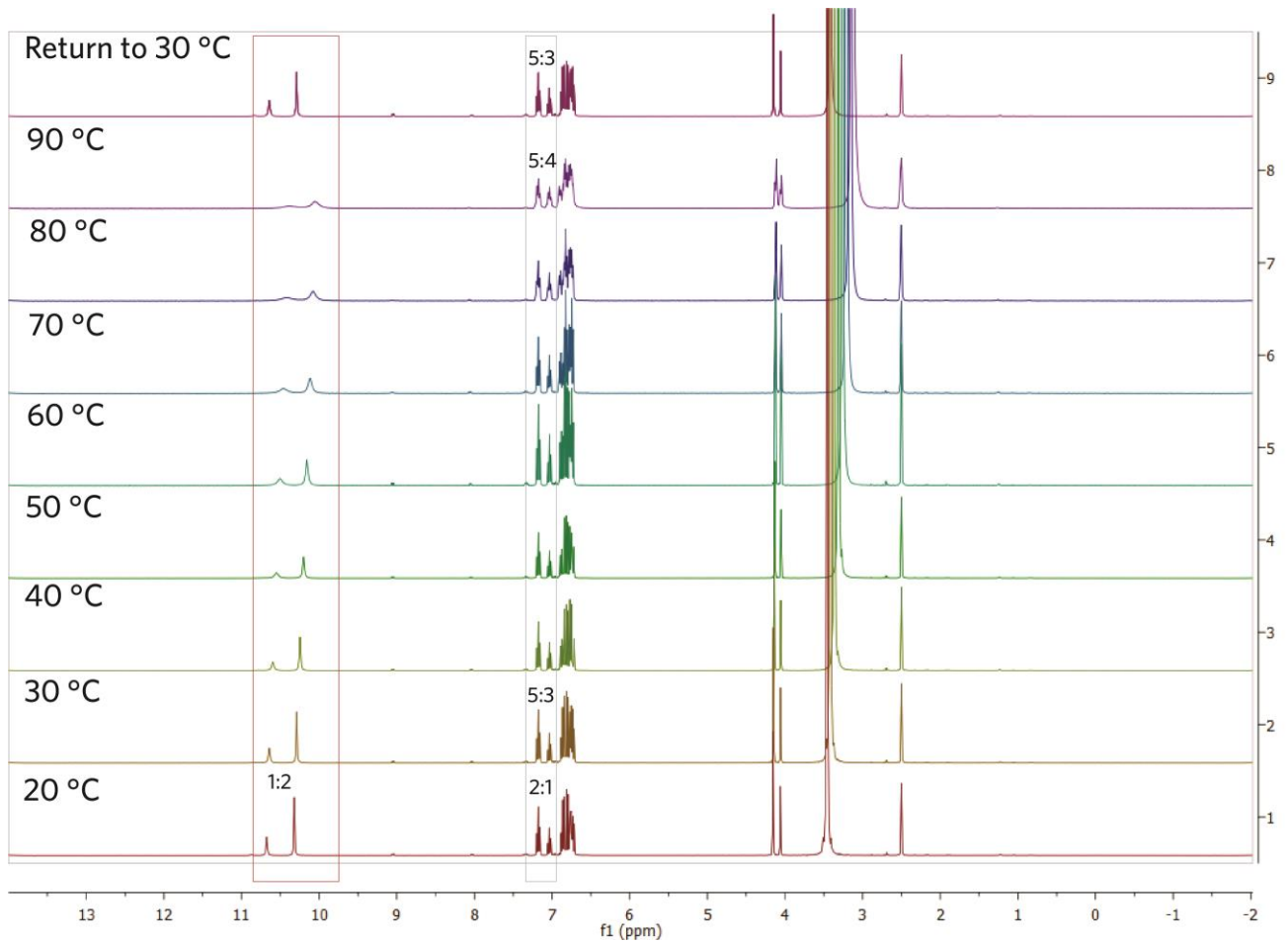
## Supplementary Figures



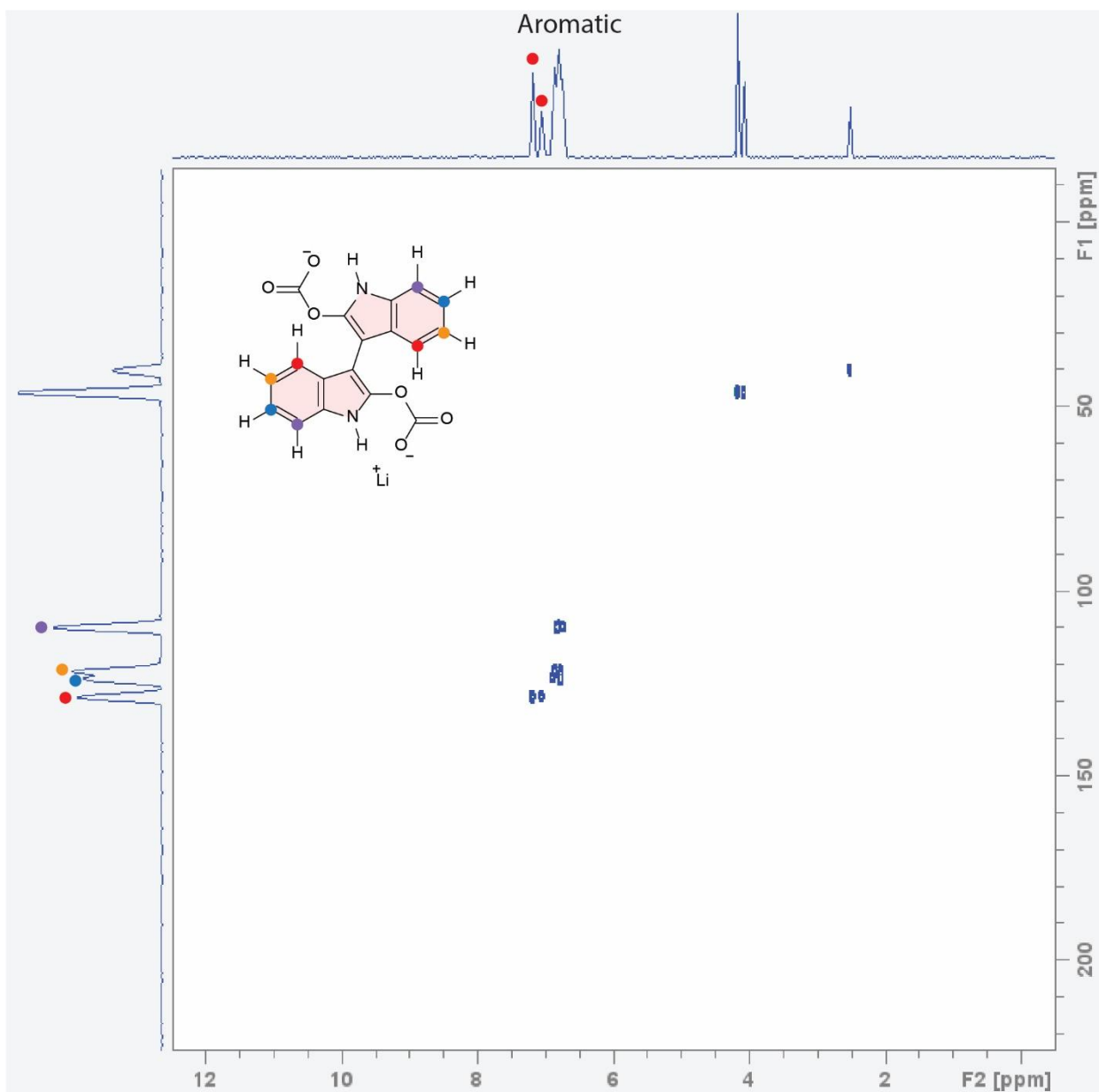
**Supplementary Fig. 1** | A diagram showing the current limitations of organic redox-active CO<sub>2</sub> sorbents for EMCC and how the bifunctional isoindigos overcome this constraint.

**a****b**

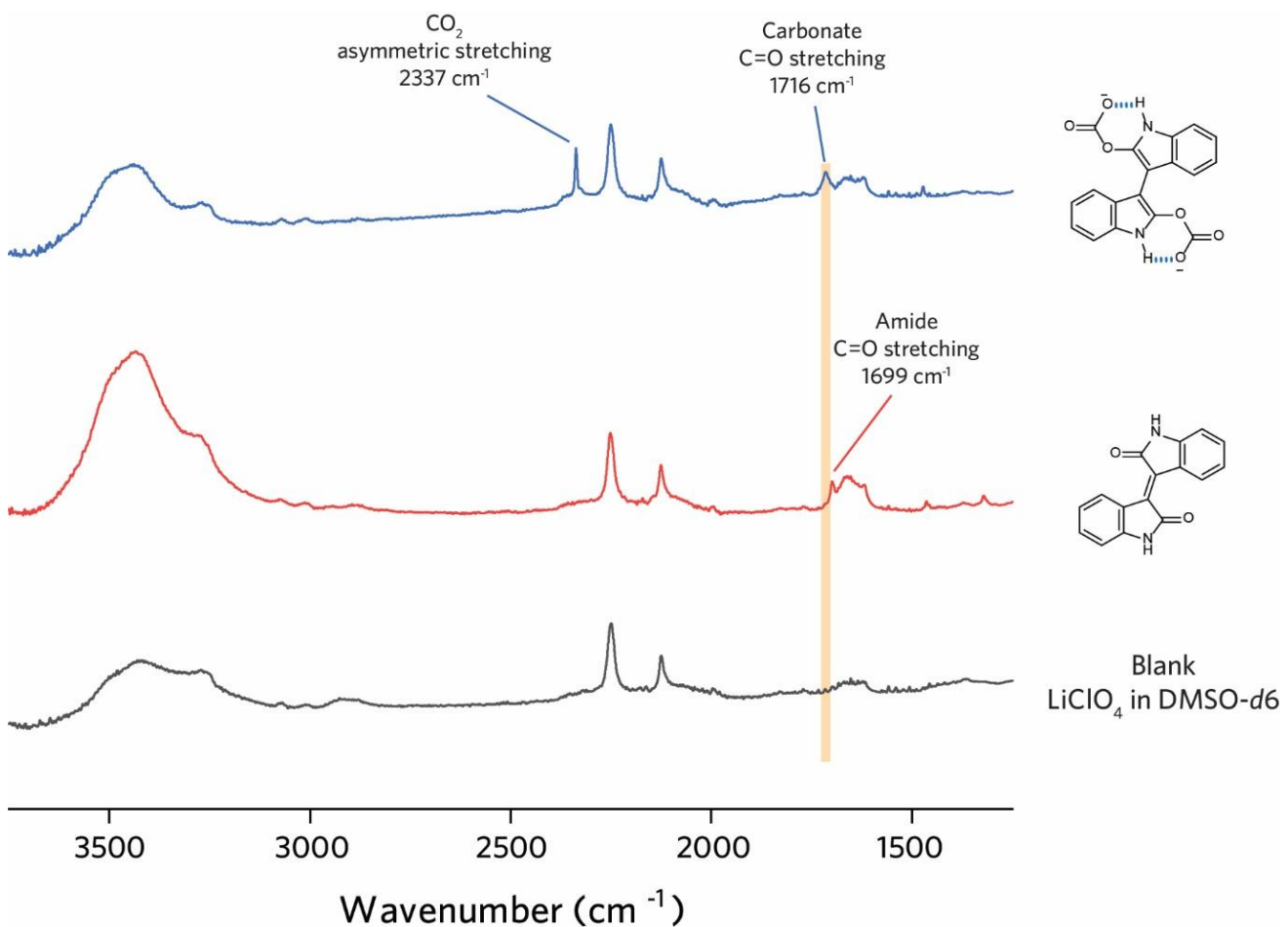
**Supplementary Fig. 2 | Full assignment of the NMR spectra of IIId (black) and IIId-CO<sub>2</sub> (red).** **a,** <sup>1</sup>H NMR. **b,** <sup>13</sup>C NMR.



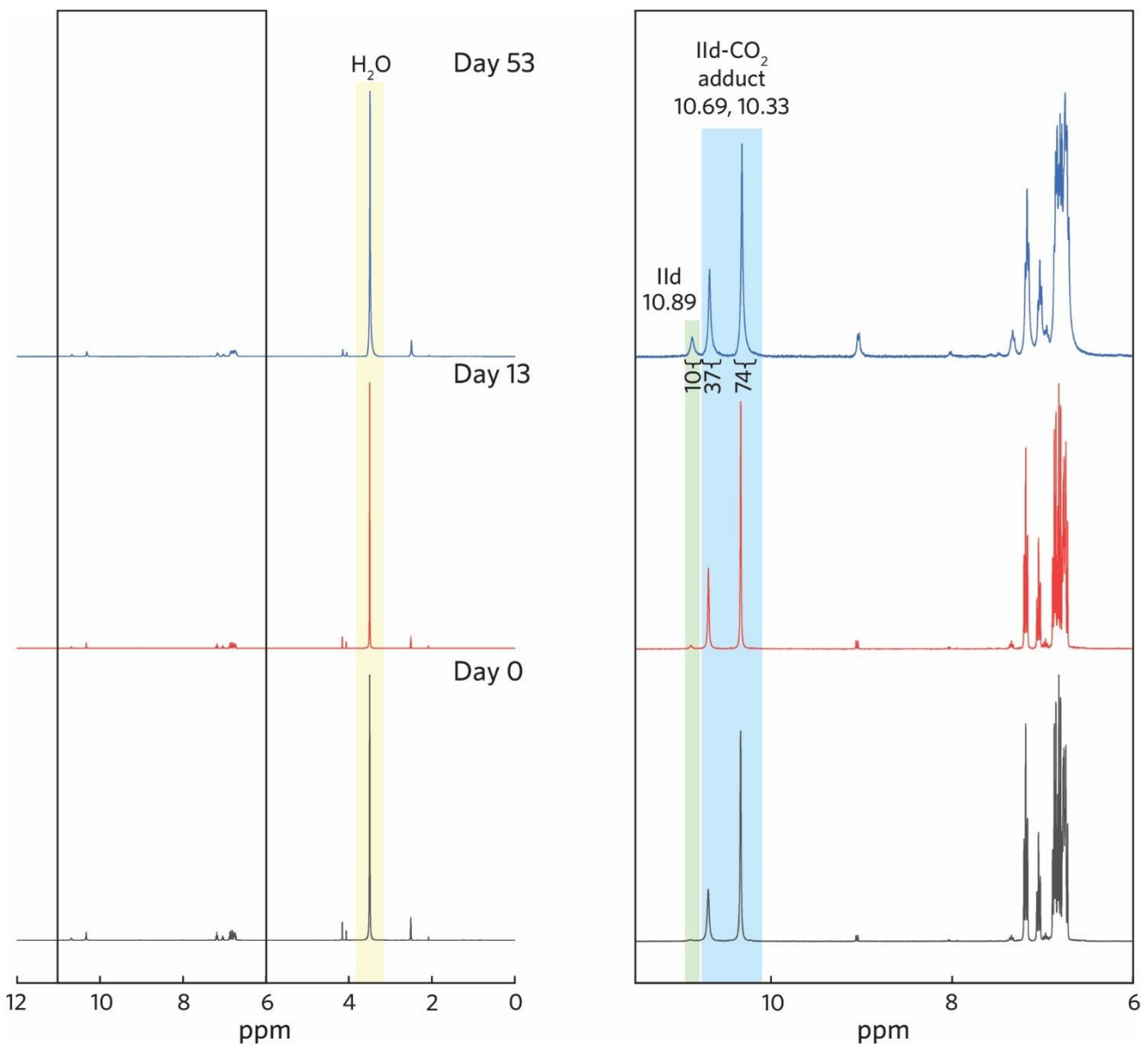
**Supplementary Fig. 3 |** Variable-Temperature  $^1\text{H}$  NMR spectra of the crude solution of IIId after the bulk reduction in  $\text{CO}_2$ .



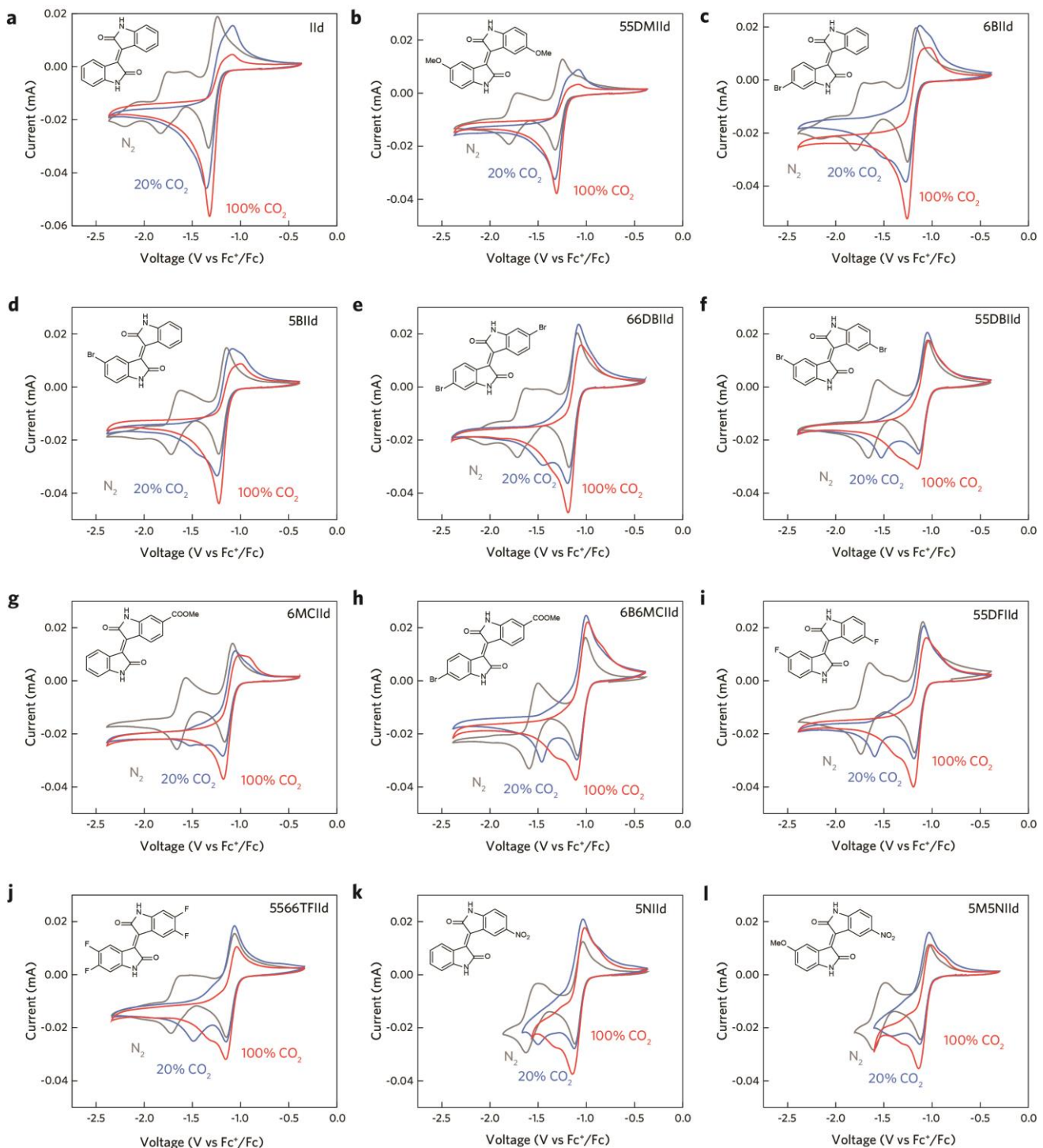
**Supplementary Fig. 4 |** 2D  $^1\text{H}$ - $^{13}\text{C}$  Heteronuclear Single Quantum Coherence (HSQC) NMR of the crude solution after bulk reduction of IIc in  $\text{CO}_2$ .



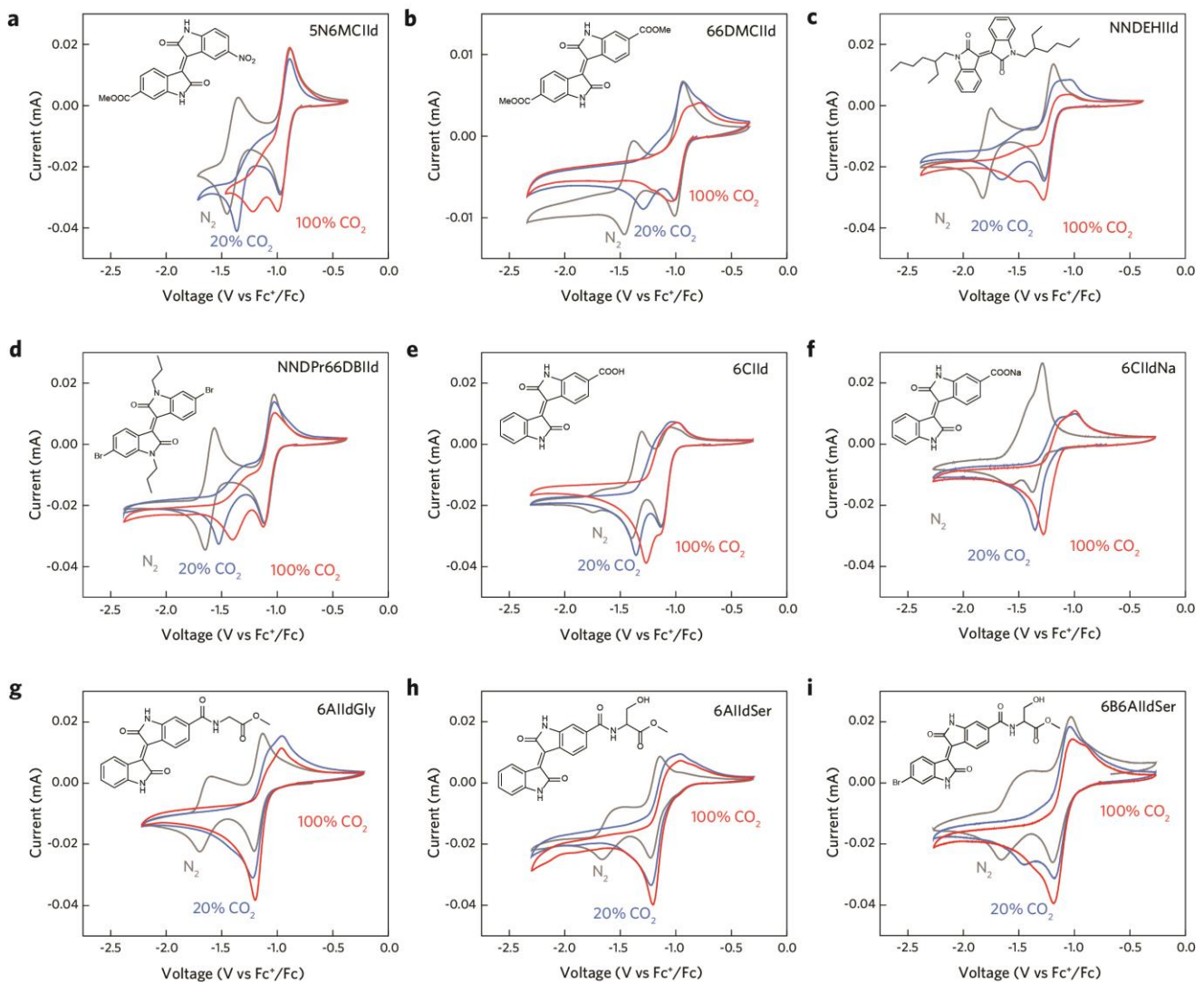
**Supplementary Fig. 5 |** FT-IR spectra of II d and the II d-CO<sub>2</sub> adduct after bulk electrolysis in DMSO with LiClO<sub>4</sub> as the supporting salt.



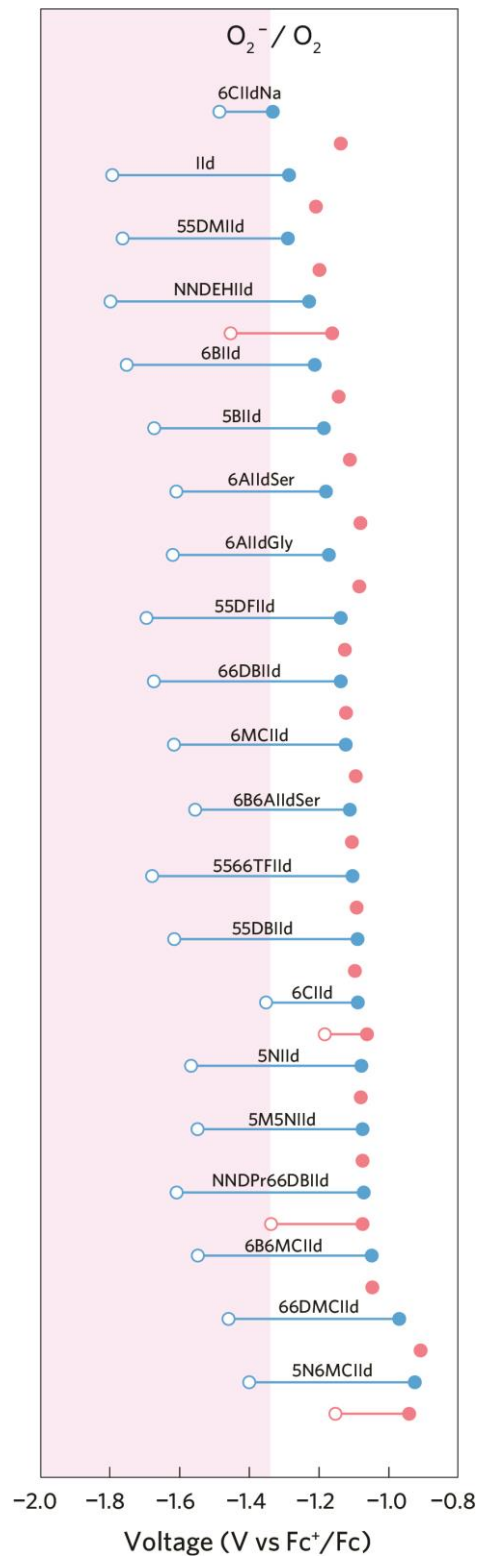
**Supplementary Fig. 6 | Stability test of the isoindigo-CO<sub>2</sub> adduct.** Less than 9 mol% of the IId-CO<sub>2</sub> adduct was oxidised back to IId after the solution was stored in the air in the presence of high water content for 53 days (based on <sup>1</sup>H NMR relative integrals).



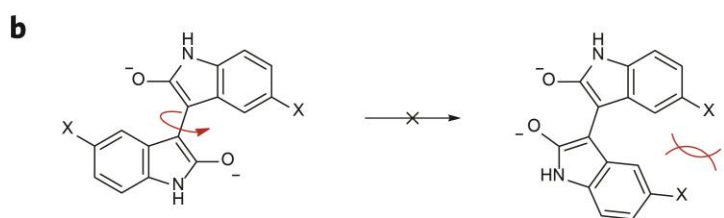
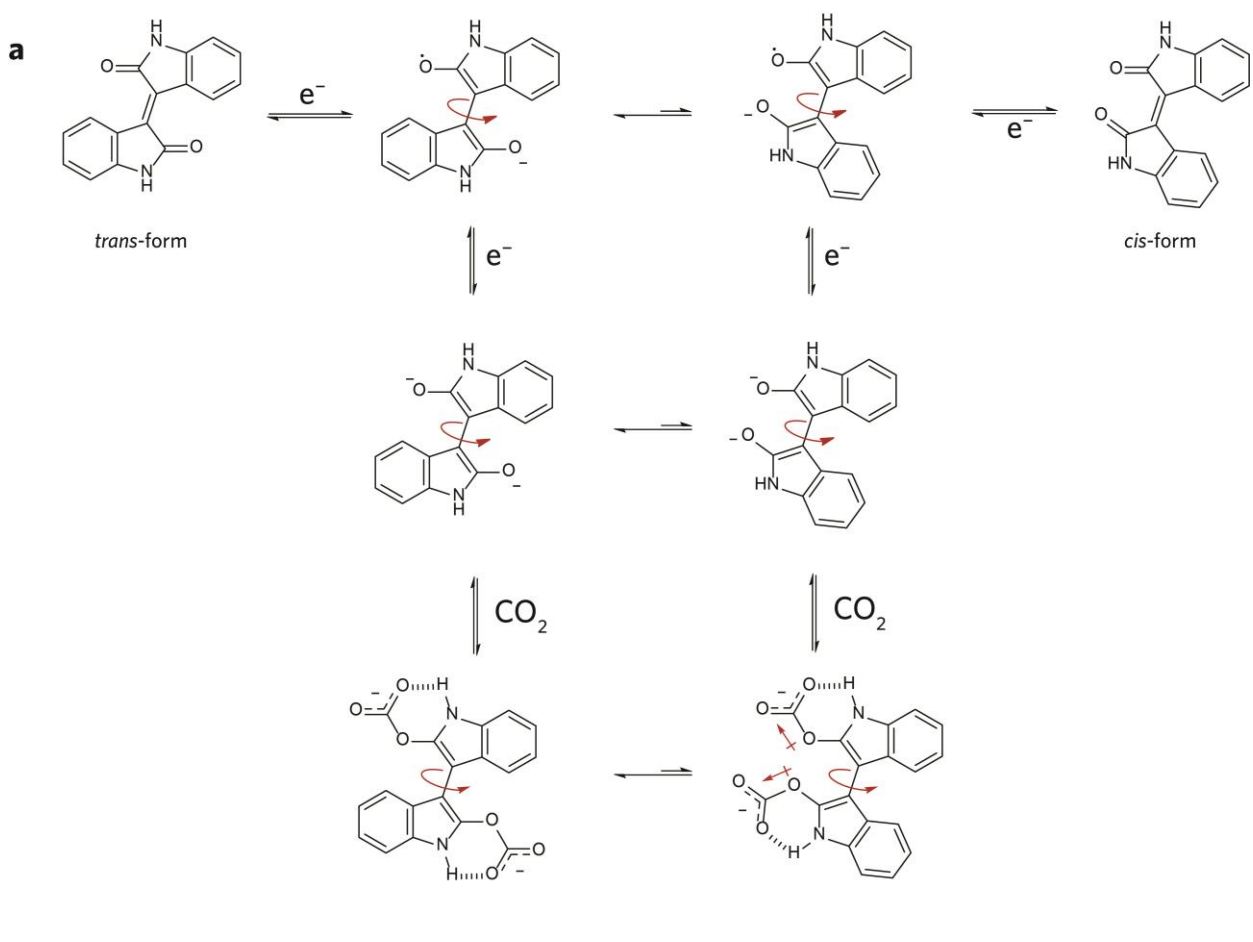
**Supplementary Fig. 7 | CVs of isoindigos with various chemical modifications under different atmospheres.** **a**, IIId. **b**, 55DMIId. **c**, 6BIIId. **d**, 5BIId. **e**, 66DBIIId. **f**, 55DBIIId. **g**, 6MCIIId. **h**, 6B6MCIIId. **i**, 55DFIIId. **j**, 5566TFIIId. **k**, 5NIId. **l**, 5M5NIId. The CV was recorded using 2.5 mM compound in anhydrous DMF with 0.1 M NBu<sub>4</sub>PF<sub>6</sub> saturated by N<sub>2</sub> (grey), 20% CO<sub>2</sub> (balanced with N<sub>2</sub>, blue), and CO<sub>2</sub> (red), respectively, at a scan rate of  $-50 \text{ mV s}^{-1}$  at 298 K.



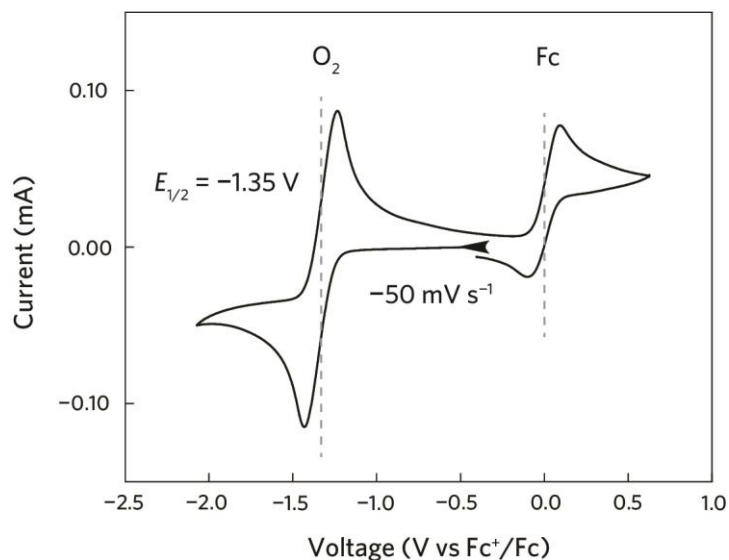
**Supplementary Fig. 8 | CVs of isoindigos with various chemical modifications under different atmospheres.** **a**, 5N6MCIIId. **b**, 66DMCIIId. **c**, NNDEHIIId. **d**, NNDPr66DBIIId. **e**, 6CIId. **f**, 6CIIdNa. **g**, 6AIIdGly. **h**, 6AIIdSer. **i**, 6B6AIIdSer. The CV was recorded using 2.5 mM compound in anhydrous DMF with 0.1 M  $\text{NBu}_4\text{PF}_6$  saturated by  $\text{N}_2$  (grey), 20%  $\text{CO}_2$  (balanced with  $\text{N}_2$ , blue), and  $\text{CO}_2$  (red), respectively, at a scan rate of  $-50 \text{ mV s}^{-1}$  at 298 K.



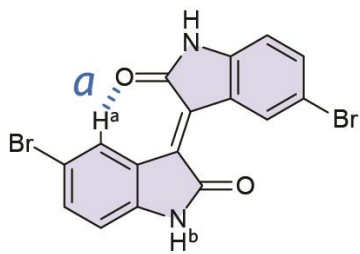
**Supplementary Fig. 9 | Tabulated half-wave potentials of isoindigos under  $\text{N}_2$  or  $\text{CO}_2$ .** Half-wave potentials are summarised from the CVs of various isoindigos using 2.5 mM compound in DMF with 0.1 M  $\text{NBu}_4\text{PF}_6$  under  $\text{N}_2$  (blue) or  $\text{CO}_2$  (pink) (filled circle: first redox potential; empty circle: second redox potential). The oxygen reduction reaction to superoxide occurs at  $-1.35$  V vs.  $\text{Fc}^+/\text{Fc}$  in DMF.



**Supplementary Fig. 10 |** Proposed mechanism for the rotational isomerisation of isoindigo radical anion.



**Supplementary Fig. 11 | CV of  $\text{O}_2$  saturated DMF with 0.1 M  $\text{NBu}_4\text{PF}_6$  at a scan rate of  $-50 \text{ mV s}^{-1}$  with a cathodic sweeping direction initially at 298 K.**

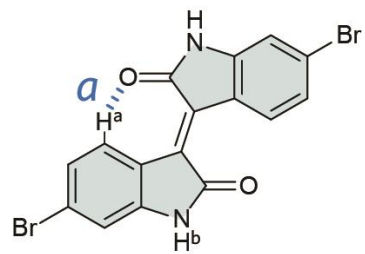


**55DBIId**

$$H^a = 9.32 \text{ ppm}$$

$$H^b = 11.11 \text{ ppm}$$

$$E_{1/2}(\text{IIId}/\text{IIId}^{\bullet-}) = -1.09 \text{ V}$$



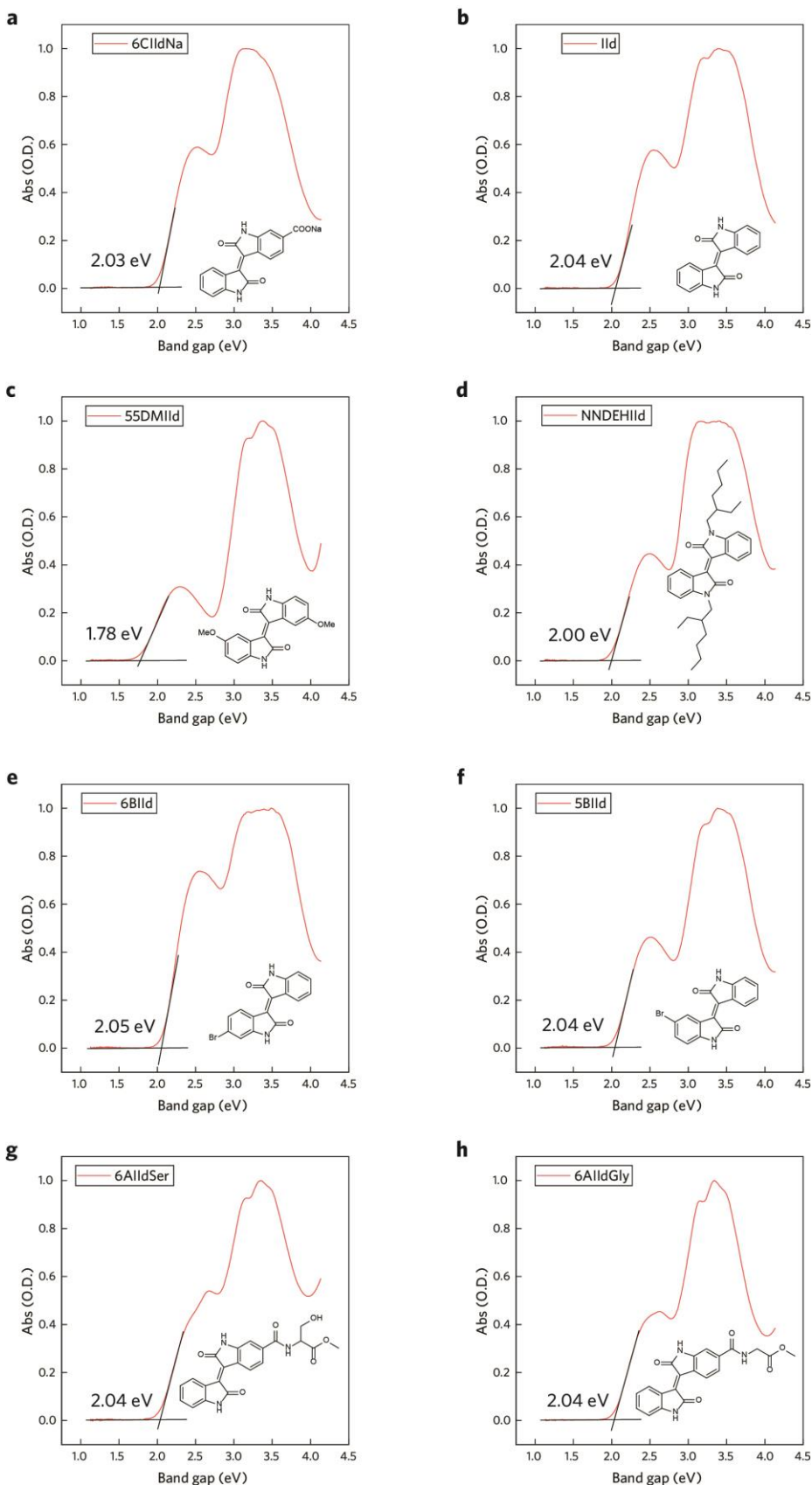
**66DBIId**

$$H^a = 8.99 \text{ ppm}$$

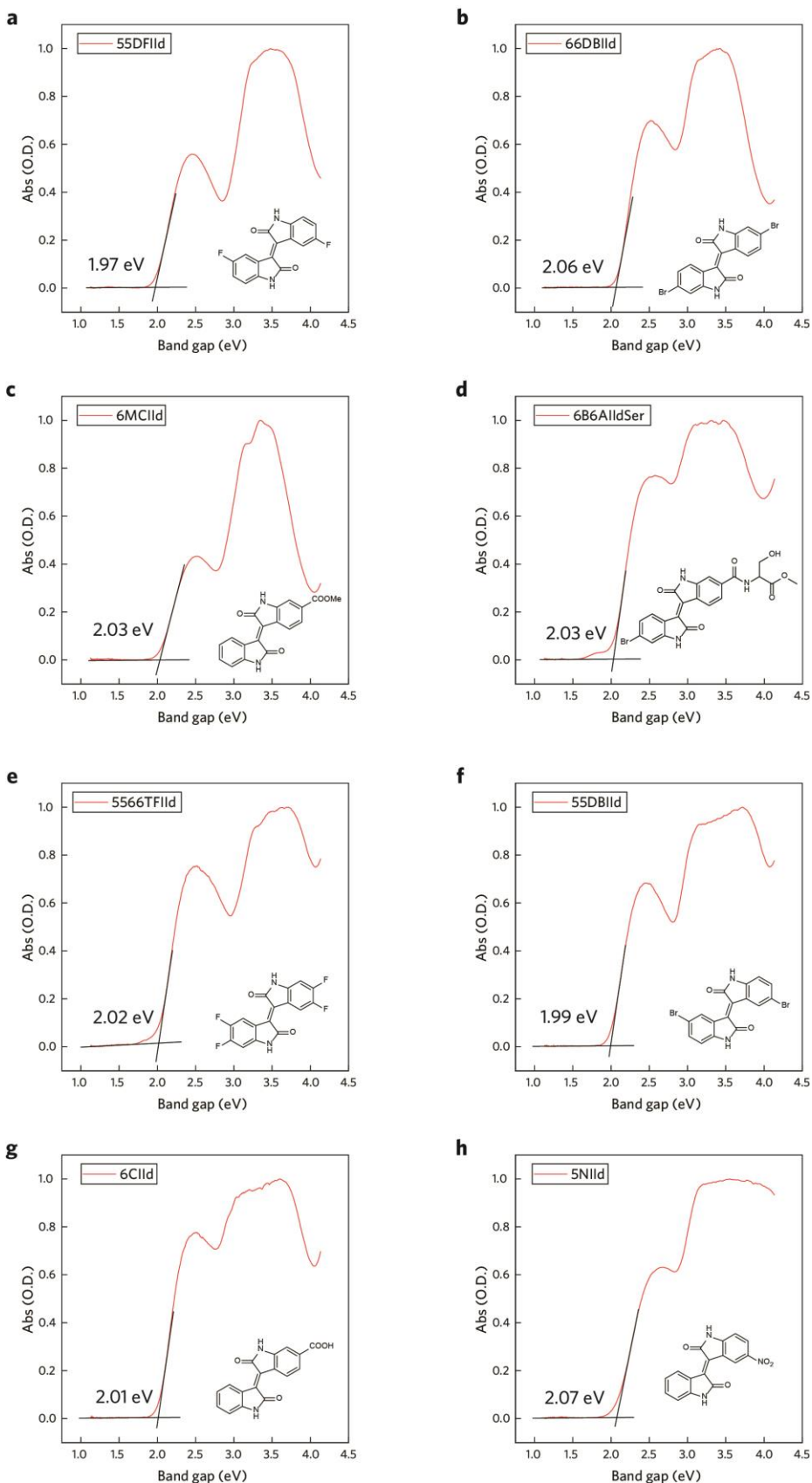
$$H^b = 11.10 \text{ ppm}$$

$$E_{1/2}(\text{IIId}/\text{IIId}^{\bullet-}) = -1.12 \text{ V}$$

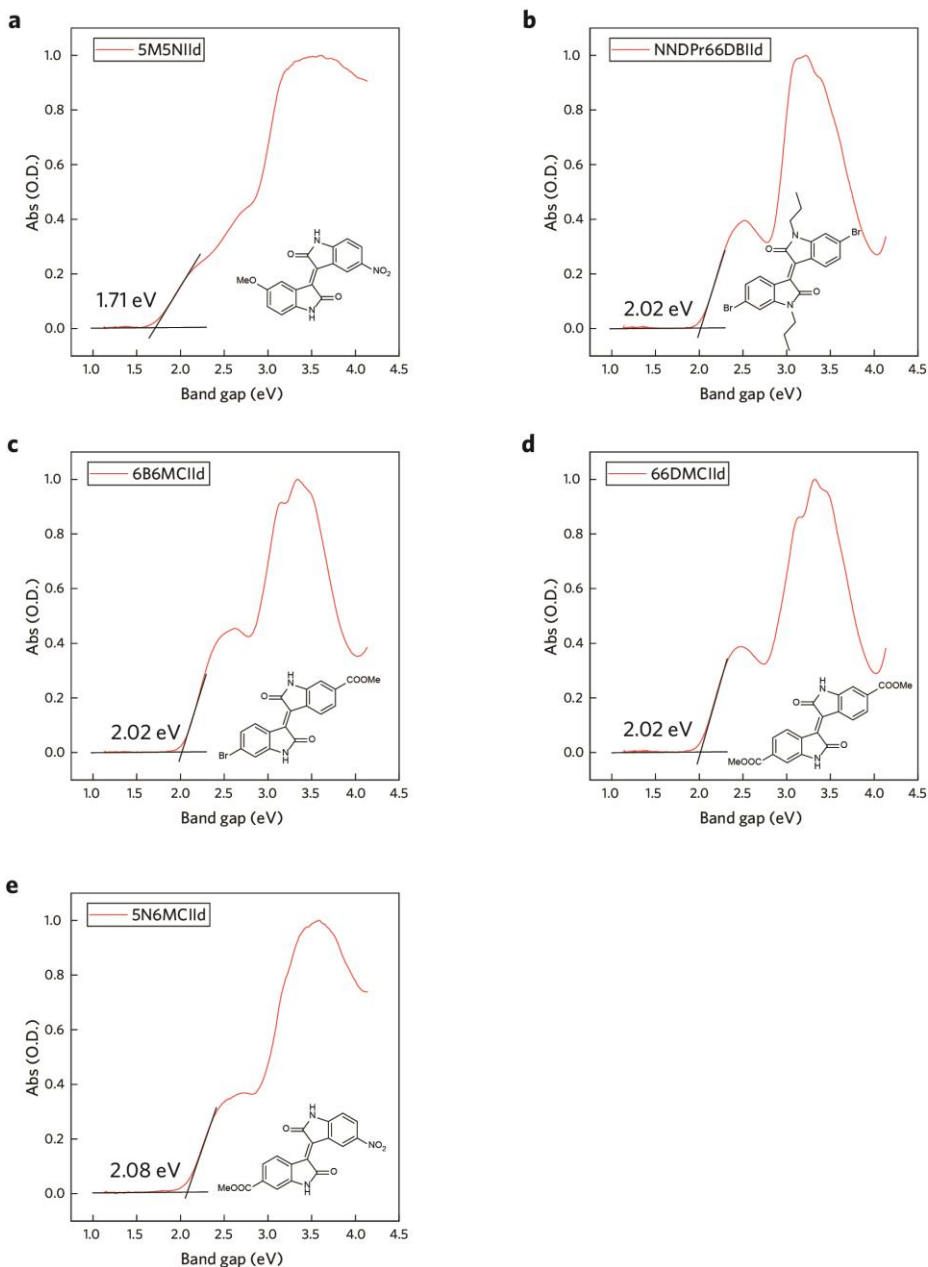
**Supplementary Fig. 12 |** A summary of characteristic  $^1\text{H}$  NMR for  $\text{H}^a$  and  $\text{H}^b$  and half-wave redox potential of 55DBIId and 66DBIId under  $\text{CO}_2$ .



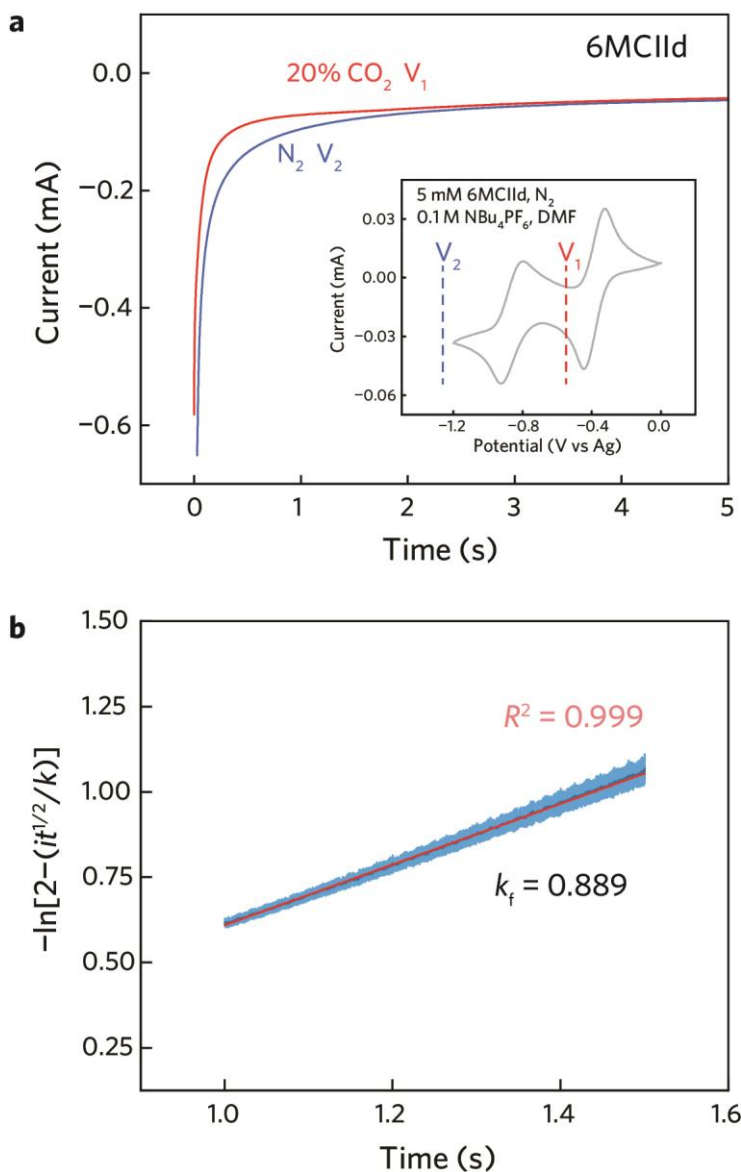
**Supplementary Fig. 13 | Kubelka-Munk spectra of various isoindigos.**



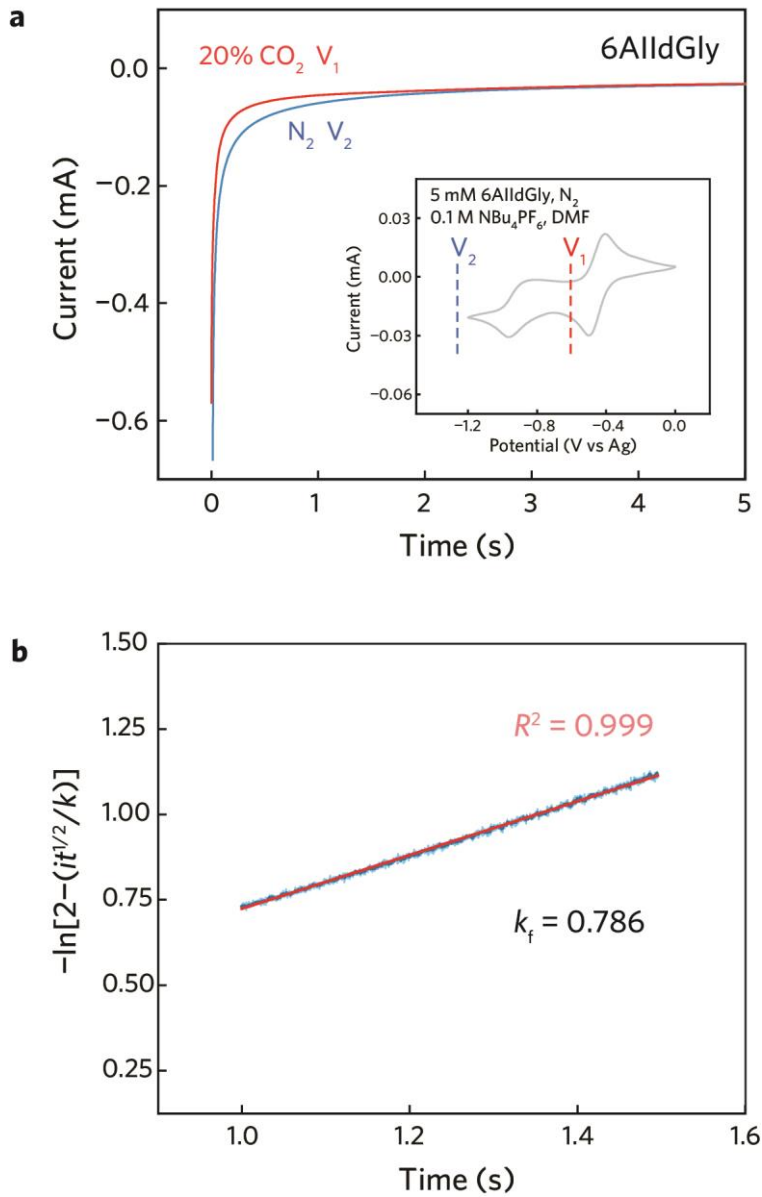
**Supplementary Fig. 14 | Kubelka-Munk spectra of various isoindigos.**



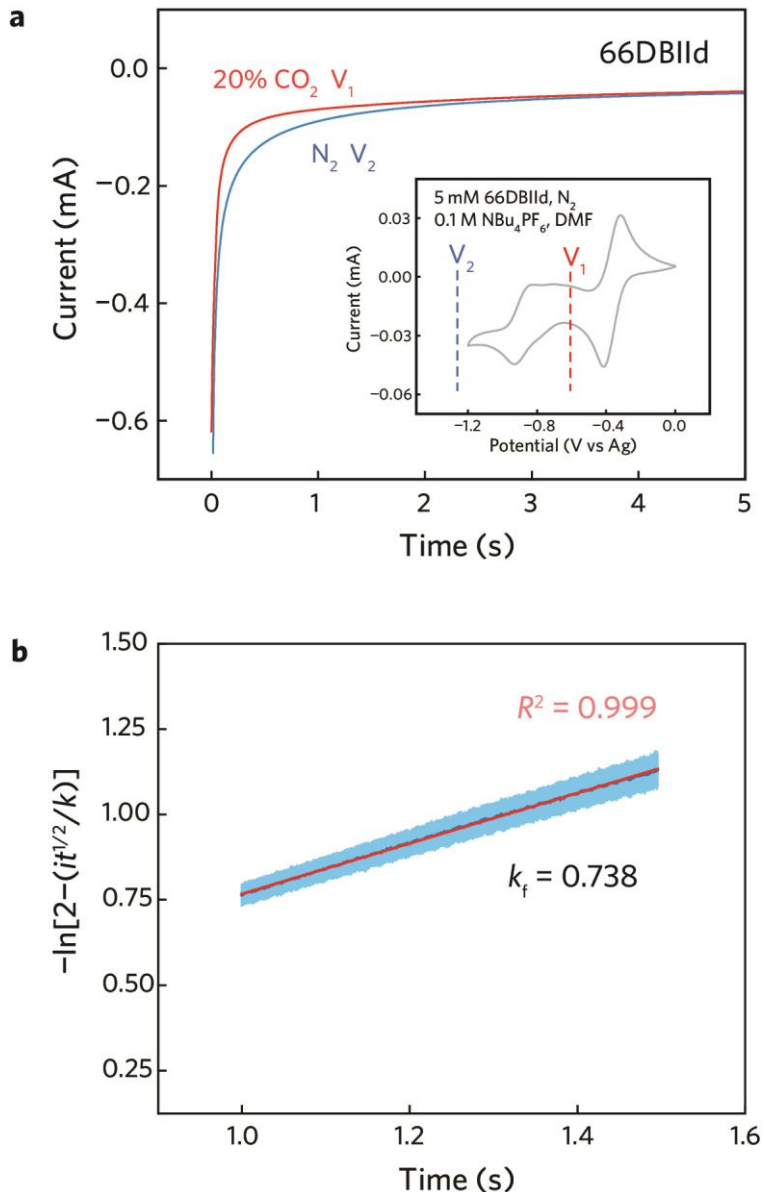
**Supplementary Fig. 15 |** Kubelka-Munk spectra of various isoindigos.



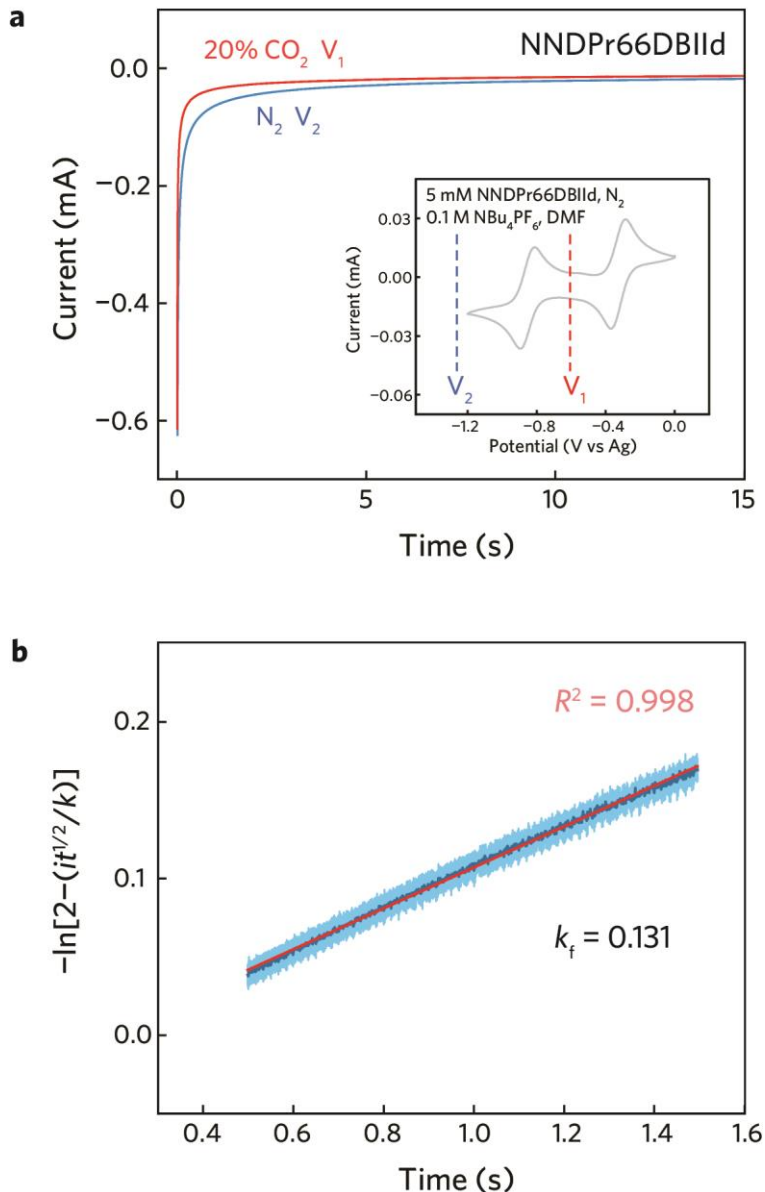
**Supplementary Fig. 16 | Calculation of the reaction rate constant between 6MCIIId radical anion and  $\text{CO}_2$ .** **a**, Plots of current vs. time for 5 mM 6MCIIId in DMF with 0.1 M  $\text{NBu}_4\text{PF}_6$  as the supporting salt for potential steps from open circuit voltage to  $-0.55$  V vs. Ag ( $V_1$ ) with 20%  $\text{CO}_2$ , and from open circuit voltage to  $-1.26$  V vs. Ag ( $V_2$ ) without  $\text{CO}_2$ . The inset is the CV of the electrolyte under  $N_2$  with the corresponding voltage steps ( $V_1$  and  $V_2$ ). **b**, Determination of the forward rate constant ( $k_f$ ) for the addition of  $\text{CO}_2$  to  $6\text{MCIIId}^{\bullet-}$ . The measurements were done in triplicate, and the data is shown for the time interval where the current is between one- and two-electron transfer processes. The slope of the plot gives  $k_f$ .



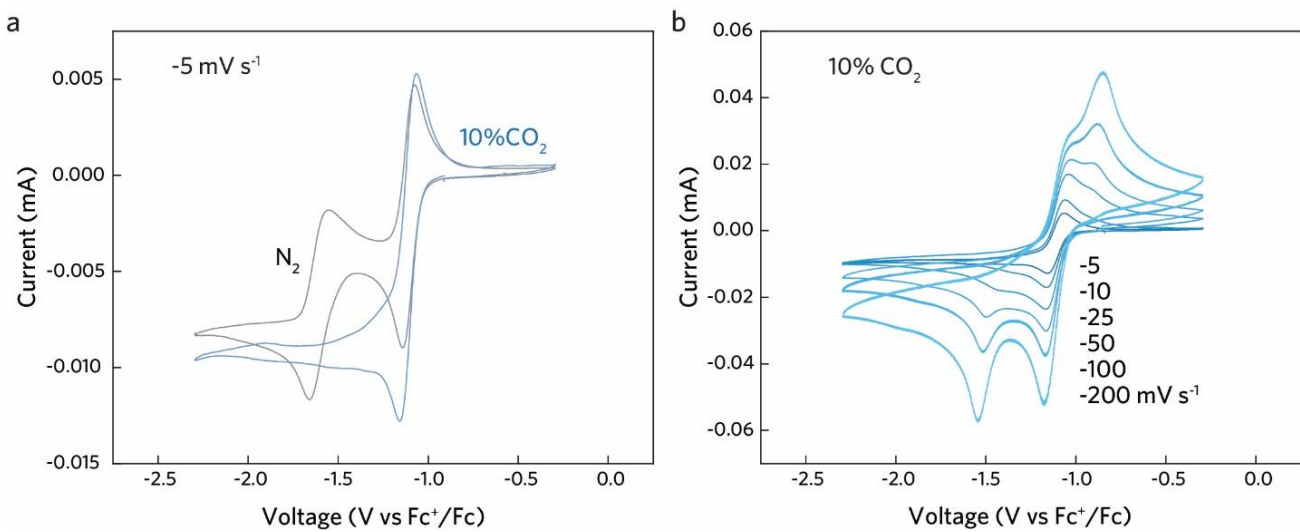
**Supplementary Fig. 17 | Calculation of the reaction rate constant between 6AlldGly radical anion and  $\text{CO}_2$ .** **a**, Plots of current vs. time for 5 mM 6AlldGly in DMF with 0.1 M  $\text{NBu}_4\text{PF}_6$  as the supporting salt for potential steps from open circuit voltage to  $-0.6$  V vs. Ag ( $V_1$ ) with 20%  $\text{CO}_2$ , and from open circuit voltage to  $-1.282$  V vs. Ag ( $V_2$ ) without  $\text{CO}_2$ . The inset is the CV of the electrolyte under  $N_2$  with the corresponding voltage steps ( $V_1$  and  $V_2$ ). **b**, Determination of the forward rate constant ( $k_f$ ) for the addition of  $\text{CO}_2$  to  $6\text{AlldGly}^{\bullet-}$ . The measurements were done in triplicate, and the data is shown for the time interval where the current is between one- and two-electron transfer processes. The slope of the plot gives  $k_f$ .



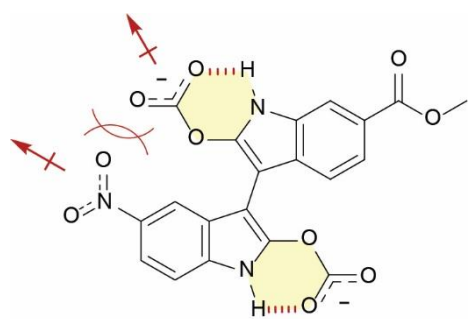
**Supplementary Fig. 18 | Calculation of the reaction rate constant between 66DBIId radical anion and  $\text{CO}_2$ .** **a**, Plots of current vs time for 5 mM 66DBIId in DMF with 0.1 M  $\text{NBu}_4\text{PF}_6$  as the supporting salt for potential steps from open circuit voltage to  $-0.6$  V vs Ag ( $V_1$ ) with 20%  $\text{CO}_2$ , and from open circuit voltage to  $-1.275$  V vs Ag ( $V_2$ ) without  $\text{CO}_2$ . The inset is the cyclic voltammogram of the electrolyte under  $\text{N}_2$  with the corresponding voltage steps ( $V_1$  and  $V_2$ ). **b**, Determination of the forward rate constant ( $k_f$ ) for the addition of  $\text{CO}_2$  to  $66\text{DBIId}^{\bullet-}$ . The measurements were done in triplicate, and the data is shown for the time interval where the current is between that of one- and two-electron transfer processes. The slope of the plot gives  $k_f$ .



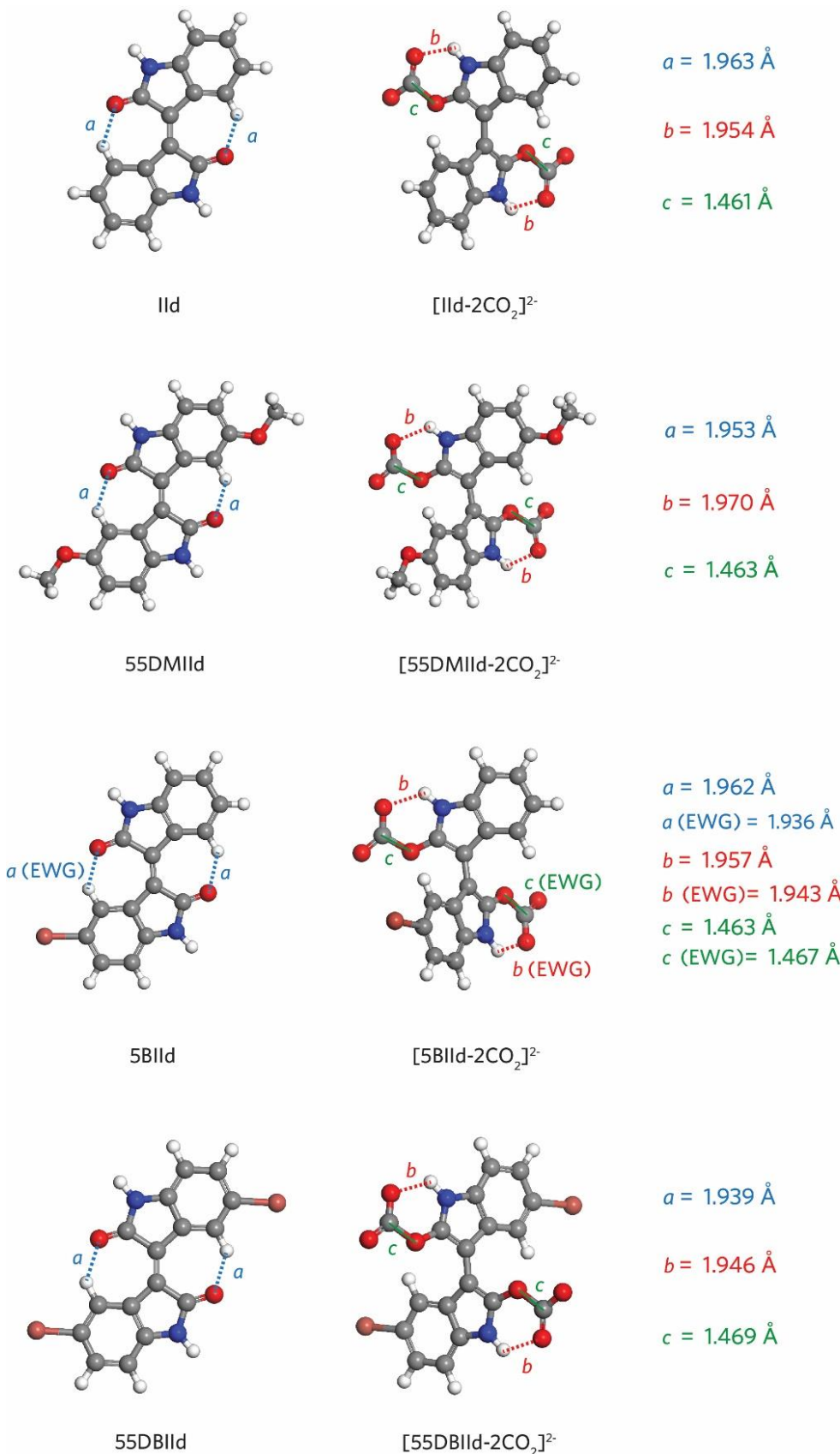
**Supplementary Fig. 19 | Calculation of the reaction rate constant between NNDPr66DBIId radical anion and  $\text{CO}_2$ .** **a**, Plots of current vs time for 5 mM NNDPr66DBIId in DMF with 0.1 M  $\text{NBu}_4\text{PF}_6$  as the supporting salt for potential steps from open circuit voltage to  $-0.6$  V vs Ag ( $V_1$ ) with 20%  $\text{CO}_2$ , and from open circuit voltage to  $-1.252$  V vs Ag ( $V_2$ ) without  $\text{CO}_2$ . The inset is the cyclic voltammogram of the electrolyte under  $\text{N}_2$  with the corresponding voltage steps ( $V_1$  and  $V_2$ ). **b**, Determination of the forward rate constant ( $k_f$ ) for the addition of  $\text{CO}_2$  to  $\text{NNDPr66DBIId}^{\bullet-}$ . The measurements were done in triplicate, and the data is shown for the time interval where the current is between that of one- and two-electron transfer processes. The slope of the plot gives  $k_f$ .



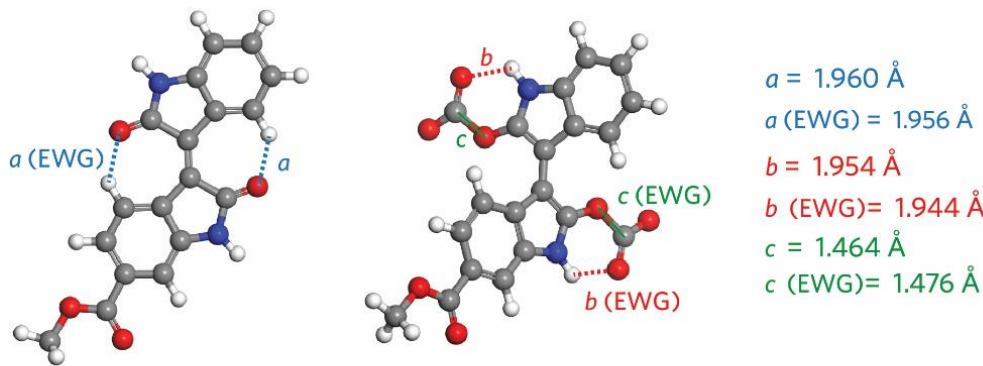
**Supplementary Fig. 20** | CV of 6MCIId under different atmospheres or at different scan rates. **a**, CV curves under N<sub>2</sub> or 10% CO<sub>2</sub> at a cathodic scan rate of  $-5 \text{ mV s}^{-1}$ . **b**, CV curves under 10% CO<sub>2</sub> at various scan rates from  $-5$  to  $-200 \text{ mV s}^{-1}$ . The CV curves were recorded using 2.5 mM 6MCIId in anhydrous DMF with 0.1 M NBu<sub>4</sub>PF<sub>6</sub>.



**Supplementary Fig. 21 |** Proposed mechanism of  $\text{CO}_2$  binding inhibition in 5N6MCIIId.

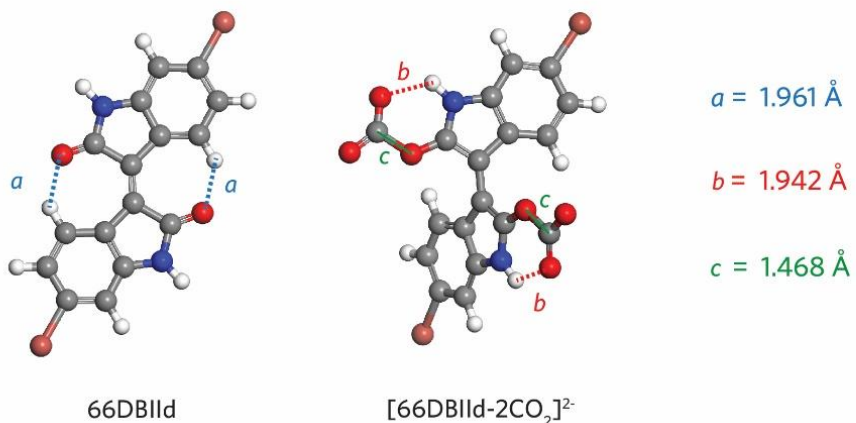


**Supplementary Fig. 22 |** DFT-optimised structures of isoindigos in the neutral state and CO<sub>2</sub>-complexed state (colour of atoms: grey: C; red: O; blue: N; brown: Br; white: H).



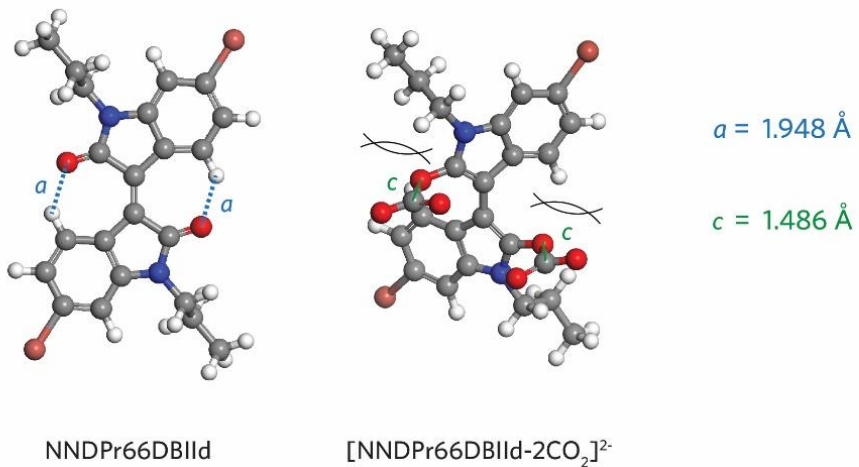
6MCIIId

$[6\text{MCIIId}-2\text{CO}_2]^{2-}$



66DBIIId

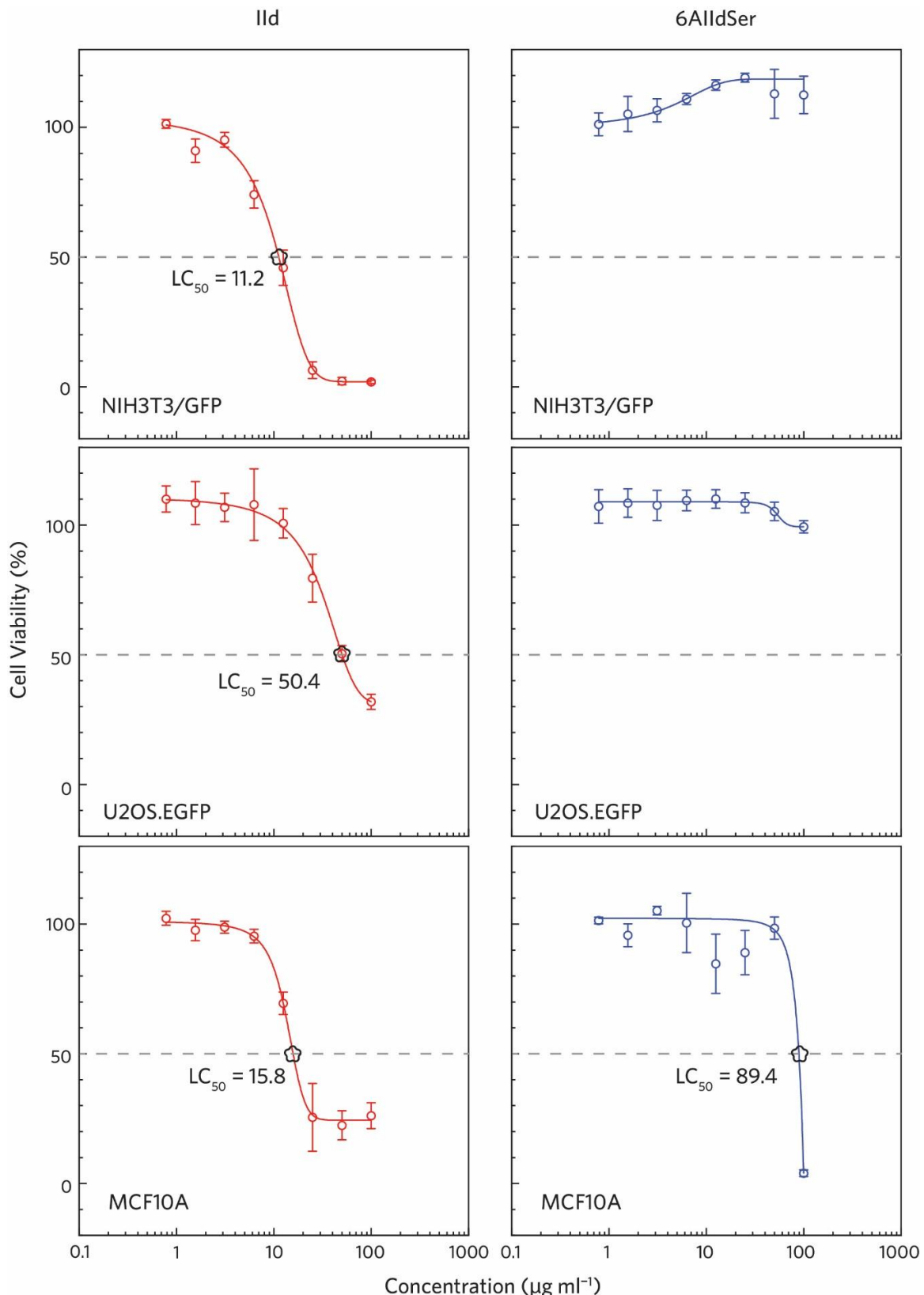
$[66\text{DBIIId}-2\text{CO}_2]^{2-}$



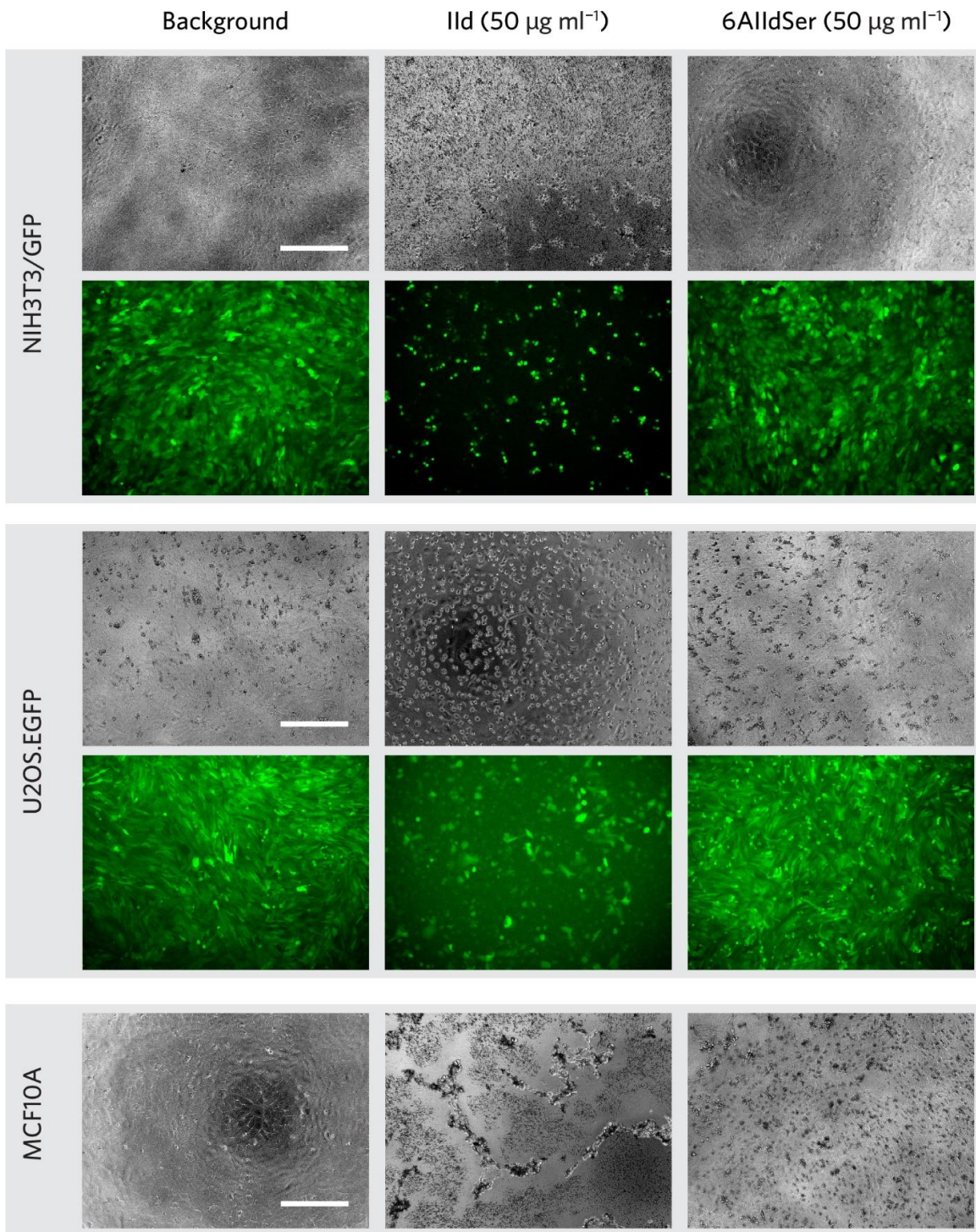
NNDPr66DBIIId

$[\text{NNDPr}66\text{DBIIId}-2\text{CO}_2]^{2-}$

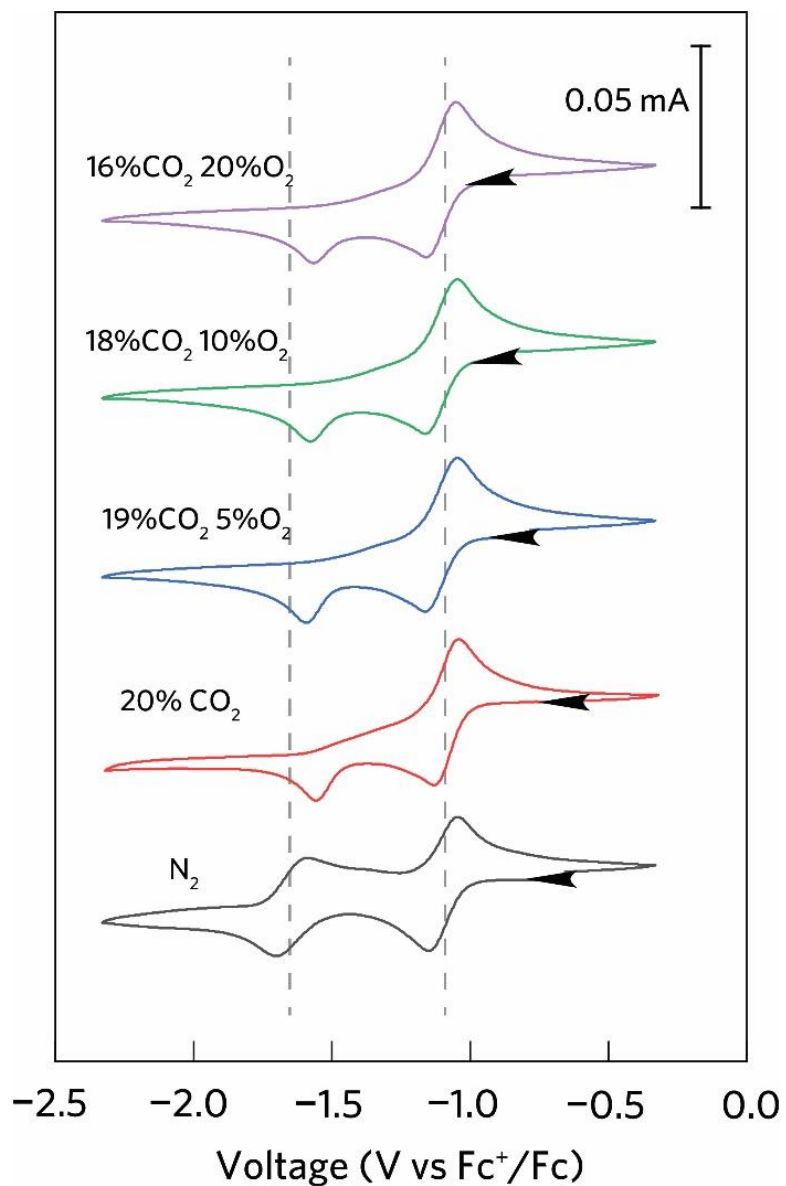
**Supplementary Fig. 23 |** DFT-optimised structures of isoindigos in the neutral state and  $\text{CO}_2$ -complexed state (colour of atoms: grey: C; red: O; blue: N; brown: Br; white: H).



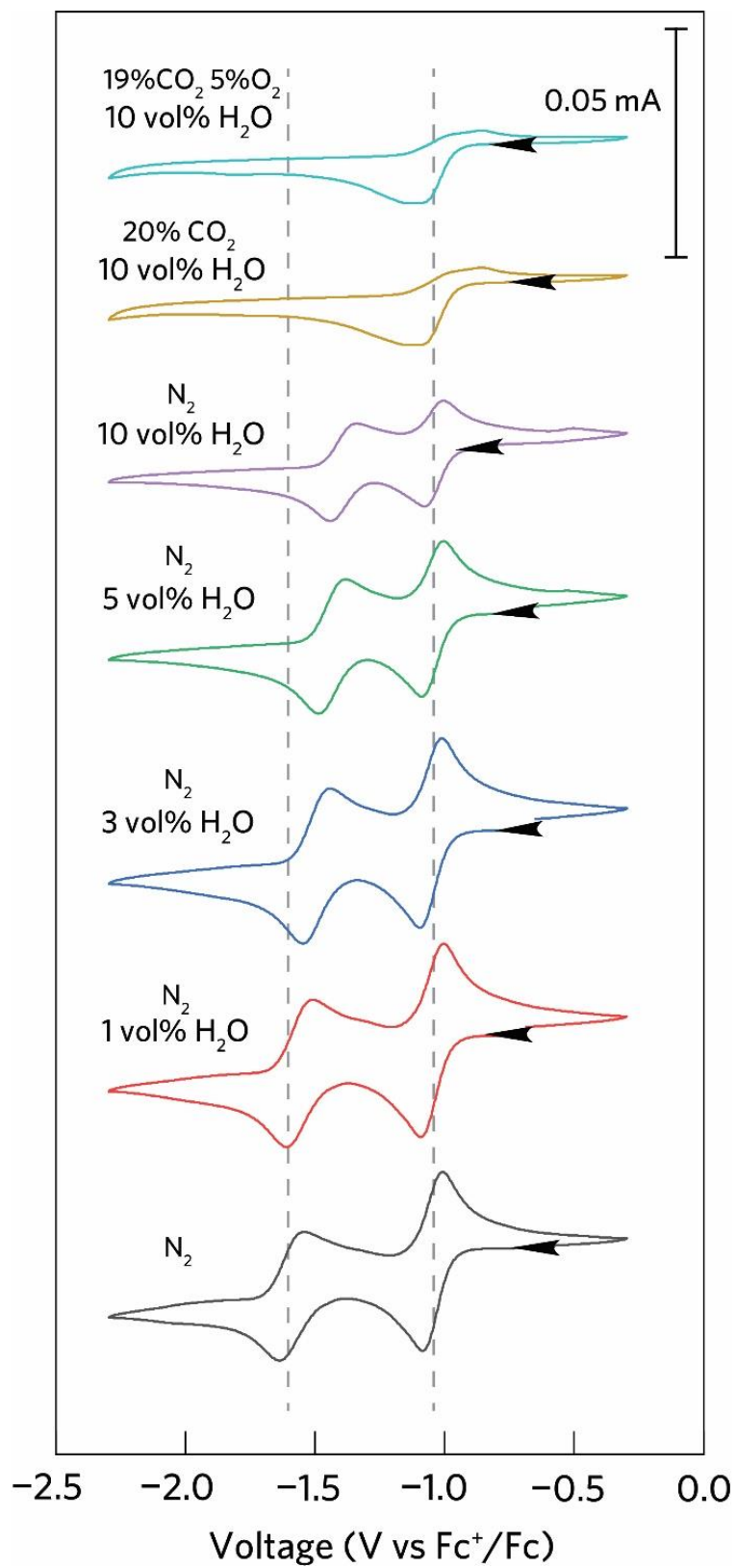
**Supplementary Fig. 24 | Cytotoxicity test of IIId and 6AIIdSer using different mammalian cells.**  
 Cells were cultured in the absence or presence of isoindigos under various concentrations from 0.78 to 100  $\mu\text{g ml}^{-1}$  for 48 h. The number of replicates (n=3). The amino ester modified 6AIIdSer exhibits much better biocompatibility than its unmodified counterparts.



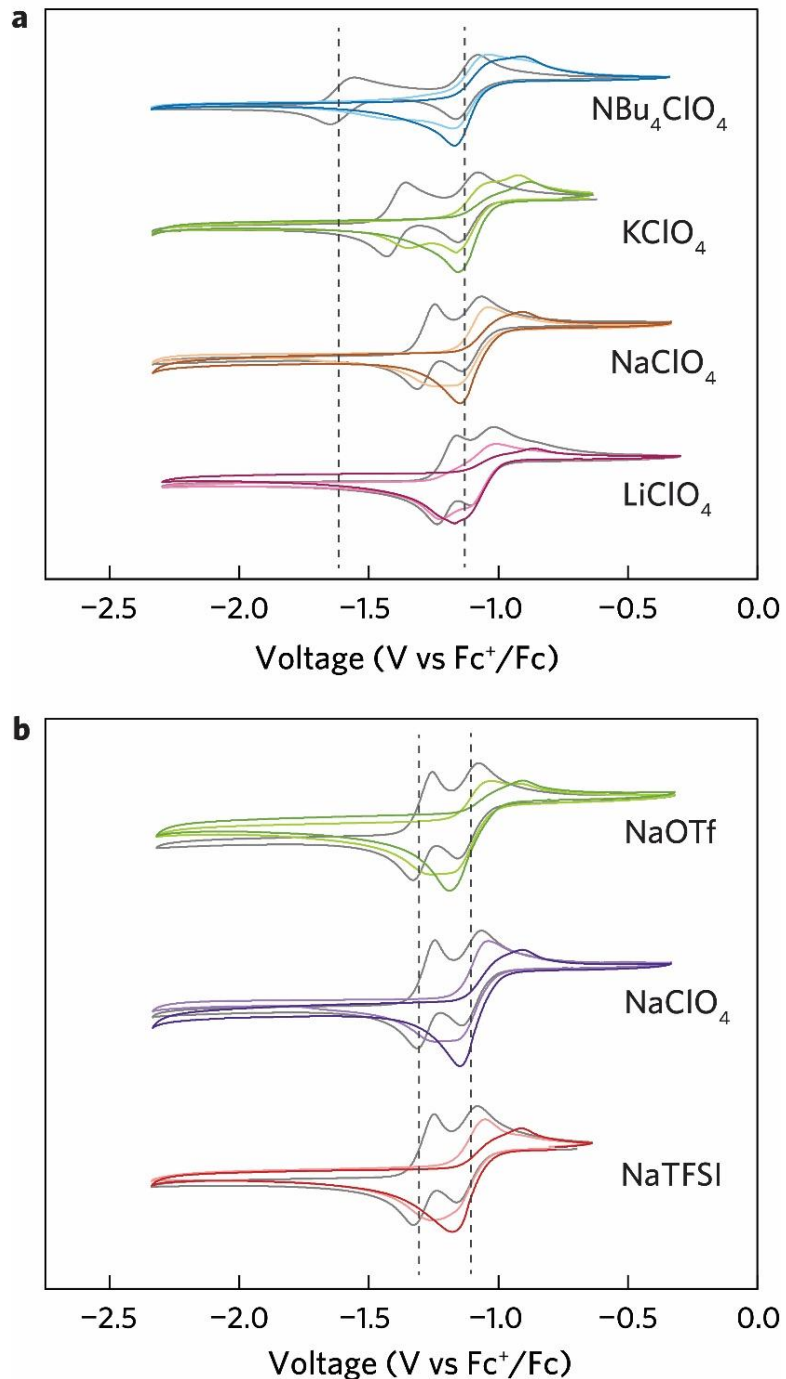
**Supplementary Fig. 25 | Optical microscopic images of mammalian cells after 48 h culture with isoindigos.** Different types of cells were cultured in the presence of  $50 \mu\text{g ml}^{-1}$  of IId or 6AIIdSer, and cells remained much healthier under the 6AIIdSer condition. The solvent DMF (1 vol%) was used as the background reference/control. The scale bars are  $300 \mu\text{m}$ . NIH3T3/GFP and U2OS.EGFP express green fluorescent protein (GFP).



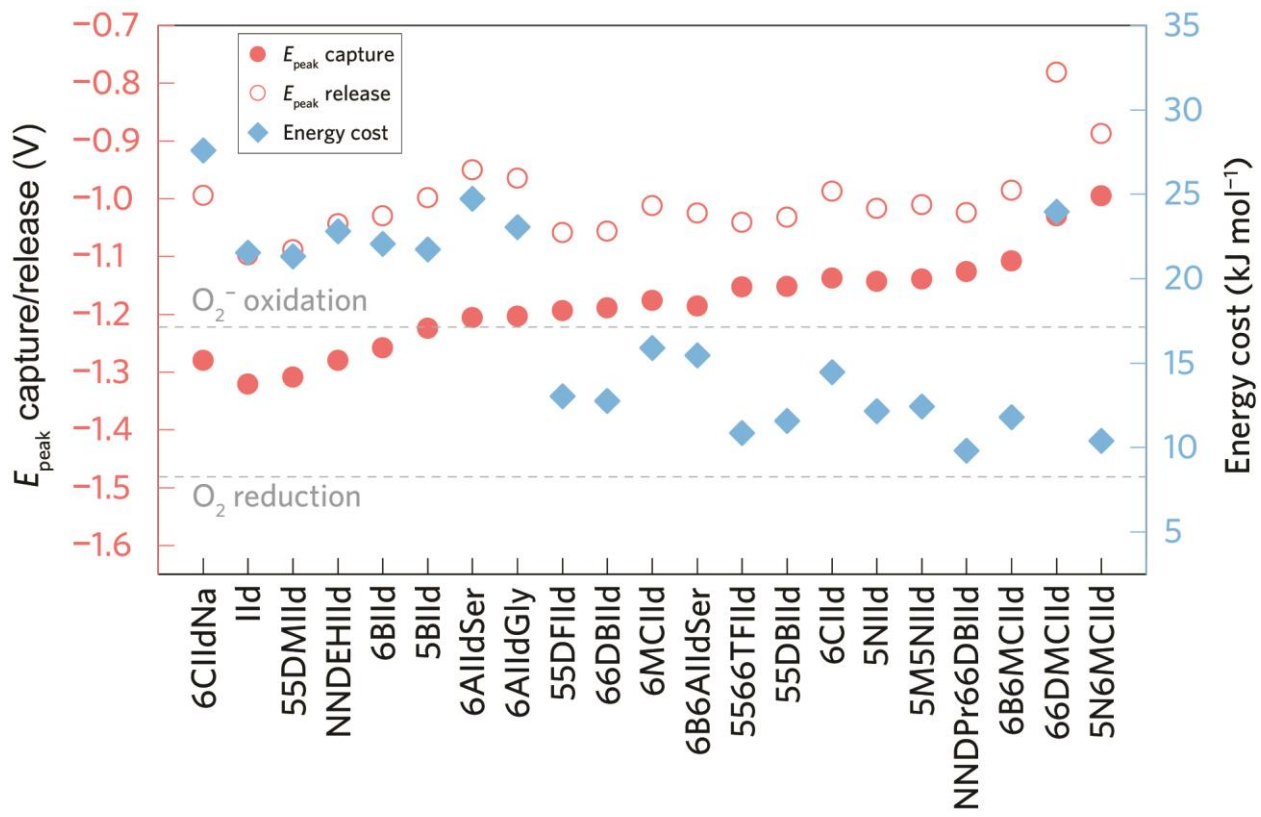
**Supplementary Fig. 26 | The impact of  $\text{O}_2$  on the redox properties and  $\text{CO}_2$  binding behaviours of 55DBIId.** The CV curves were recorded using 2.5 mM 55DBIId in DMF with 0.1 M  $\text{NBu}_4\text{PF}_6$  under mixtures of gases at a scan rate of  $-50 \text{ mV s}^{-1}$  with a cathodic sweeping direction initially at 298 K.



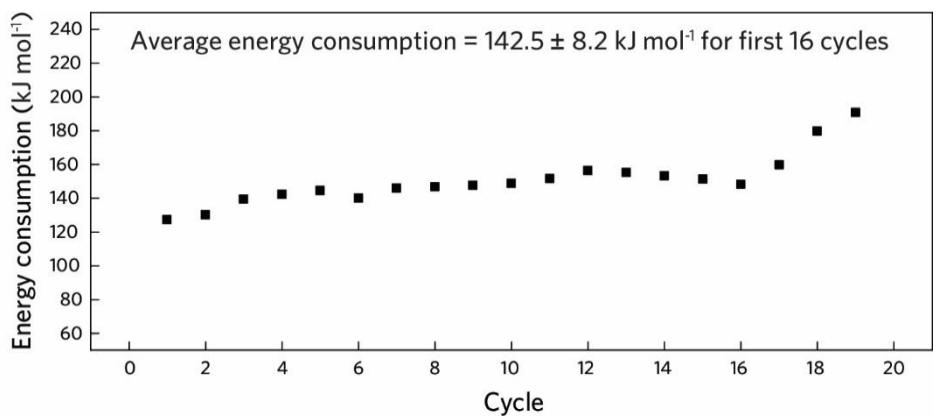
**Supplementary Fig. 27 | The impact of water on the redox properties and CO<sub>2</sub> binding behaviours of 55DBIId.** The CV was recorded using 2.5 mM 55DBIId in DMF with 0.1 M NBu<sub>4</sub>PF<sub>6</sub> with various water contents under various atmospheres at a scan rate of  $-50\text{ mV s}^{-1}$  with an initial cathodic sweeping direction at 298 K.



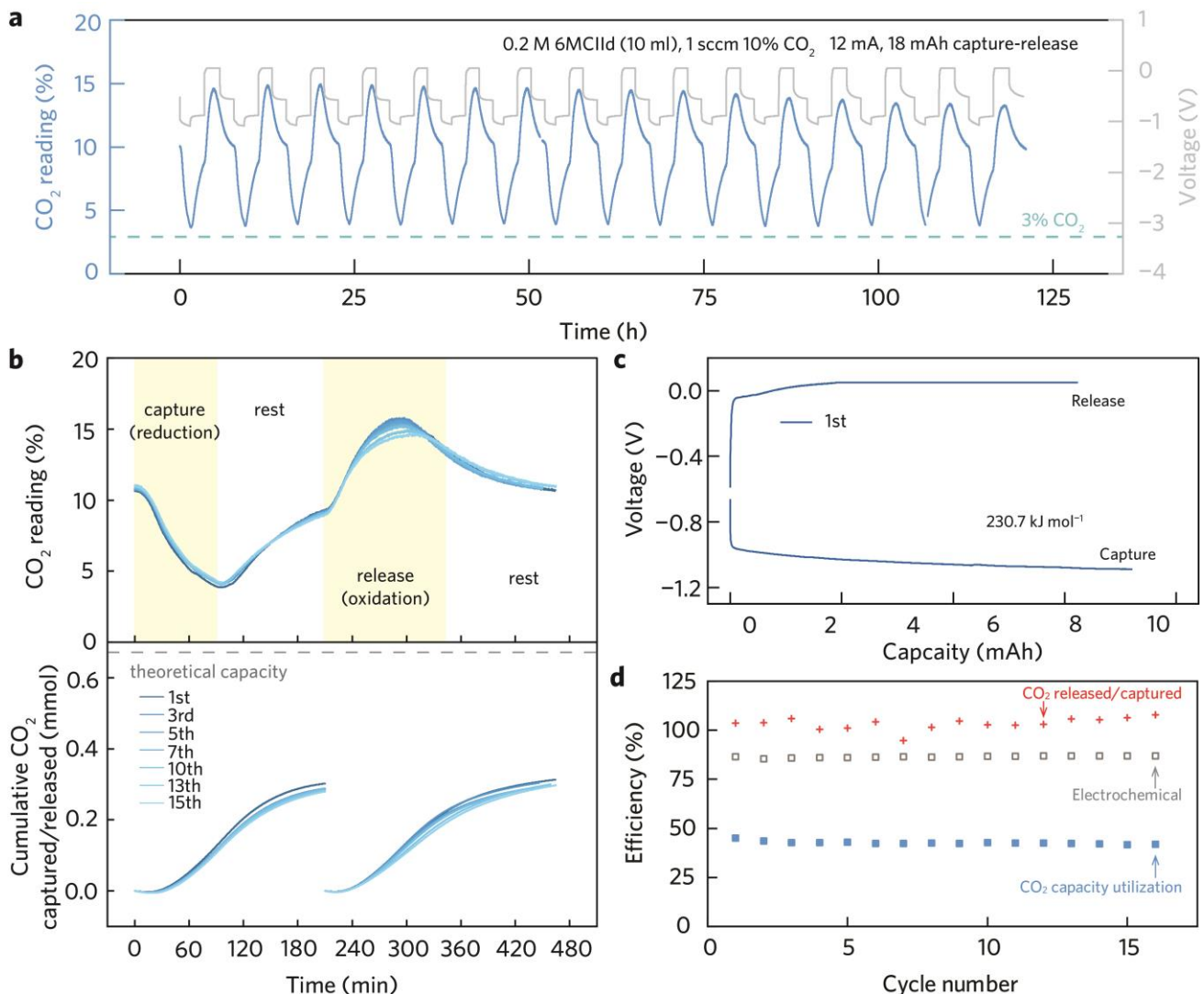
**Supplementary Fig. 28 | The effect of supporting salts on the redox properties and  $\text{CO}_2$  binding behaviours of 6MCIId. a,** CV curves of 6MCIId in electrolytes with various supporting salt cations under  $\text{N}_2$ , 20%  $\text{CO}_2$ , and  $\text{CO}_2$ , respectively. **b,** CV curves of 6MCIId in electrolytes with various counter anions under  $\text{N}_2$ , 20%  $\text{CO}_2$ , and 100%  $\text{CO}_2$ . The CV was recorded using 2.5 mM 6MCIId in DMF with 0.1 M supporting salt at a scan rate of  $-50 \text{ mV s}^{-1}$  with an initial cathodic sweeping direction at 298 K. (Grey:  $\text{N}_2$ ; lighter colour: 20%  $\text{CO}_2$ ; colour: 100%  $\text{CO}_2$ ).



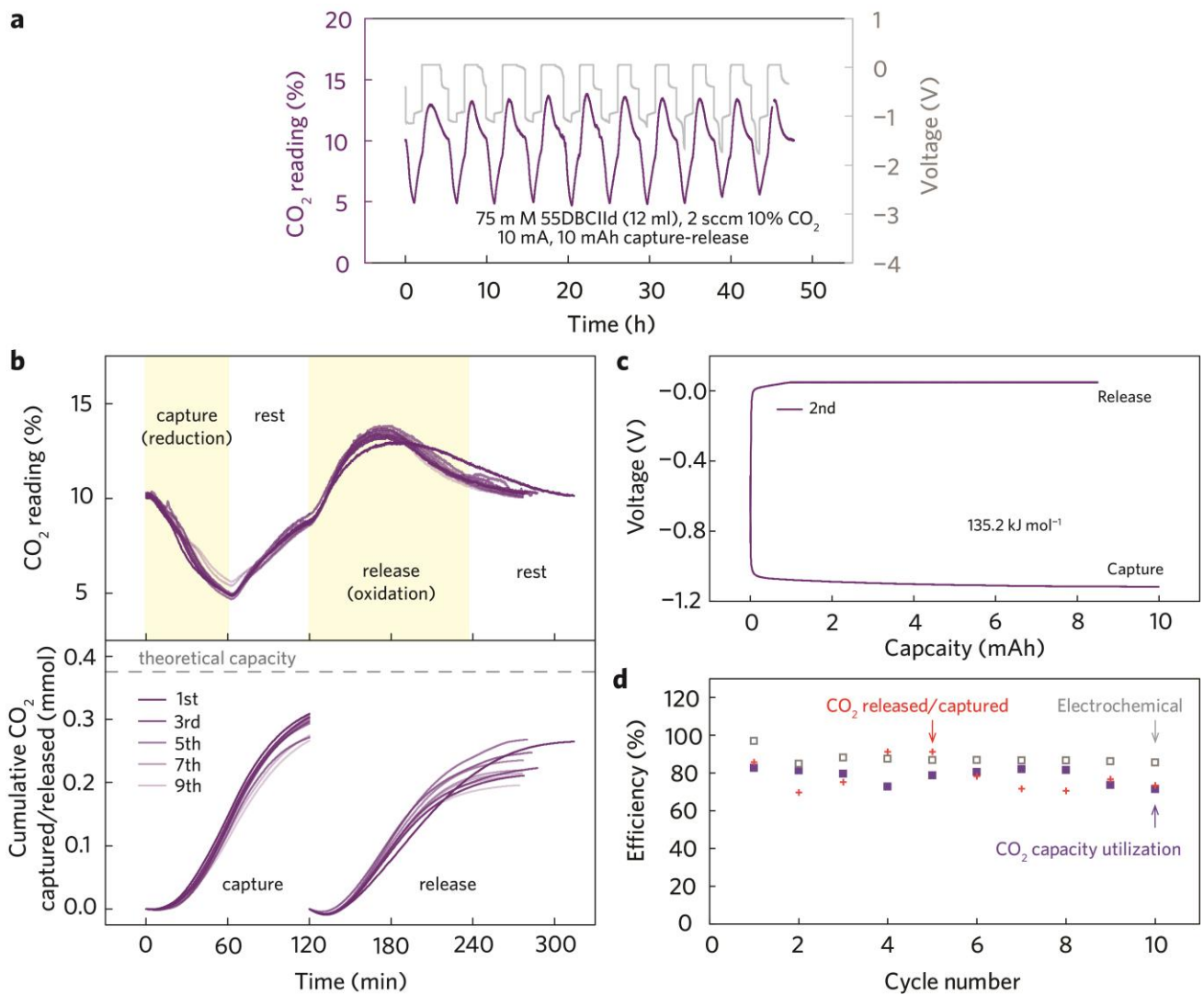
**Supplementary Fig. 29 | Summary of the peak potentials for CO<sub>2</sub> capture (filled symbols) and release (empty symbols) of isoindigos from Supplementary Fig. 2 and 3.** The theoretical energy costs for CO<sub>2</sub> capture and release were estimated based on the voltage gap ( $E_{\text{peak}} \text{ release} - E_{\text{peak}} \text{ capture}$ ). The peak potentials for O<sub>2</sub> reduction and oxidation are shown as grey dashed lines.



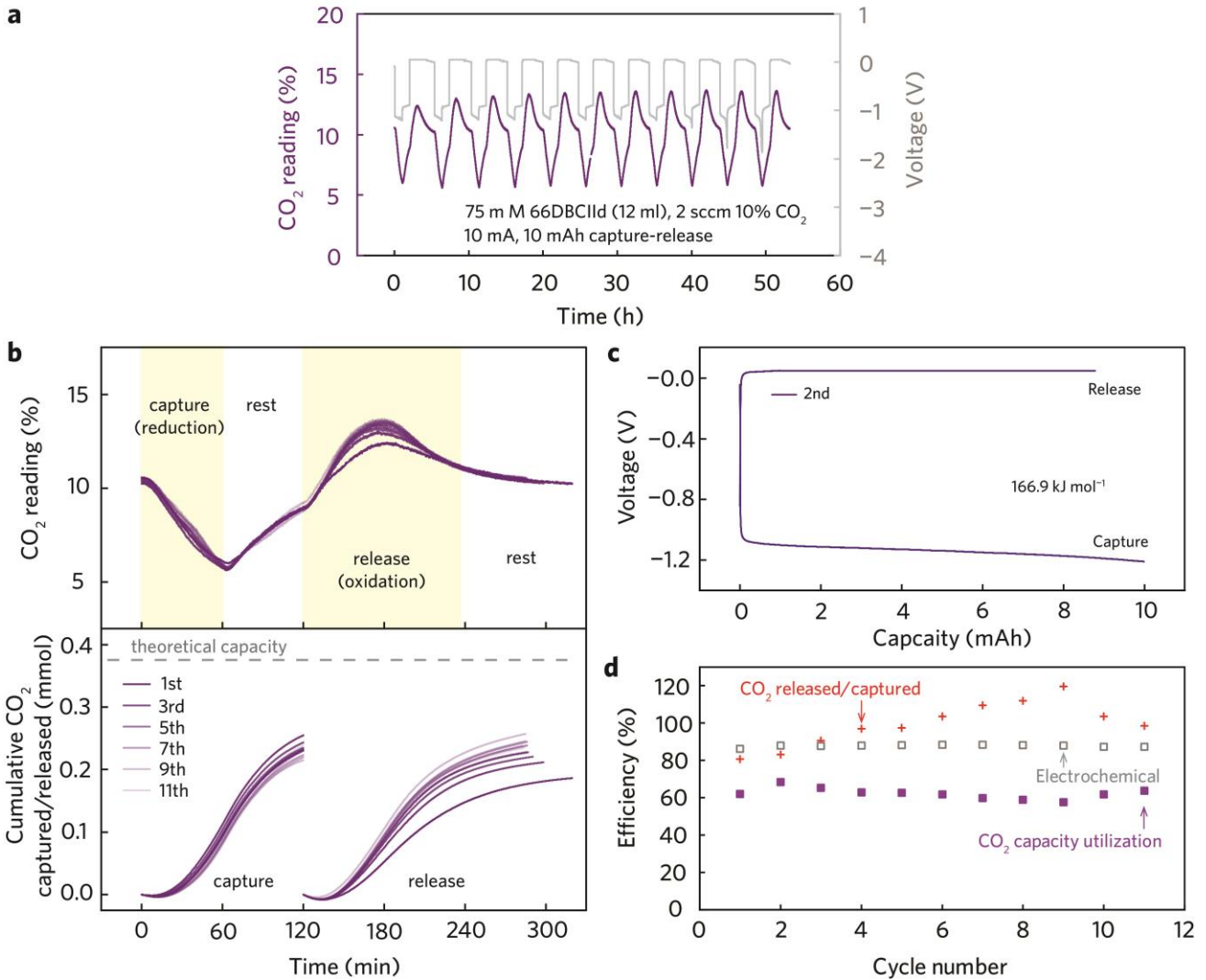
**Supplementary Fig. 30 |** Energy consumption of CO<sub>2</sub> concentration for each cycle in Fig. 6.



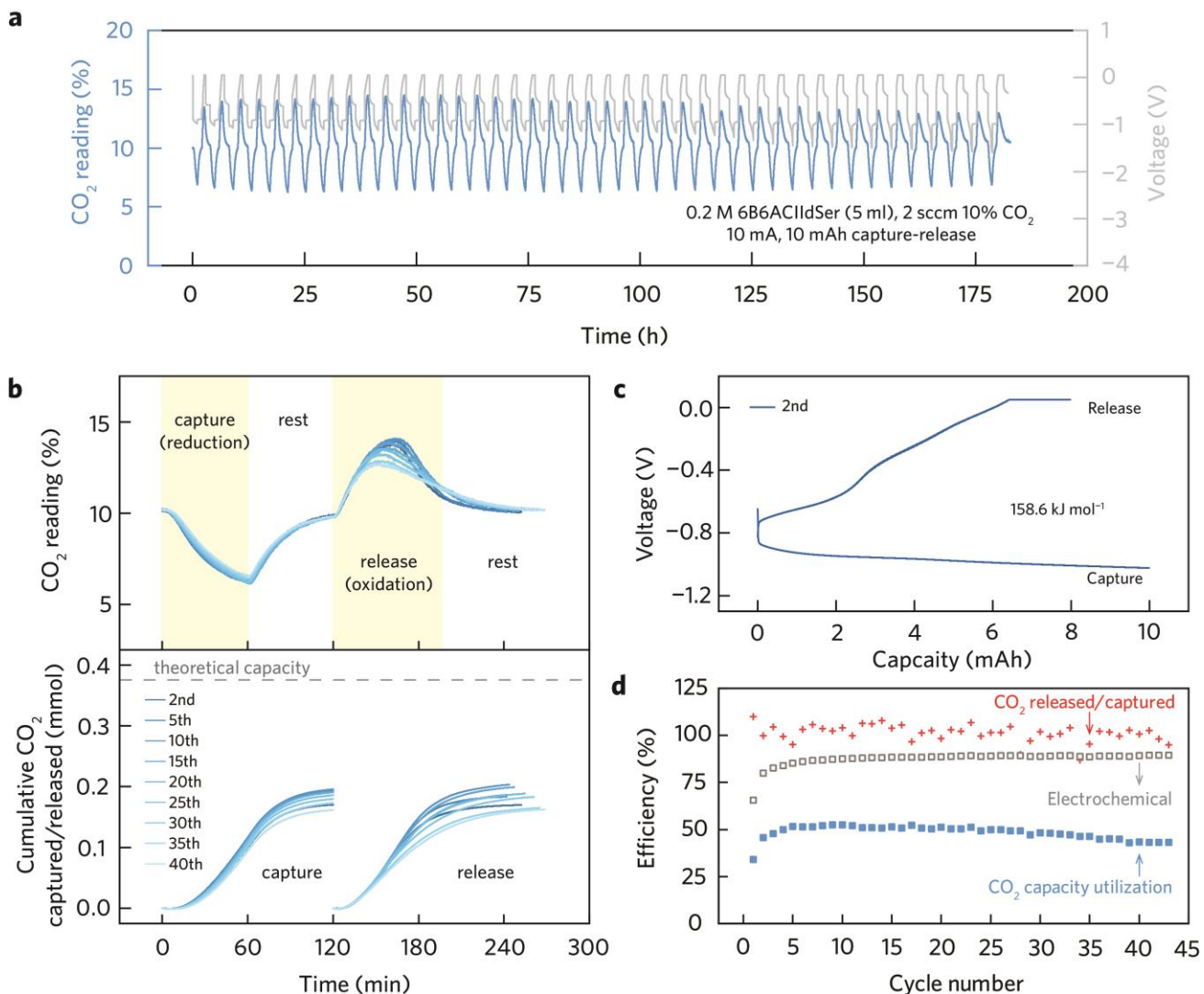
**Supplementary Fig. 31 | Evaluating the performance of 6MCIIId at a higher percentage of CO<sub>2</sub> removal.** **a**, CO<sub>2</sub> reading at the exit of the sorbent tank and voltage curve over 16 repeating capture/release cycles for ~120 h operation. **b**, CO<sub>2</sub> reading for selected capture/release cycles overlaid, with the cumulative amount of CO<sub>2</sub> captured/released in each cycle relative to the theoretical capacity. Lighter colours represent later cycles. Capture, rest, release, and rest steps are indicated by the shaded regions. For CO<sub>2</sub> capture, 6MCIIId was reduced at 12 mA for 90 min followed by a 120 min rest. For CO<sub>2</sub> release, the adducts were oxidised at 12 mA to 0.05 mV followed by a ~120 min constant voltage hold, and finally rested for another 120 min. **c**, The voltage-capacity curve for the 2<sup>nd</sup> capture/release cycle, indicating an early-stage energy consumption of 230.7 kJ per mol CO<sub>2</sub> concentrated. **d**, The CO<sub>2</sub> capacity utilisation efficiency (blue squares), release/capture efficiency (red crosses), and electrochemical efficiency (grey empty squares) of the system. The liquid sorbent was composed of 10 ml 0.2 M 6MCIIId in DMF with 0.5 M NaTFSI as the supporting salt. The sorbent tank was filled with plastic beads and purged with 10% CO<sub>2</sub> balanced in N<sub>2</sub> at a flow rate of 1 sccm. On the opposite side, a Fc tank was used to balance the charge, which was filled with 20 ml 0.2 M Fc in DMF with 0.5 M NaTFSI as the supporting salt, 4 mM FcBF<sub>4</sub> to facilitate electro-reduction, and 10 mM 6MCIIId to mitigate sorbent crossover.



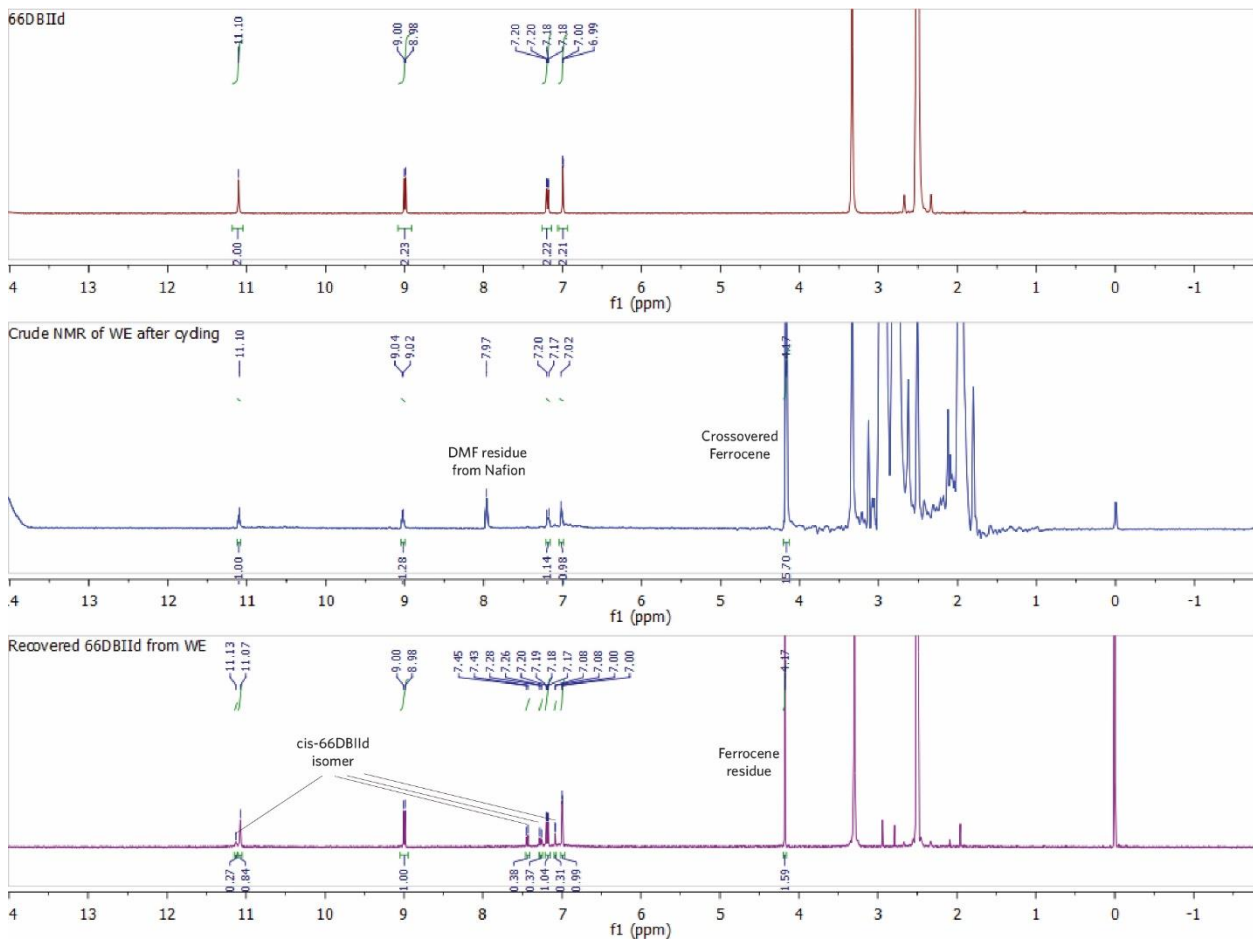
**Supplementary Fig. 32 | Evaluating the performance of 55DBIIId in the flow-based EMCC prototype.** **a**, CO<sub>2</sub> reading at the exit of the sorbent tank and voltage curve over repeating capture/release cycles for ~50 hours of operation. **b**, CO<sub>2</sub> reading of selected capture/release cycles overlaid, with the cumulative amount of CO<sub>2</sub> captured/released in each cycle relative to the theoretical capacity. Lighter colours represent later cycles. The capture, rest, release, and rest steps are indicated by the shaded regions. For CO<sub>2</sub> capture, 55DBIIId was reduced at 10 mA for 60 min followed by a 60 min rest. For CO<sub>2</sub> release, the adducts were oxidised at 10 mA to 0.05 mV followed by a ~120 min constant voltage hold, and finally rested for another 60 min. **c**, The voltage-capacity curve for the 2<sup>nd</sup> capture/release cycle, indicating an energy consumption of 135.2 kJ per mole of CO<sub>2</sub> concentrated. **d**, The CO<sub>2</sub> capacity utilisation efficiency (purple squares), release/capture efficiency (red crosses), and Coulombic efficiency (empty grey squares) of the system. The liquid sorbent was composed of 12 ml 75 mM 55DBIIId slurry in DMAc with 0.25 M NaClO<sub>4</sub> as the supporting salt. On the opposite side, a Fc tank was used to balance the charge, which was filled with 30 ml 0.1 M Fc in DMAc with 0.25 M NaClO<sub>4</sub> as the supporting salt.



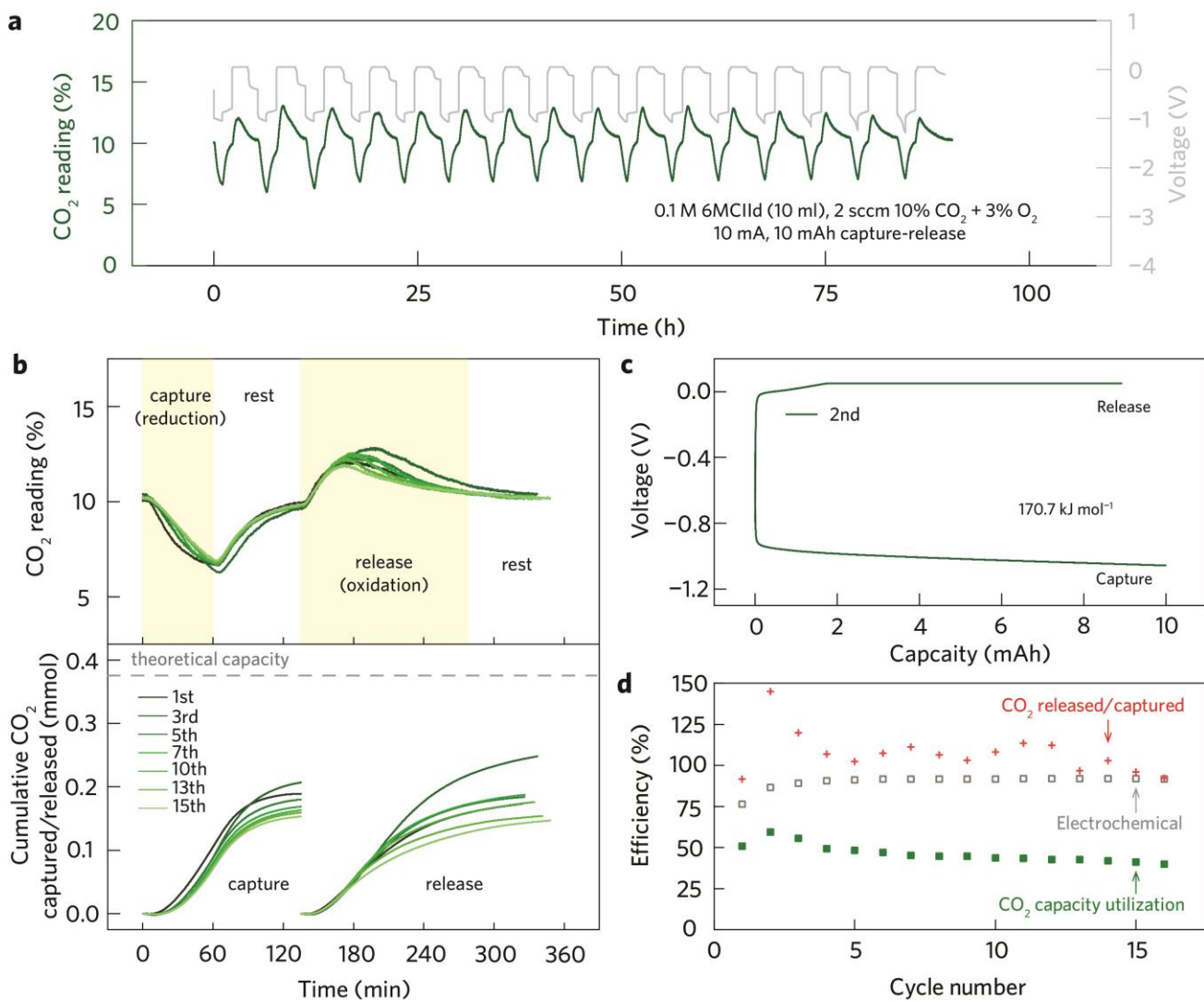
**Supplementary Fig. 33 | Evaluating the performance of 66DBIIId in the flow-based EMCC prototype.** **a**, CO<sub>2</sub> reading at the exit of the sorbent tank and voltage curve over repeating capture/release cycles for ~50 h operation. **b**, The CO<sub>2</sub> reading for selected capture/release cycles overlaid, with the cumulative amount of CO<sub>2</sub> captured/released in each cycle relative to the theoretical capacity. Lighter colours represent later cycles. The capture, rest, release, and rest steps are indicated by the shaded regions. For CO<sub>2</sub> capture, 66DBIIId was reduced at 10 mA for 60 min followed by a 60 min rest. For CO<sub>2</sub> release, the adducts were oxidised at 10 mA to 0.05 mV followed by a ~120 min constant voltage hold, and finally rested for another 60 min. **c**, The voltage-capacity curve for the 2<sup>nd</sup> capture/release cycle, indicating an early-stage energy consumption of 166.9 kJ per mol CO<sub>2</sub> concentrated. **d**, The CO<sub>2</sub> capacity utilisation efficiency (purple squares), release/capture efficiency (red crosses), and Coulombic efficiency (grey empty squares) of the system. The liquid sorbent was composed of 12 ml 75 mM 66DBIIId slurry in DMAc with 0.25 M NaClO<sub>4</sub> as the supporting salt. On the opposite side, a Fc tank was used to balance the charge, which was filled with 30 ml 0.1 M Fc in DMAc with 0.25 M NaClO<sub>4</sub> as the supporting salt.



**Supplementary Fig. 34 | Evaluating the performance of 6B6AIIdSer in the flow-based EMCC prototype.** **a**, CO<sub>2</sub> reading at the exit of the sorbent tank and voltage curve over 43 repeating capture/release cycles for ~190 h operation. **b**, CO<sub>2</sub> reading for selected capture/release cycles overlaid, with the cumulative amount of CO<sub>2</sub> captured/released in each cycle relative to the theoretical capacity. Lighter colours represent later cycles. The capture, rest, release, and rest steps are indicated by the shaded regions. For CO<sub>2</sub> capture, 6B6AIIdSer was reduced at 10 mA for 60 min followed by a 60 min rest. For CO<sub>2</sub> release, the adducts were oxidised at 10 mA to 0.05 mV followed by a ~80 min constant voltage hold, and finally rested for another 60 min. **c**, The voltage-capacity curve for the 2<sup>nd</sup> capture/release cycle, indicating an early-stage energy consumption of 158.6 kJ per mol CO<sub>2</sub> concentrated. **d**, The CO<sub>2</sub> capacity utilisation efficiency (blue squares), release/capture efficiency (red crosses), and electrochemical efficiency (grey empty squares) of the system. The liquid sorbent was composed of 5 ml 0.2 M 6B6AIIdSer in DMF with 0.5 M NaTFSI as the supporting salt. On the opposite side, a Fc tank was used to balance the charge, which was filled with 10 ml 0.22 M Fc in DMF with 0.5 M NaTFSI as the supporting salt, and 10 mM 6B6AIIdSer to mitigate sorbent crossover.

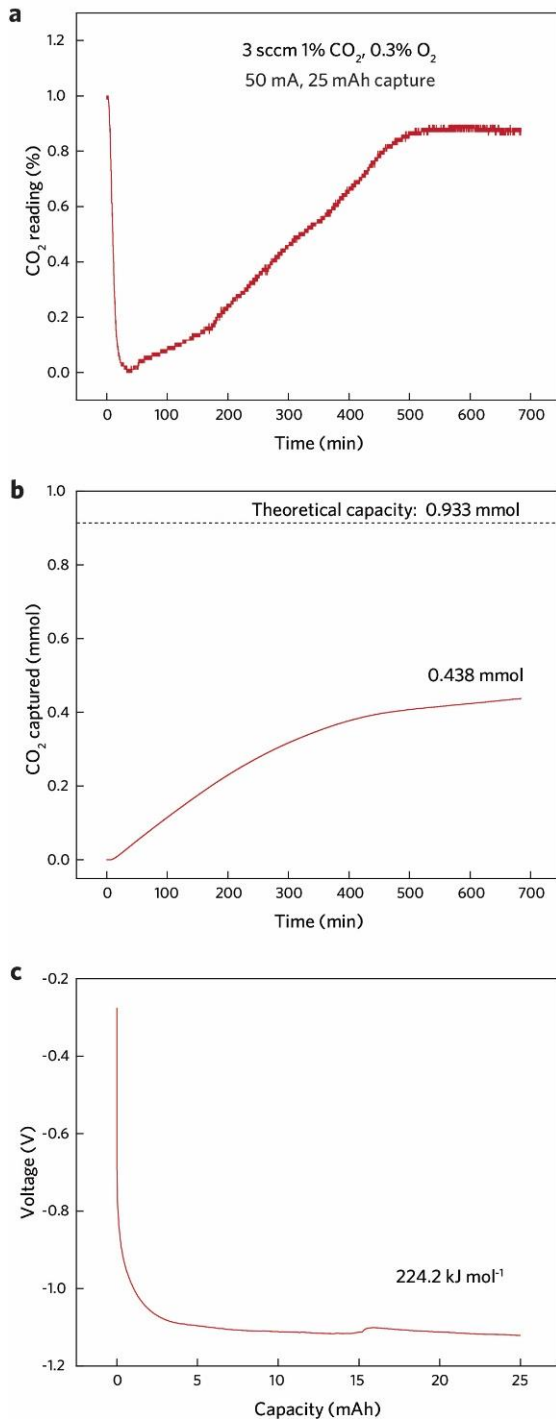


**Supplementary Fig. 35 | NMR analysis of the sorbent electrolyte after CO<sub>2</sub> capture-release cycling of 66DBIID.** The corresponding cycling data are presented in Supplementary Fig. 33. <sup>1</sup>H NMR of 66DBIID (up), crude <sup>1</sup>H NMR of sorbent electrolyte after 11 capture-release cycles (middle), and <sup>1</sup>H NMR of recovered 66DBIID from the sorbent electrolyte.

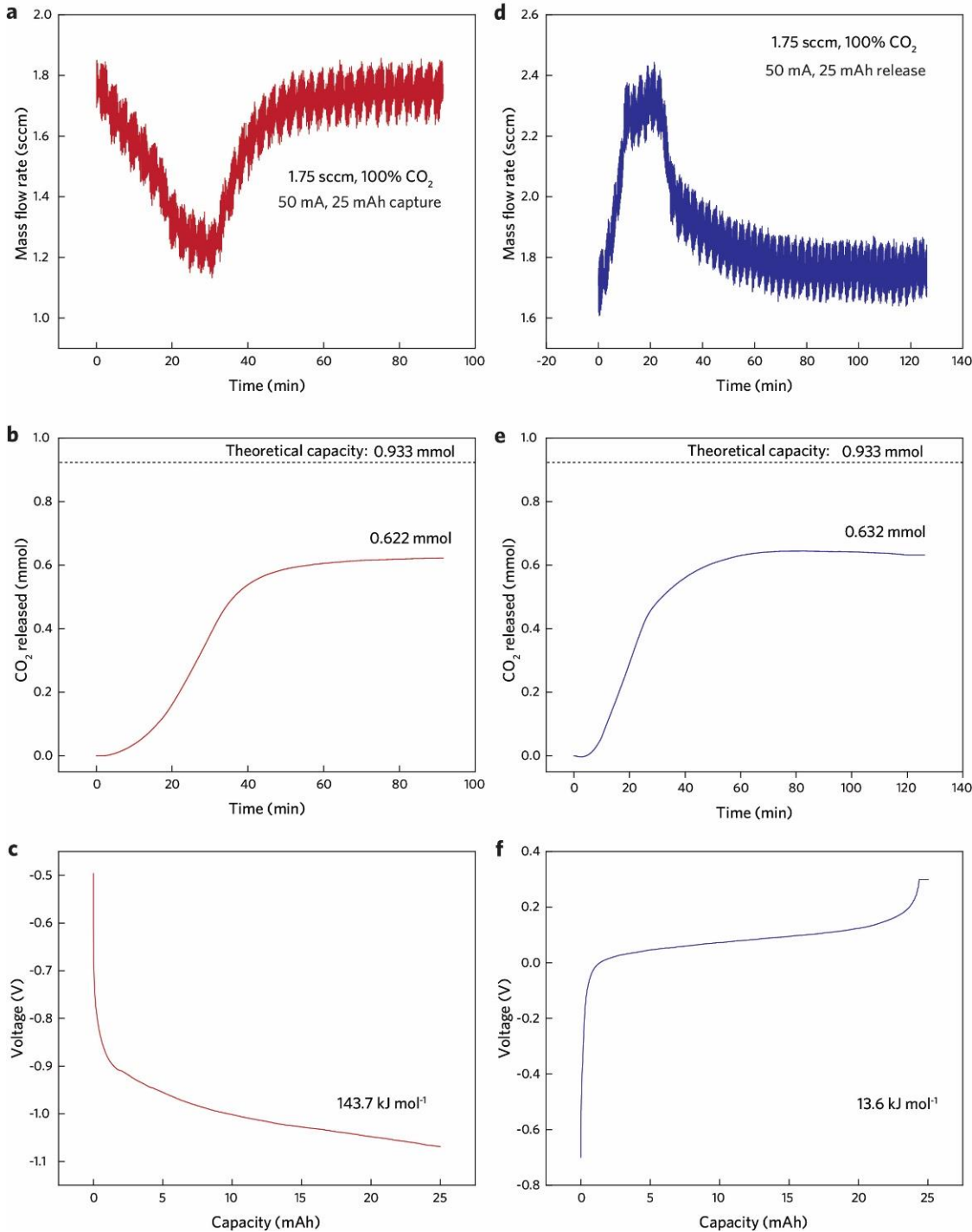


**Supplementary Fig. 36 | Evaluating the performance of 6MCIId in simulated flue gas condition.**

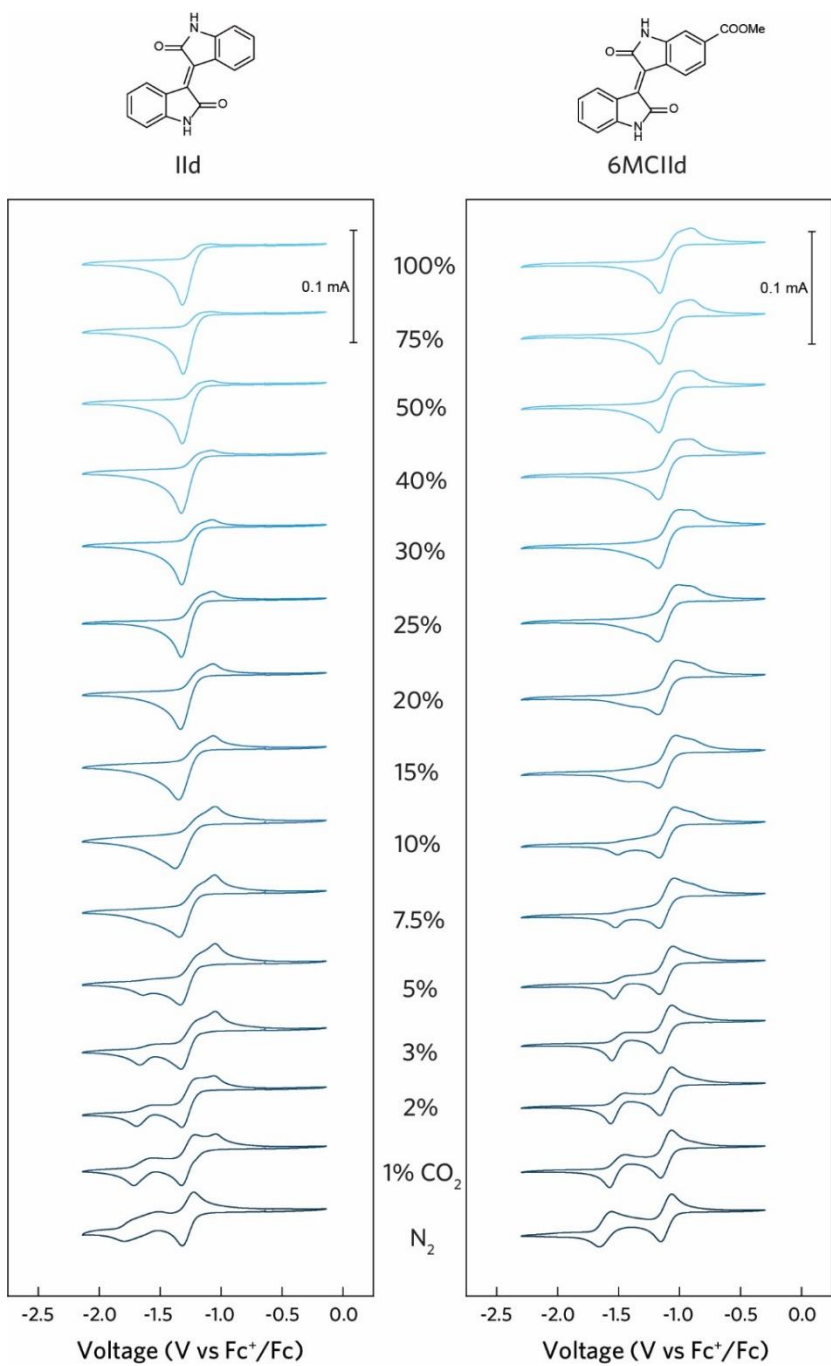
**a**, CO<sub>2</sub> reading at the exit of the sorbent tank and voltage curve over 16 repeating capture/release cycles for ~90 h operation. **b**, CO<sub>2</sub> reading of selected capture/release cycles overlaid, with the cumulative amount of CO<sub>2</sub> captured/released in each cycle relative to the theoretical capacity. Lighter colours represent later cycles. Capture, rest, release, and rest steps are indicated by the shaded regions. For CO<sub>2</sub> capture, 6MCIId was reduced at 10 mA for 60 min followed by a 75 min rest. For CO<sub>2</sub> release, the adducts were oxidised at 10 mA to 0.05 mV followed by a ~120 min constant voltage hold, and finally rested for another 75 min. **c**, The voltage-capacity curve for the 2<sup>nd</sup> capture/release cycle, indicating an energy consumption of 170.7 kJ per mole of CO<sub>2</sub> concentrated. **d**, The CO<sub>2</sub> capacity utilisation efficiency (green squares), release/capture efficiency (red crosses), and electrochemical efficiency (empty grey squares) of the system. The liquid sorbent was composed of 10 ml 0.1 M 6MCIId in DMF with 0.5 M NaTFSI as the supporting salt. The sorbent tank was filled with plastic beads and purged with 10% CO<sub>2</sub> and 3% O<sub>2</sub> balanced in N<sub>2</sub> at a flow rate of 2 sccm. On the opposite side, a Fc tank was used to balance the charge, which was filled with 20 ml 0.1 M Fc in DMF with 0.5 M NaTFSI as the supporting salt, 4 mM FcBF<sub>4</sub> to facilitate Fc oxidation, and 10 mM 6MCIId to mitigate sorbent crossover.



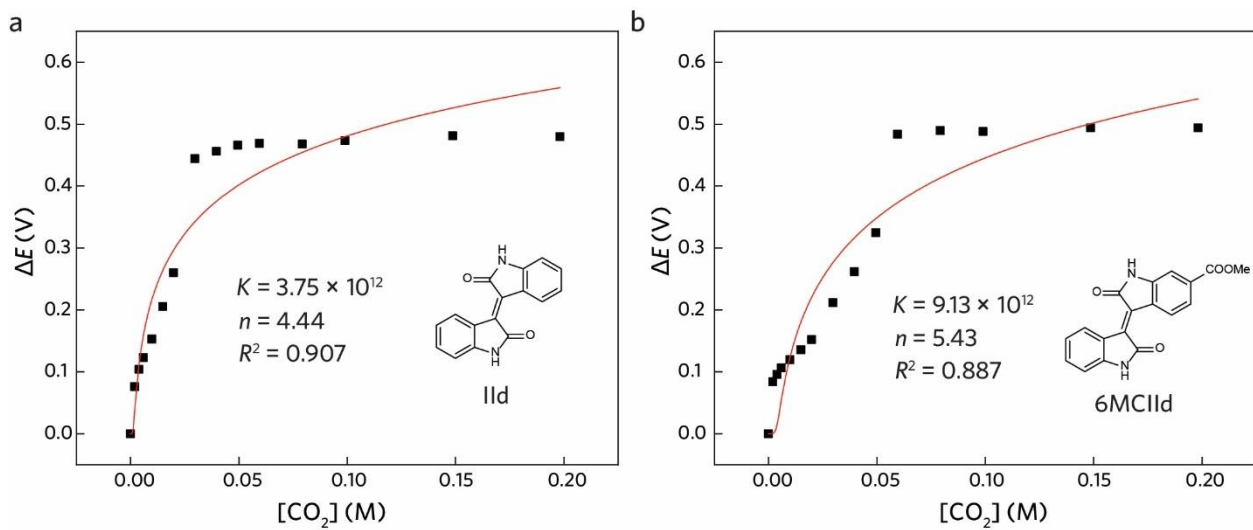
**Supplementary Fig. 37 | Evaluating CO<sub>2</sub> capture performance of 6MCIId in flow-based EMCC prototype with low-concentration CO<sub>2</sub> feed.** 3 sccm 1% CO<sub>2</sub> with 0.3% O<sub>2</sub> was used as the feed gas. **a**, CO<sub>2</sub> reading from an IR-based sensor at the exit of the sorbent tank. **b**, Cumulative amount of CO<sub>2</sub> captured over time. **c**, The voltage-capacity curve of the capture process, indicating an early-stage energy consumption of 224.2 kJ per mole of CO<sub>2</sub> captured. The area of the flow field and the carbon paper electrode was 25 cm<sup>2</sup>. The liquid sorbent was composed of 10 ml 0.25 M 6MCIId in DMF with 0.5 M NaTFSI as the supporting salt. On the opposite side, a Fc tank was used to balance the charge, which was filled with 20 ml 0.25 M Fc in DMF with 0.5 M NaTFSI as the supporting salt and 12.5 mM 6MCIId to mitigate sorbent crossover. We observed faster redox molecule crossover in this system as the membrane area was increased from 5 to 25 cm<sup>2</sup>, resulting in lower CO<sub>2</sub> capacity utilization efficiency.



**Supplementary Fig. 38 | Evaluating CO<sub>2</sub> capture-release performance of 6MCIId in flow-based EMCC prototype under 100% CO<sub>2</sub>.** **a** and **d**, CO<sub>2</sub> flow rate on a mass flow metre at the exit of the sorbent tank. **b** and **e**, Cumulative amount of CO<sub>2</sub> captured and released over time, respectively. **c** and **f**, The voltage-capacity curve of the capture and release process, indicating an early-stage energy consumption of 143.7 kJ per mole of CO<sub>2</sub> captured and 13.6 kJ per mole of CO<sub>2</sub> released, respectively. The area of the flow field and the carbon paper electrode was 25 cm<sup>2</sup>. The liquid sorbent was composed of 10 ml 0.25 M 6MCIId in DMF with 0.5 M NaTFSI as the supporting salt. On the opposite side, a Fc tank was used to balance the charge, which was filled with 20 ml 0.25 M Fc in DMF with 0.5 M NaTFSI as the supporting salt and 12.5 mM 6MCIId to mitigate sorbent crossover.



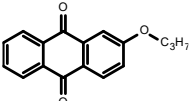
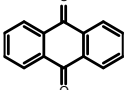
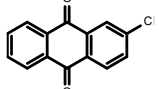
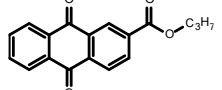
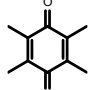
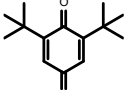
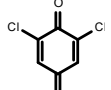
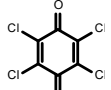
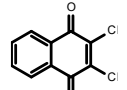
**Supplementary Fig. 39 | CV of IId and 6MCIIId under different concentrations of  $\text{CO}_2$ . a, IId. b, 6MCIIId.** The CV curves were recorded using 2.5 mM compound in anhydrous DMF with 0.1 M  $\text{NBu}_4\text{PF}_6$  at a scan rate of  $-50 \text{ mV s}^{-1}$ .



**Supplementary Fig. 40 |** Shifts in second reduction peak potentials ( $\Delta E_{\text{peak}(2)}$ ) in the presence of various concentrations of  $CO_2$  calculated using data from Response Fig. 1, and corresponding fitted values of  $n$  and  $CO_2$  binding constant  $K$ . **a**, IIId. **b**, 6MCIIId.

## Supplementary Tables

**Supplementary Table 1** | A summary of existing redox-active quinone sorbents with their redox potentials (V vs.  $\text{Fc}^+/\text{Fc}$ ) and  $\text{CO}_2$  binding constants in DMF<sup>1</sup>.

Quinoids	$E_{1/2} (\mathbf{1})^{\text{A}}$ in $\text{CO}_2$ (V)	$E_{1/2} (\mathbf{2})^{\text{B}}$ in $\text{N}_2$ (V)	$E_{1/2} (\mathbf{2})$ in $\text{CO}_2$ (V)	$\log K_{\text{CO}_2}$	
AQ-O-C3H7		-1.55	-2.2	-1.55	11.70
AQ		-1.4	-2.15	-1.4	13.39
AQ-Cl		-1.25	-2	-1.88	2.73
AQ-COO-C3H7		-1.29	-2	-1.89	2.56
BQ		-0.95	-1.98	-0.95	18.12
DBQ		-1.39	-2.39	-1.39	17.61
TBQ		-1.25	-2.29	-1.25	18.29
BQ-Cl2		-0.7	-1.66	-1.59	1.86
BQ-Cl4		-0.48	-1.42	-1.38	1.28
p-NQ		-1.23	-2.06	-1.23	14.74
p-NQ-Cl2		-0.9	-1.75	-1.63	2.73

<sup>A</sup> The first half-wave potential. <sup>B</sup> The second half-wave potential cathodic to the first one.

**Supplementary Table 2** | Summary of key parameters of isoindigo sorbents including their redox properties, <sup>1</sup>H NMR, and optical band gap.

	Substituents	E <sub>1/2</sub> in N <sub>2</sub> (V) <sup>A</sup>	E <sub>1/2</sub> in CO <sub>2</sub> (V) <sup>A</sup>	ΔE <sub>peak(2)</sub> <sup>B</sup> (V)	K <sub>CO<sub>2</sub></sub> (M <sup>-1</sup> )	log K <sub>CO<sub>2</sub></sub>	<sup>1</sup> H NMR (H <sup>a</sup> , H <sup>a'</sup> ) (ppm)	<sup>1</sup> H NMR (H <sup>b</sup> , H <sup>b'</sup> ) (ppm)	Optical band gap (eV)
6CIIIdNa	6-COONa	-1.33, -1.49	-1.14	0.301	6.11E+05	5.79	9.05, 8.93	10.84	2.03
IIId	-	-1.29, -1.79	-1.21	0.511	2.19E+09	9.34	9.06	10.89	2.04
55DMIIId	5,5'-OMe	-1.29, -1.76	-1.2	0.494	1.13E+09	9.05	8.85	10.69	1.78
NNDEHIId	N,N'-2-ethylhexyl	-1.23, -1.80	-1.16, -1.45	0.350	4.19E+06	6.62	9.1	N.A.	2.00
6BIIId	6-Br	-1.21, -1.75	-1.14	0.538	6.25E+09	9.8	9.04, 9.00	10.95, 11.06	2.05
5BIIId	5-Br	-1.19, -1.67	-1.11	0.494	1.12E+09	9.05	9.07, 9.31	10.96, 11.05	2.04
6AIIdSer	6-methyl serinate	-1.18, -1.60	-1.08	0.46	2.57E+08	8.41	9.07, 9.11	10.94, 11.12	2.04
6AIIdGly	6-methyl glycinate	-1.17, -1.62	-1.08	0.469	4.30E+08	8.63	9.08, 9.12	10.94, 11.12	2.04
55DFIId	5,5'-F	-1.14, -1.69	-1.13	0.547	9.13E+09	9.96	9.00	11.02	1.97
66DBIIId	6,6'-Br	-1.14, -1.67	-1.12	0.525	3.88E+04	9.59	8.99	11.1	2.06
6MCIIId	6-COOMe	-1.12, -1.62	-1.09	0.484	7.78E+08	8.89	9.07, 9.15	10.94, 11.08	2.03
6B6AIIdSer	6-Br-6'-methyl serinate	-1.11, -1.55	-1.11	0.475	5.41E+08	8.73	9.02, 9.11	11.09, 11.16	2.03
5566TFIId	5,5',6,6'-F	-1.10, -1.68	-1.1	0.570	2.17E+10	10.3	9.21	11.2	2.02
55DBIIId	5,5-Br	-1.09, -1.61	-1.09	0.510	2.16E+09	9.33	9.32	11.11	1.99
6CIIId	6-COOH	-1.09, -1.35	-1.06, -1.18	0.129	7.50E+02	2.87	9.07, 9.13	10.93, 11.05	2.01
5NIIId	5-NO <sub>2</sub>	-1.08, -1.57	-1.08	0.484	7.63E+08	8.88	9.08, 10.12	11.03, 11.63	2.07
5M5NIIId	5-OMe-5'-NO <sub>2</sub>	-1.08, -1.55	-1.08	0.470	4.45E+08	8.65	8.83, 10.14	10.84, 11.61	1.71
NNDPPr66DBIIId	N,N'-Pr-6,6'-Br	-1.07, -1.61	-1.08, -1.34	0.247	7.48E+04	4.48	9.05	N.A.	2.02
6B6MCIIId	6-Br-6-COOMe	-1.05, -1.55	-1.05	0.486	8.34E+08	8.92	9.02, 9.14	11.09, 11.12	2.02
66DMCIIId	6,6'-COOME	-0.97, -1.41	-0.91	0.435	1.17E+08	8.07	9.17	11.18	2.02
5N6MCIIId	5-NO <sub>2</sub> -6-COOMe	-0.93, -1.40	-0.94, -1.15	0.232	4.15E+04	4.62	9.15, 10.10	11.22, 11.68	2.08

<sup>A</sup>Fc<sup>+</sup>/Fc is used as the internal reference. <sup>B</sup>ΔE<sub>peak(2)</sub> was calculated based on the difference between the second reduction peak potentials (IIId<sup>•-</sup>/IIId<sup>2-</sup>) in CO<sub>2</sub> and N<sub>2</sub>.

**Supplementary Table 3** | Reaction rate constant for the first CO<sub>2</sub> binding using different isoindigo sorbents. Isoindigo (5 mM) in DMF using 0.1 M NBu<sub>4</sub>PF<sub>6</sub> as the supporting salt.

Isoindigo sorbent	<i>k<sub>bimolecular</sub></i> (M <sup>-1</sup> s <sup>-1</sup> )	<i>k<sub>f</sub></i> (s <sup>-1</sup> ) (20% CO <sub>2</sub> )
6MCIIId	22.45	0.889
6AIIdGly	19.85	0.786
66DBIID	18.64	0.738
NNDPr66DBIID	3.31	0.131

**Supplementary Table 4** | Comparison between the DFT-simulated 1<sup>st</sup> electron-transfer redox potentials (V vs. Fc<sup>+</sup>/Fc) and experimental 1<sup>st</sup> half-wave potentials in N<sub>2</sub> (V vs. Fc<sup>+</sup>/Fc) of various isoindigos.

Isoindigo sorbent	Theoretical (V)	Experimental (V)
IIId	-1.102	-1.29
5BIIId	-1.100	-1.19
66DBIIId	-1.058	-1.14
55DBIIId	-1.006	-1.09

**Supplementary Table 5** | DFT-calculated CO<sub>2</sub> binding energies of IIId<sup>•-</sup> ( $E_{\text{b}1}$ ) and [IIId-CO<sub>2</sub>]<sup>•-</sup> ( $E_{\text{b}2}$ ).

	$E_{\text{b}1}$ (eV)	$E_{\text{b}2}$ (eV)	Theoretical $\log K_{\text{CO}_2}$ <sup>A</sup>	Experimental $\log K_{\text{CO}_2}$
IIId	0.08	0.50	9.18	9.34
55DMIId	0.08	0.49	9.03	9.05
55DBIID	0.20	0.43	9.98	9.33
5BIIId	0.23	0.50	11.56	9.05
66DBIID	0.20	0.45	10.29	9.59
NNDPr66DBIID	0.07	0.35	6.65	4.48

<sup>A</sup>Theoretical  $\log K_{\text{CO}_2}$  was calculated using the equation,  $\log K_{\text{CO}_2} = \frac{E_{\text{b}1} + E_{\text{b}2}}{RT \ln 10}$ , where  $R$  is the ideal gas constant and  $T$  is the room temperature of 298 K.

**Supplementary Table 6 |** Solubilities of various isoindigos in DMF.

Isoindigo sorbent	Solubility in DMF (mM)
IIId	230
55DBIId	6.3
66DMCIIId	<2.5
6MCIIId	515
6AIIdGly	606
6AIIdSer	830
6B6AIIdSer	568

## **Supplementary Methods**

### **Materials and Methods**

Unless otherwise stated, all the chemicals were purchased from commercial sources and used without further purification.

### **Nuclear Magnetic Resonance Spectroscopy (NMR)**

NMR spectra were collected on a Bruker AMX400 (400 MHz) spectrometer. Chemical shifts were reported in parts per million (ppm). Residual solvent peak was used as an internal reference.

### **Low-Resolution Electrospray Ionisation Mass Spectroscopy (Low-Res ESI-MS)**

Low-res ESI-MS was recorded on a Thermo Scientific LCQ Fleet Ion trap Mass spectrometer.

### **High-Resolution ESI Quadrupole Time of Flight (Q-TOF) MS**

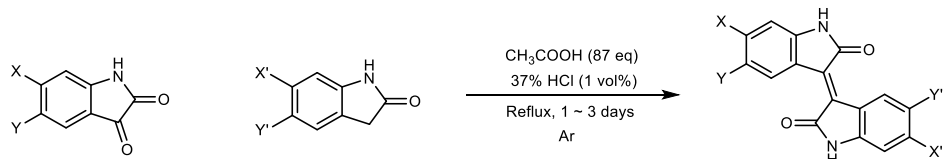
Analysis was performed using the Bruker compact Q-TOF-MS in negative ion mode using the ESI ionization source. Tuning and mass calibration was performed prior to running client samples, using 10 mM sodium formate. Mass spectra for the sample were collected from m/z 50-3000, at a rate of one spectrum per sec over a span of 30 seconds.

### **Ultraviolet-visible (UV-vis) Spectroscopy**

UV-vis absorption spectra were recorded on a Thermo Scientific Genesys 10S UV-vis spectrophotometer.

## Synthesis of isoindigos

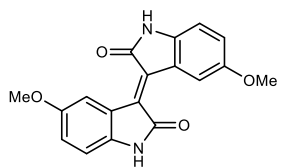
### General synthetic procedure for isoindigos:



**Supplementary Fig. 41 |** Synthesis of isoindigos.

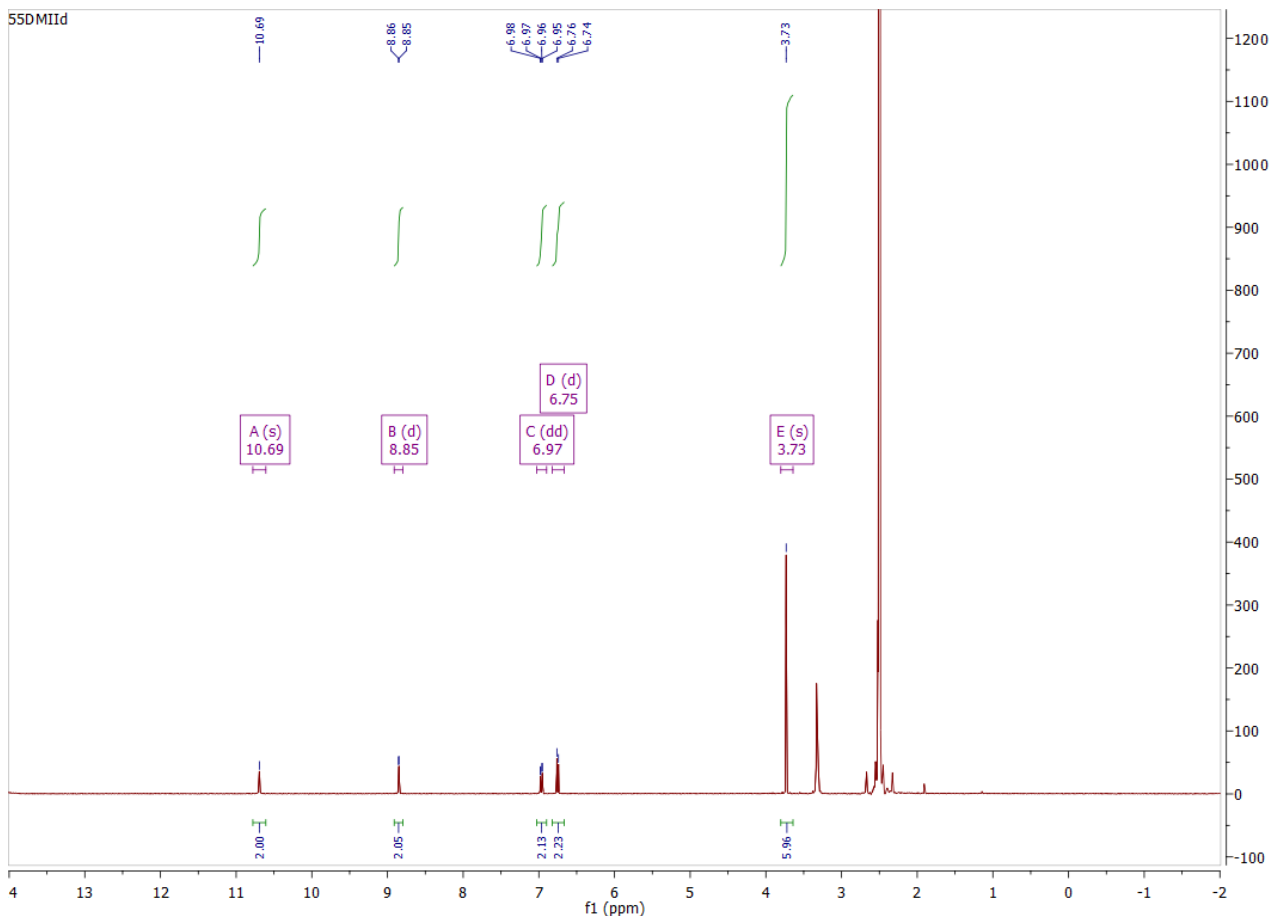
To a mixture of isatin (1.106 ~20 mmol, 1.0 equiv) and 2-oxindole (1.106~20 mmol, 1.0 equiv) in acetic acid (~87 equiv) was added 37% HCl solution (1 vol% of acetic acid). The suspension was heated at reflux for 1 to 3 days under Ar atmosphere before being cooled to room temperature (most reactions were completed in 1 day except for those substrates with strong electron-withdrawing groups which required further reaction time). The mixture was filtered and washed with copious water, ethanol, and ethyl acetate (EA). The product was dried in the vacuum oven at 60 °C for 15 h to afford the desired isoindigos in 50~97% yield.

**5,5'-Dimethoxylisoindigo (55DMIId):**



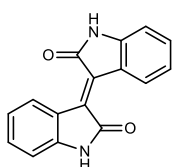
**Supplementary Fig. 42 |** Chemical structure of 55DMIId.

The target was synthesised by the general procedure starting with 5-methoxyisatin (209 mg, 1.18 mmol) and 5-methoxy-2-oxindole (192.6 mg, 1.18 mmol) in a day to afford the desired product (324 mg, 85%).  $^1\text{H}$  NMR (400 MHz, DMSO)  $\delta$  10.69 (s, 2H), 8.85 (d,  $J$  = 2.6 Hz, 2H), 6.97 (dd,  $J$  = 8.5, 2.7 Hz, 2H), 6.75 (d,  $J$  = 8.5 Hz, 2H), 3.73 (s, 6H).



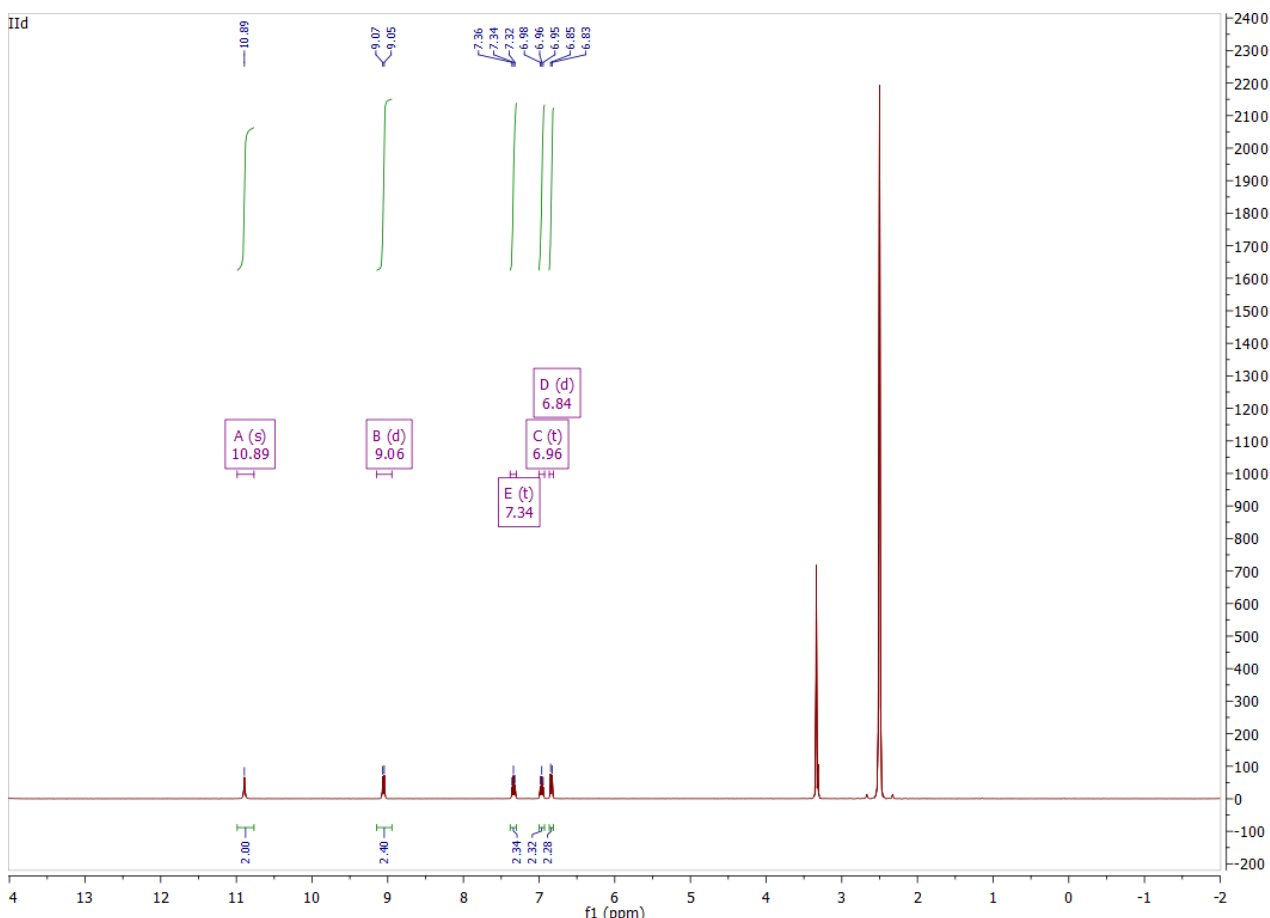
**Supplementary Fig. 43 |**  $^1\text{H}$  NMR spectra of 55DMIId.

**Isoindigo (IId):**

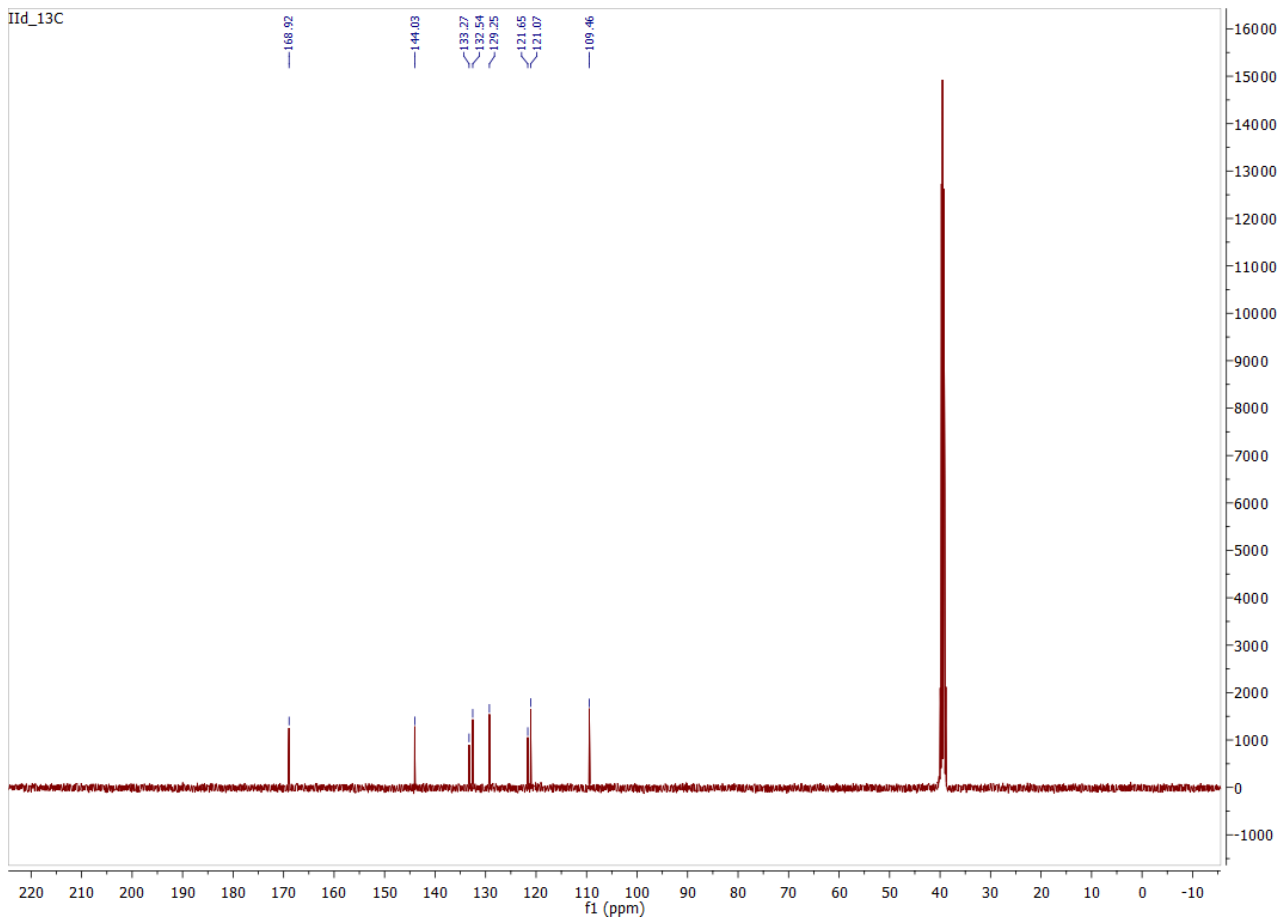


**Supplementary Fig. 44 |** Chemical structure of IId.

The target was synthesised by the general procedure starting with isatin (2.94 g, 20 mmol) and 2-oxindole (2.66 g, 20 mmol) in a day to afford the desired product (5.01 g, 96%).  $^1\text{H}$  NMR (400 MHz, DMSO)  $\delta$  10.89 (s, 2H), 9.06 (d,  $J$  = 7.9 Hz, 2H), 7.34 (t,  $J$  = 7.6 Hz, 2H), 6.96 (t,  $J$  = 7.8 Hz, 2H), 6.84 (d,  $J$  = 7.7 Hz, 2H).  $^{13}\text{C}$  NMR (101 MHz, DMSO)  $\delta$  168.92, 144.03, 133.27, 132.54, 129.25, 121.65, 121.07, 109.46.

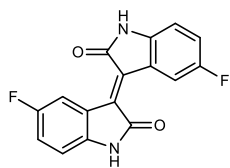


**Supplementary Fig. 45 |**  $^1\text{H}$  NMR spectra of IId.



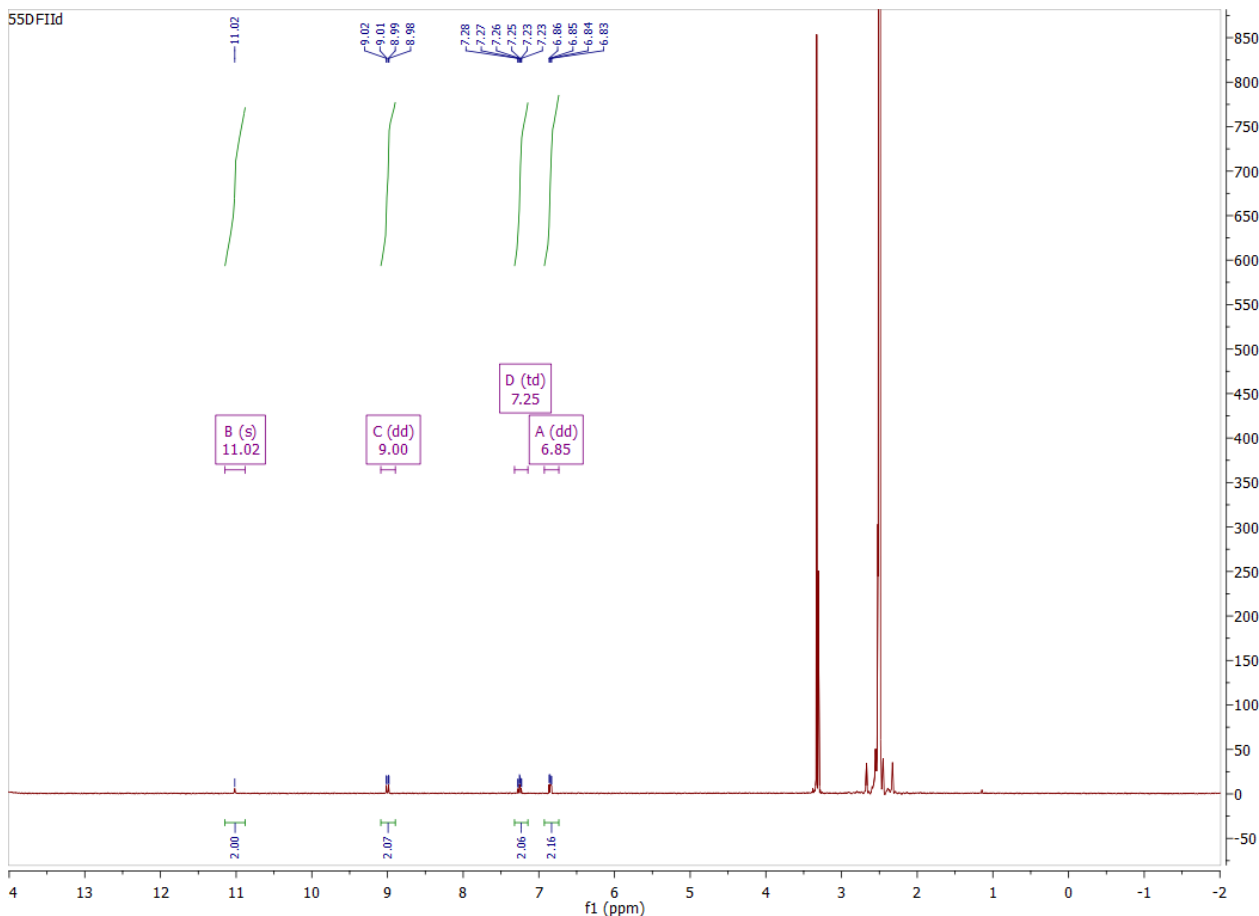
**Supplementary Fig. 46 |**  $^{13}\text{C}$  NMR spectra of IId.

**5,5'-Difluoroisoindigo (55DFIID):**



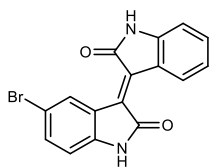
**Supplementary Fig. 47 |** Chemical structure of 55DFIID.

The target was synthesised by the general procedure starting with 5-fluoroisatin (195 mg, 1.18 mmol) and 5-fluoro-2-oxindole (178.3 mg, 1.18 mmol) in a day to afford the desired product (177 mg, 50%).  $^1\text{H}$  NMR (400 MHz, DMSO)  $\delta$  11.02 (s, 2H), 9.00 (dd,  $J = 11.4, 2.7$  Hz, 2H), 7.25 (td,  $J = 8.7, 2.8$  Hz, 2H), 6.85 (dd,  $J = 8.6, 4.9$  Hz, 2H).



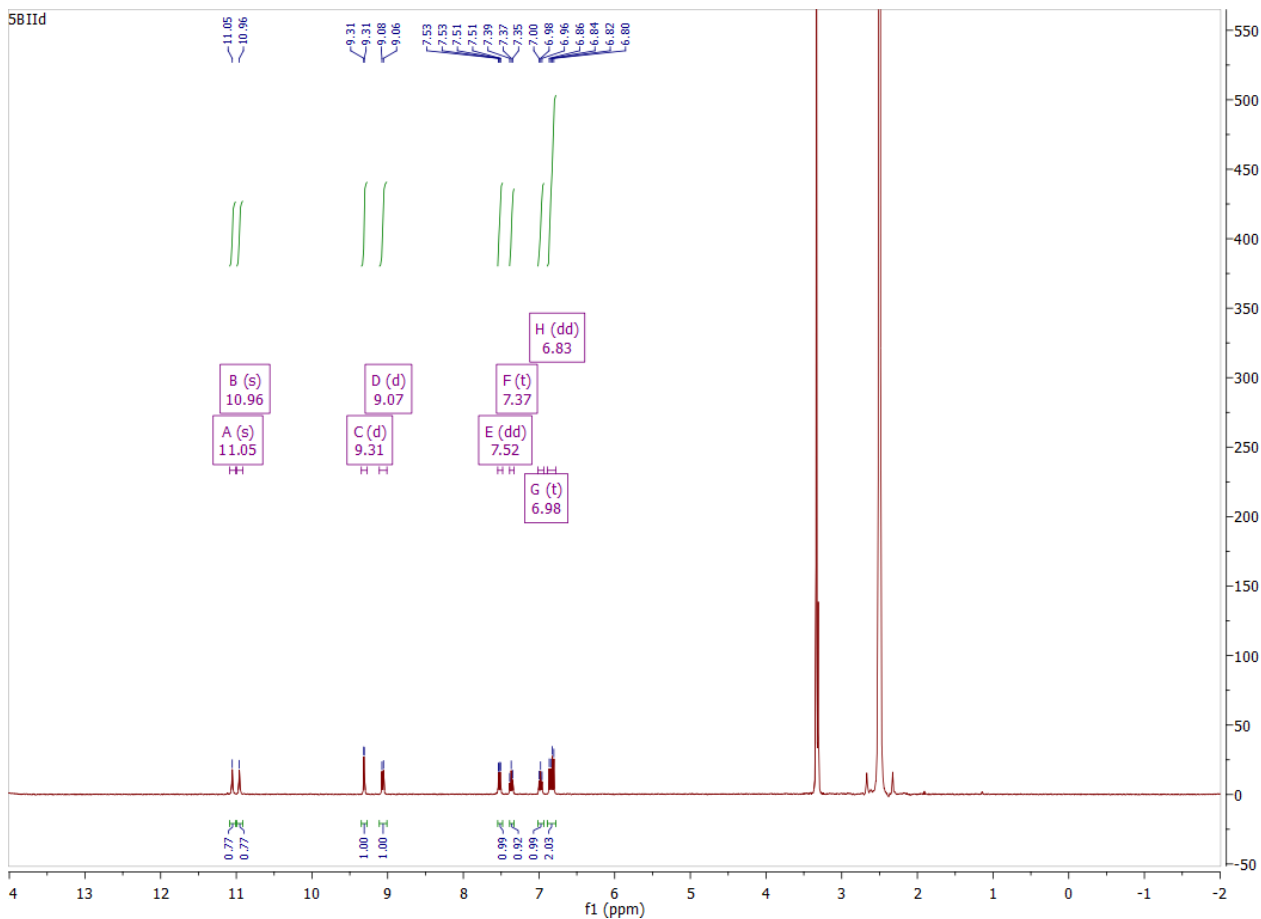
**Supplementary Fig. 48 |**  $^1\text{H}$  NMR spectra of 55DFIID.

**5-Bromoisoindigo (5BIId):**



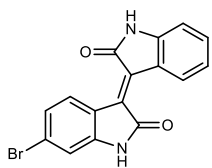
**Supplementary Fig. 49 |** Chemical structure of 5BIId.

The target was synthesised by the general procedure starting with isatin (323.7 mg, 2.2 mmol) and 5-bromo-2-oxindole (466.5 mg, 2.2 mmol) in a day to afford the desired product (691 mg, 92%).  $^1\text{H}$  NMR (400 MHz, DMSO)  $\delta$  11.05 (s, 1H), 10.96 (s, 1H), 9.31 (d,  $J$  = 1.8 Hz, 1H), 9.07 (d,  $J$  = 8.0 Hz, 1H), 7.52 (dd,  $J$  = 8.3, 2.0 Hz, 1H), 7.37 (t,  $J$  = 7.6 Hz, 1H), 6.98 (t,  $J$  = 7.8 Hz, 1H), 6.83 (dd,  $J$  = 16.1, 8.0 Hz, 2H).



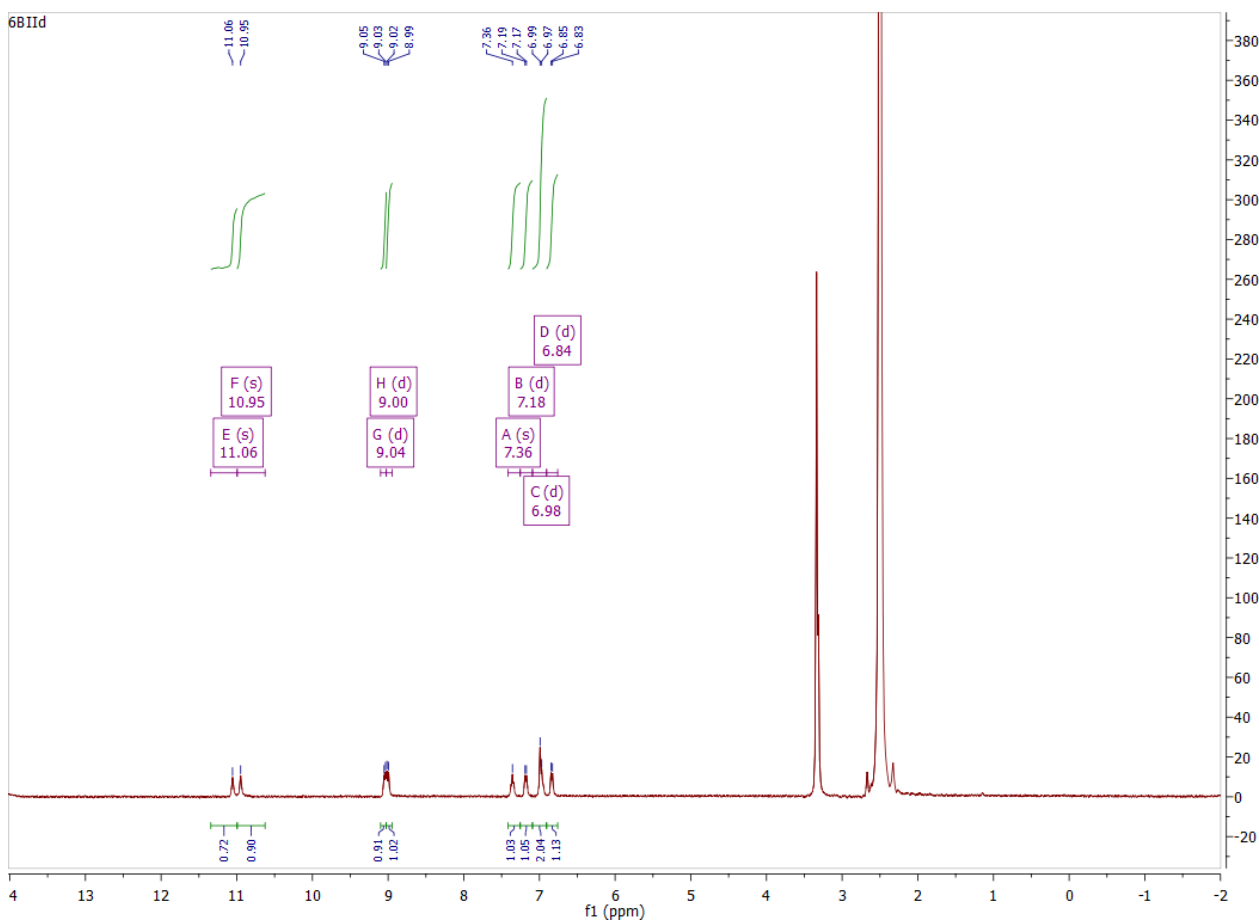
**Supplementary Fig. 50 |**  $^1\text{H}$  NMR spectra of 5BIId.

**6-Bromoisoindigo (6BIId):**



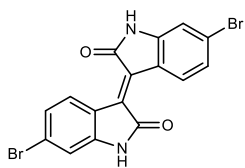
**Supplementary Fig. 51 |** Chemical structure of 6BIId.

The target was synthesised by the general procedure starting with 6-bromoisatin (250 mg, 1.106 mmol) and 2-oxindole (147 mg, 1.106 mmol) in a day to afford the desired product (261 mg, 69%).  $^1\text{H}$  NMR (400 MHz, DMSO)  $\delta$  11.06 (s, 1H), 10.95 (s, 1H), 9.04 (d,  $J$  = 7.2 Hz, 1H), 9.00 (d,  $J$  = 8.9 Hz, 1H), 7.36 (s, 1H), 7.18 (d,  $J$  = 7.1 Hz, 1H), 6.98 (d,  $J$  = 8.6 Hz, 2H), 6.84 (d,  $J$  = 7.5 Hz, 1H).



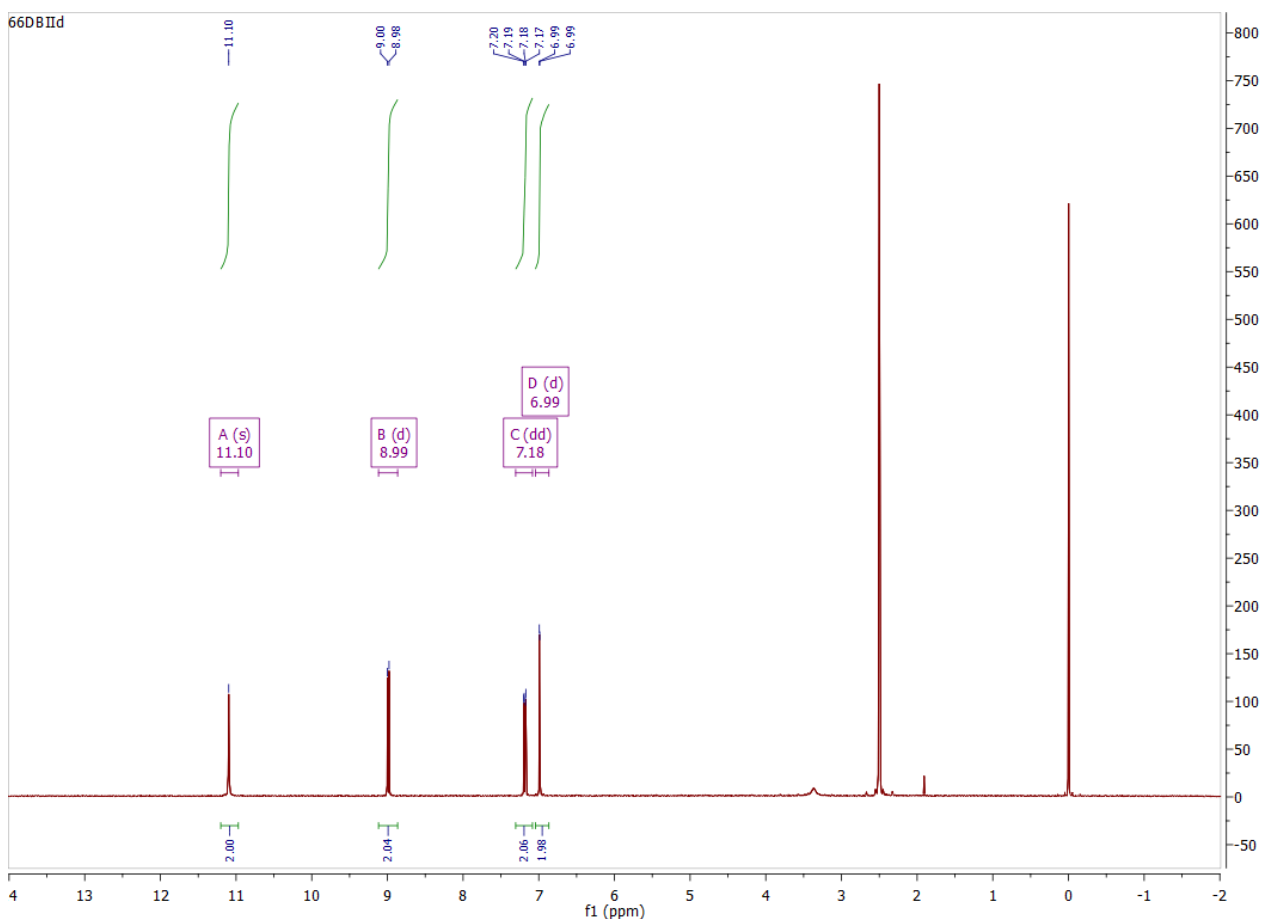
**Supplementary Fig. 52 |**  $^1\text{H}$  NMR spectra of 6BIId.

**6,6'-Dibromoisoindigo (66DBIID):**



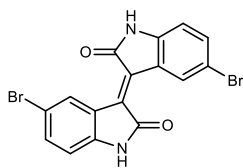
**Supplementary Fig. 53 |** Chemical structure of 66DBIID.

The target was synthesised by the general procedure starting with 6-bromoisatin (533 mg, 2.36 mmol) and 6-bromo-2-oxindole (500 mg, 2.36 mmol) in a day to afford the desired product (776 mg, 78%).  $^1\text{H}$  NMR (400 MHz, DMSO)  $\delta$  11.10 (s, 2H), 8.99 (d,  $J$  = 8.7 Hz, 2H), 7.18 (dd,  $J$  = 8.7, 2.0 Hz, 2H), 6.99 (d,  $J$  = 2.0 Hz, 2H).



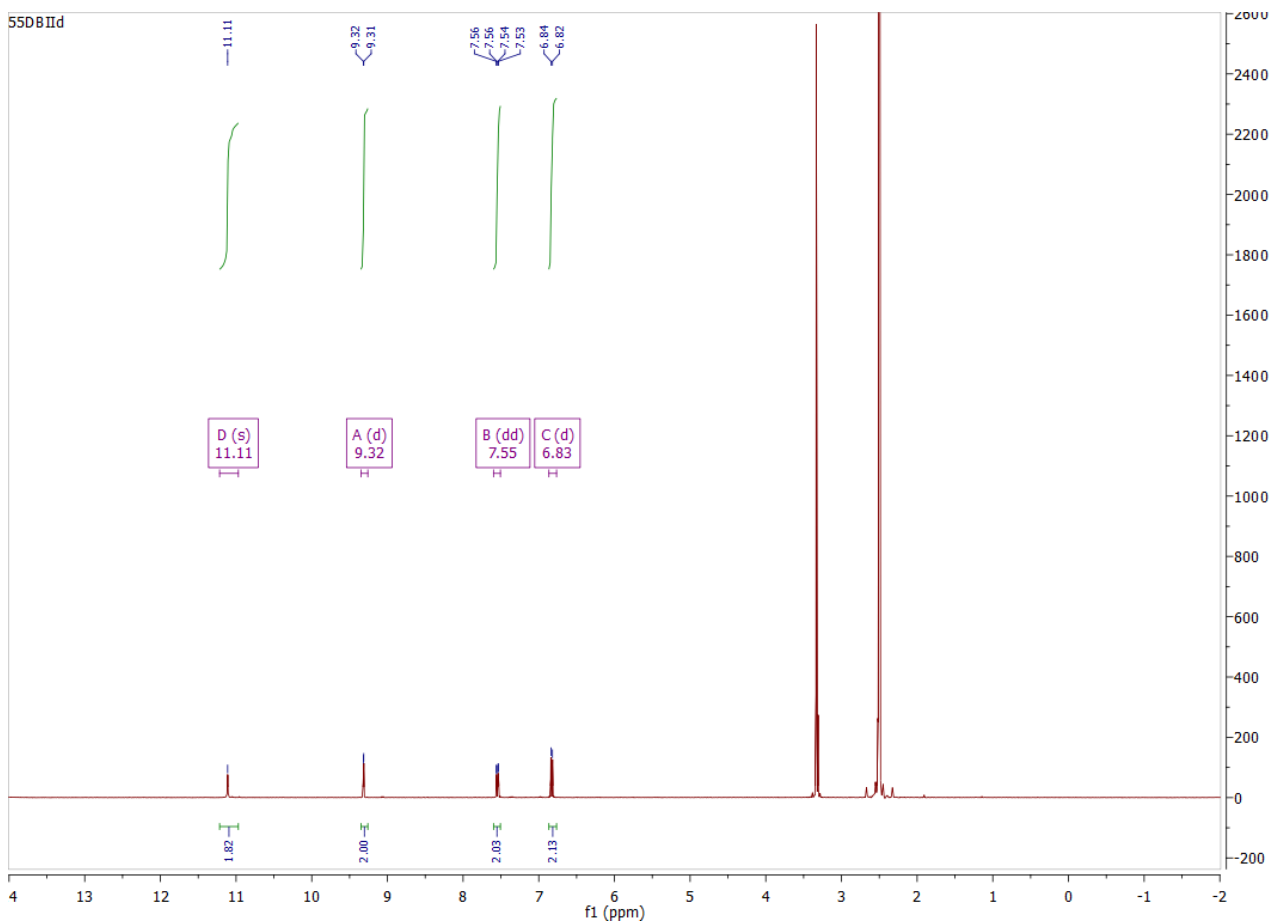
**Supplementary Fig. 54 |**  $^1\text{H}$  NMR spectra of 66DBIID.

**5,5'-Dibromoisoindigo (55DBIID):**



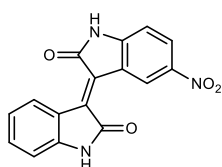
**Supplementary Fig. 55 |** Chemical structure of 55DBIID.

The target was synthesised by the general procedure starting with 5-bromoisatin (2.132 g, 9.44 mmol) and 5-bromo-2-oxindole (2 g, 9.44 mmol) in a day to afford the desired product (3.87, 97%).  $^1\text{H}$  NMR (400 MHz, DMSO)  $\delta$  11.11 (s, 2H), 9.32 (d,  $J$  = 2.0 Hz, 2H), 7.55 (dd,  $J$  = 8.3, 2.1 Hz, 2H), 6.83 (d,  $J$  = 8.3 Hz, 2H).



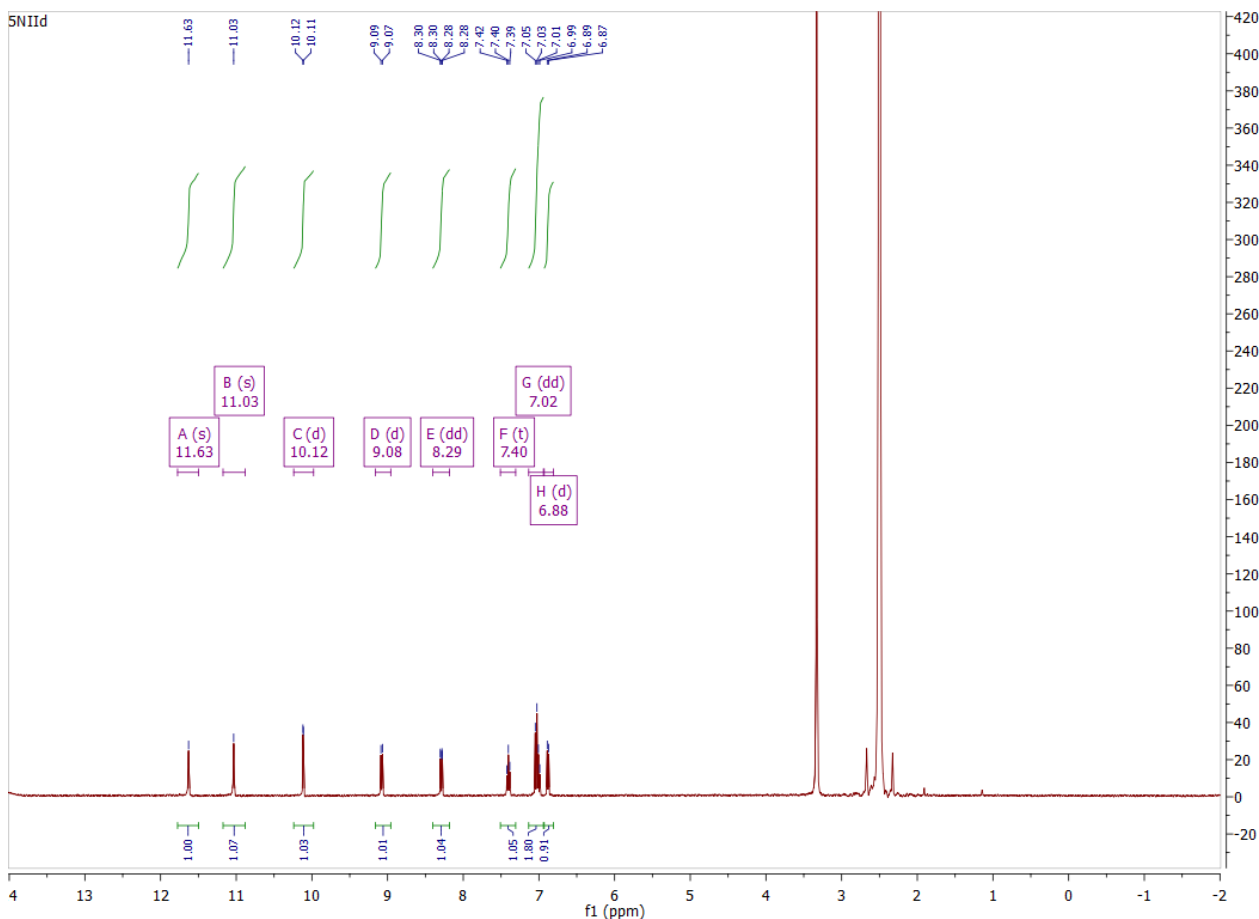
**Supplementary Fig. 56 |**  $^1\text{H}$  NMR spectra of 55DBIID.

**5-Nitroisoindigo (5NIId):**



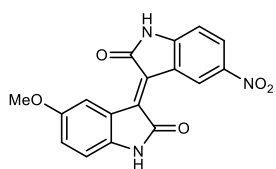
**Supplementary Fig. 57 |** Chemical structure of 5NIId.

The target was synthesised by the general procedure starting with 5-nitroisatin (227 mg, 1.18 mmol) and 2-oxindole (157.1 mg, 1.18 mmol) in three days to afford the desired product (339 mg, 93%).  $^1\text{H}$  NMR (400 MHz, DMSO)  $\delta$  11.63 (s, 1H), 11.03 (s, 1H), 10.12 (d,  $J$  = 2.3 Hz, 1H), 9.08 (d,  $J$  = 8.1 Hz, 1H), 8.29 (dd,  $J$  = 8.7, 2.4 Hz, 1H), 7.40 (t,  $J$  = 7.6 Hz, 1H), 7.02 (dd,  $J$  = 15.7, 8.0 Hz, 2H), 6.88 (d,  $J$  = 7.6 Hz, 1H).



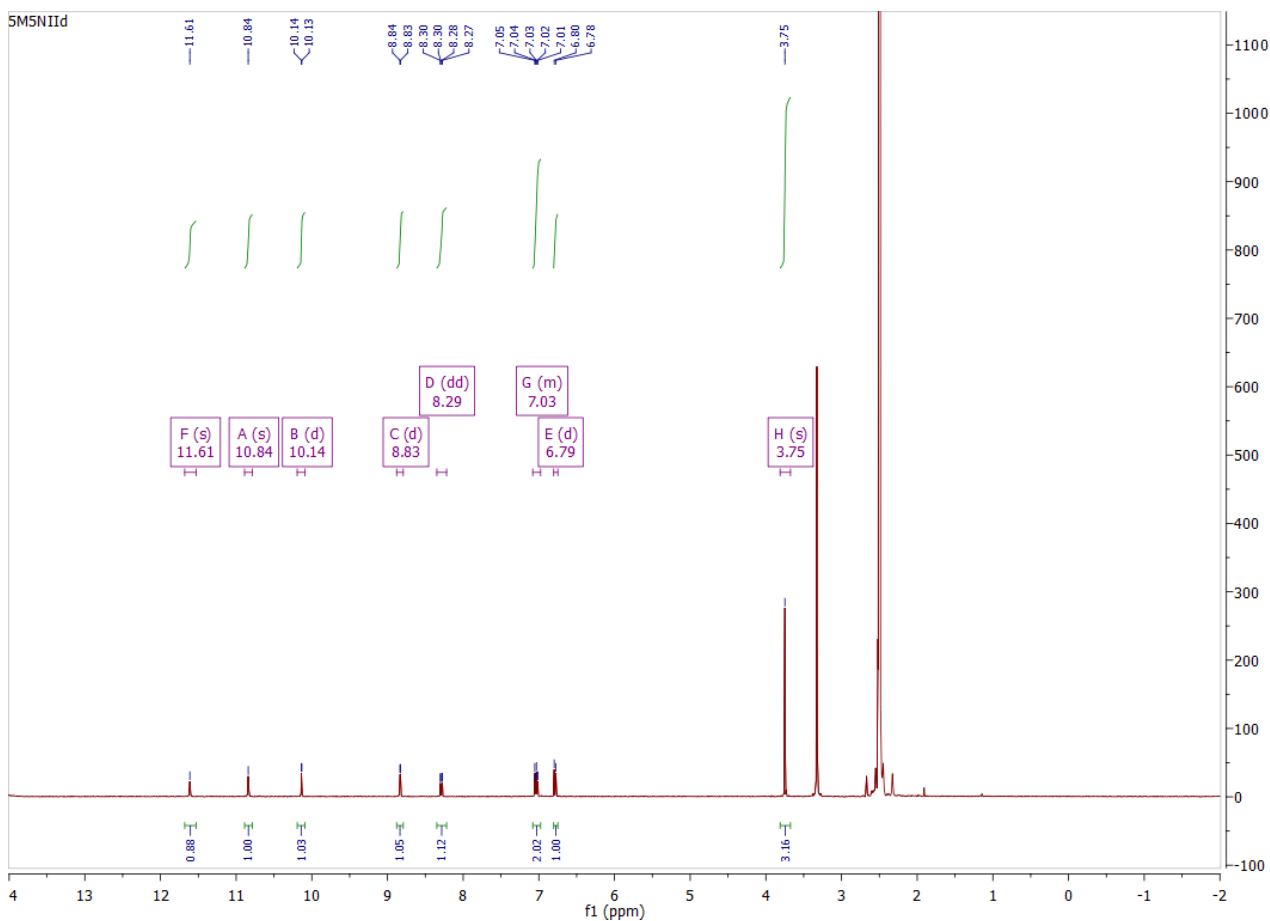
**Supplementary Fig. 58 |**  $^1\text{H}$  NMR spectra of 5NIId.

**5-Methoxyl-5'-nitroisoindigo (5M5NIIId):**

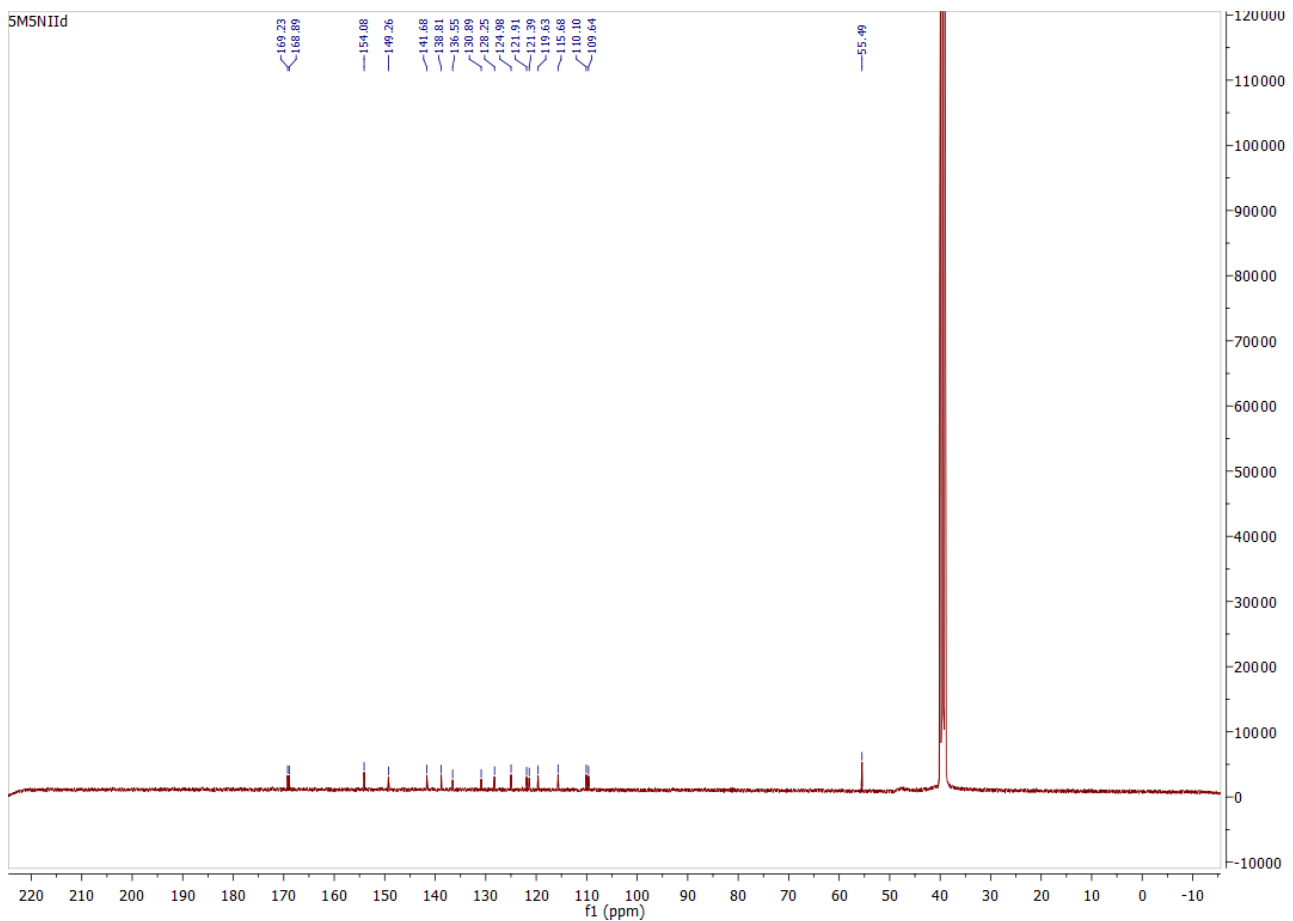


**Supplementary Fig. 59 |** Chemical structure of 5M5NIIId.

The target was synthesised by the general procedure starting with 5-nitroisatin (227 mg, 1.18 mmol) and 5-methoxy-2-oxindole (192.6 mg, 1.18 mmol) in three days to afford the desired product (309 mg, 78%).  $^1\text{H}$  NMR (400 MHz, DMSO)  $\delta$  11.61 (s, 1H), 10.84 (s, 1H), 10.14 (d,  $J$  = 2.3 Hz, 1H), 8.83 (d,  $J$  = 2.6 Hz, 1H), 8.29 (dd,  $J$  = 8.7, 2.4 Hz, 1H), 7.08 – 6.98 (m, 2H), 6.79 (d,  $J$  = 8.5 Hz, 1H), 3.75 (s, 3H).  $^{13}\text{C}$  NMR (101 MHz, DMSO)  $\delta$  169.23, 168.89, 154.08, 149.26, 141.68, 138.81, 136.55, 130.89, 128.25, 124.98, 121.91, 121.39, 119.63, 115.68, 110.10, 109.64, 55.49. Low-res ESI-MS ( $m/z$ ): [M-H]<sup>-</sup> calcd. for C<sub>17</sub>H<sub>10</sub>N<sub>3</sub>O<sub>5</sub>, 336; found, 336.

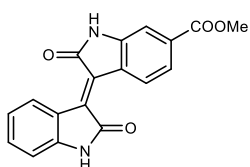


**Supplementary Fig. 60 |**  $^1\text{H}$  NMR spectra of 5M5NIIId.



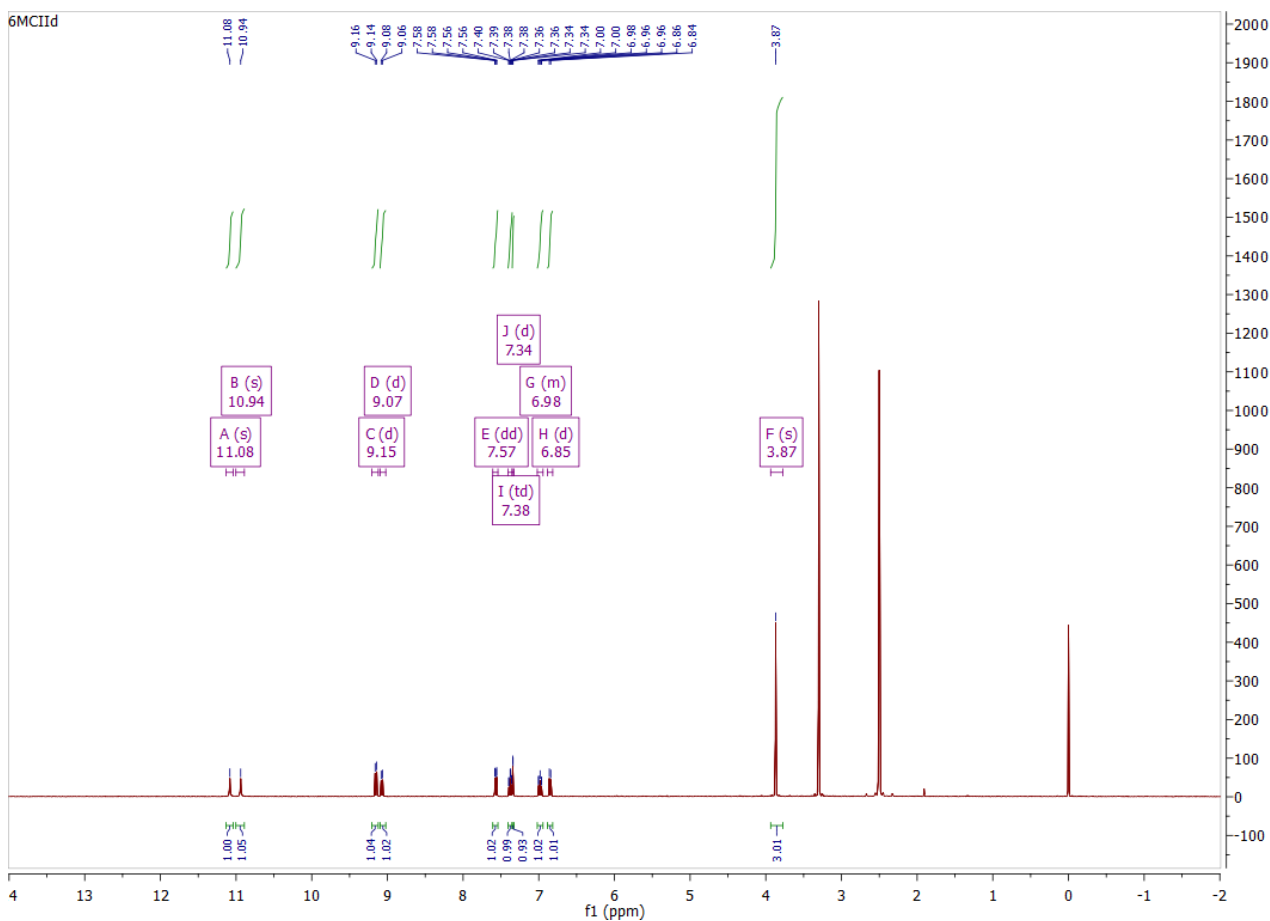
**Supplementary Fig. 61 |**  $^{13}\text{C}$  NMR spectra of 5M5NIId.

**Methyl isoindigo-6-carboxylate (6MCIIId):**

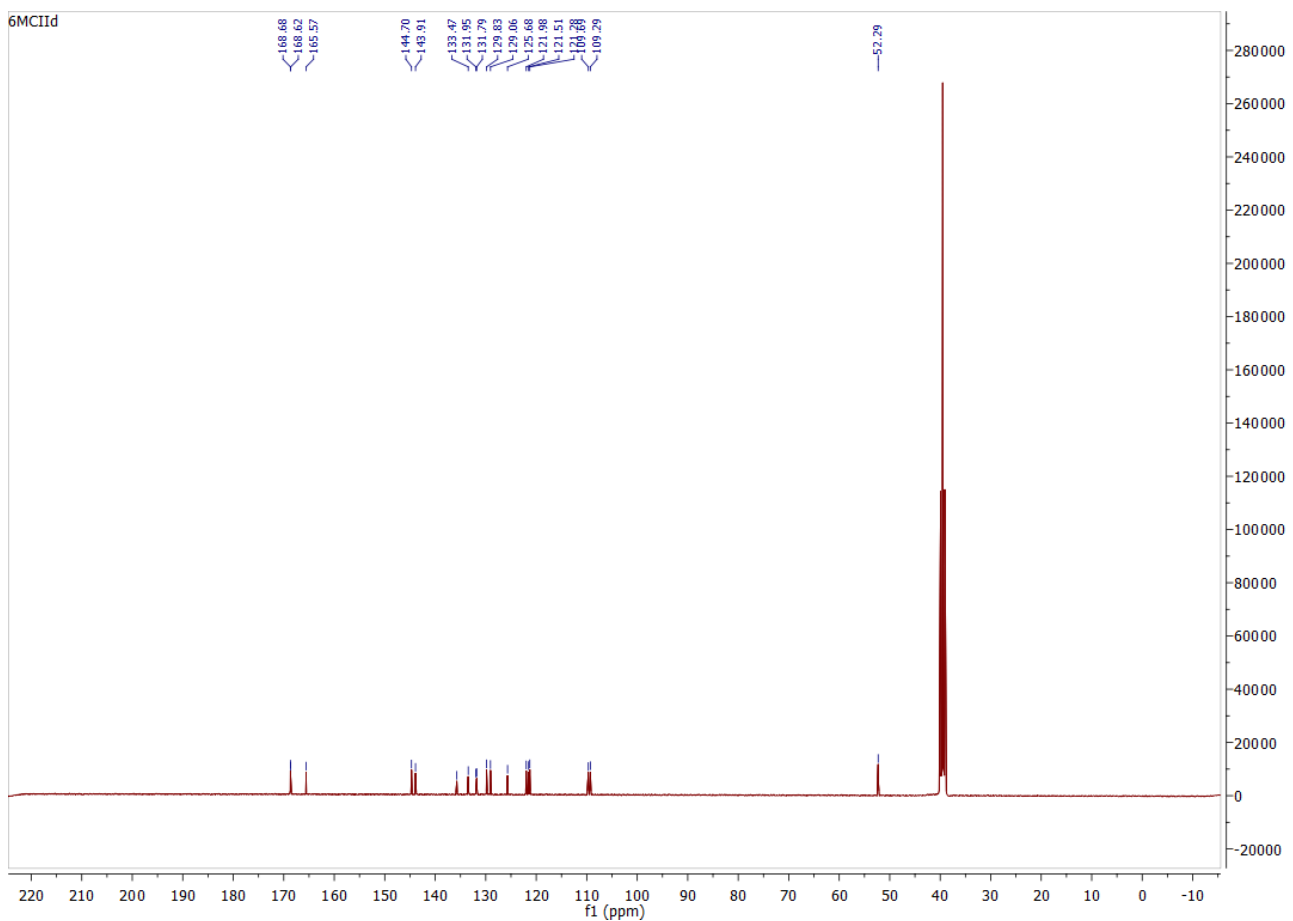


**Supplementary Fig. 62 |** Chemical structure of 6MCIIId.

The target was synthesised by the general procedure starting with isatin (1.47 g, 10 mmol) and methyl 2-oxindole-6-carboxylate (1.91 g, 10 mmol) in a day to afford the desired product (2.93 g, 92%).  $^1\text{H}$  NMR (400 MHz, DMSO)  $\delta$  11.08 (s, 1H), 10.94 (s, 1H), 9.15 (d,  $J$  = 8.4 Hz, 1H), 9.07 (d,  $J$  = 8.0 Hz, 1H), 7.57 (dd,  $J$  = 8.4, 1.7 Hz, 1H), 7.38 (td,  $J$  = 7.7, 1.2 Hz, 1H), 7.34 (d,  $J$  = 1.6 Hz, 1H), 7.02 – 6.94 (m, 1H), 6.85 (d,  $J$  = 7.3 Hz, 1H), 3.87 (s, 3H).  $^{13}\text{C}$  NMR (101 MHz, DMSO)  $\delta$  168.68, 168.62, 165.57, 144.70, 143.91, 135.73, 133.47, 131.95, 131.79, 129.83, 129.06, 125.68, 121.98, 121.51, 121.28, 109.69, 109.29, 52.29. Low-res ESI-MS ( $m/z$ ): [M–H] $^-$  calcd. for  $\text{C}_{18}\text{H}_{11}\text{N}_2\text{O}_4$ , 319; found, 319.

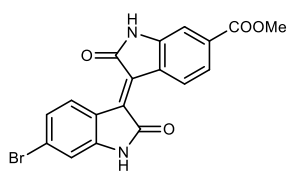


**Supplementary Fig. 63 |**  $^1\text{H}$  NMR spectra of 6MCIIId.



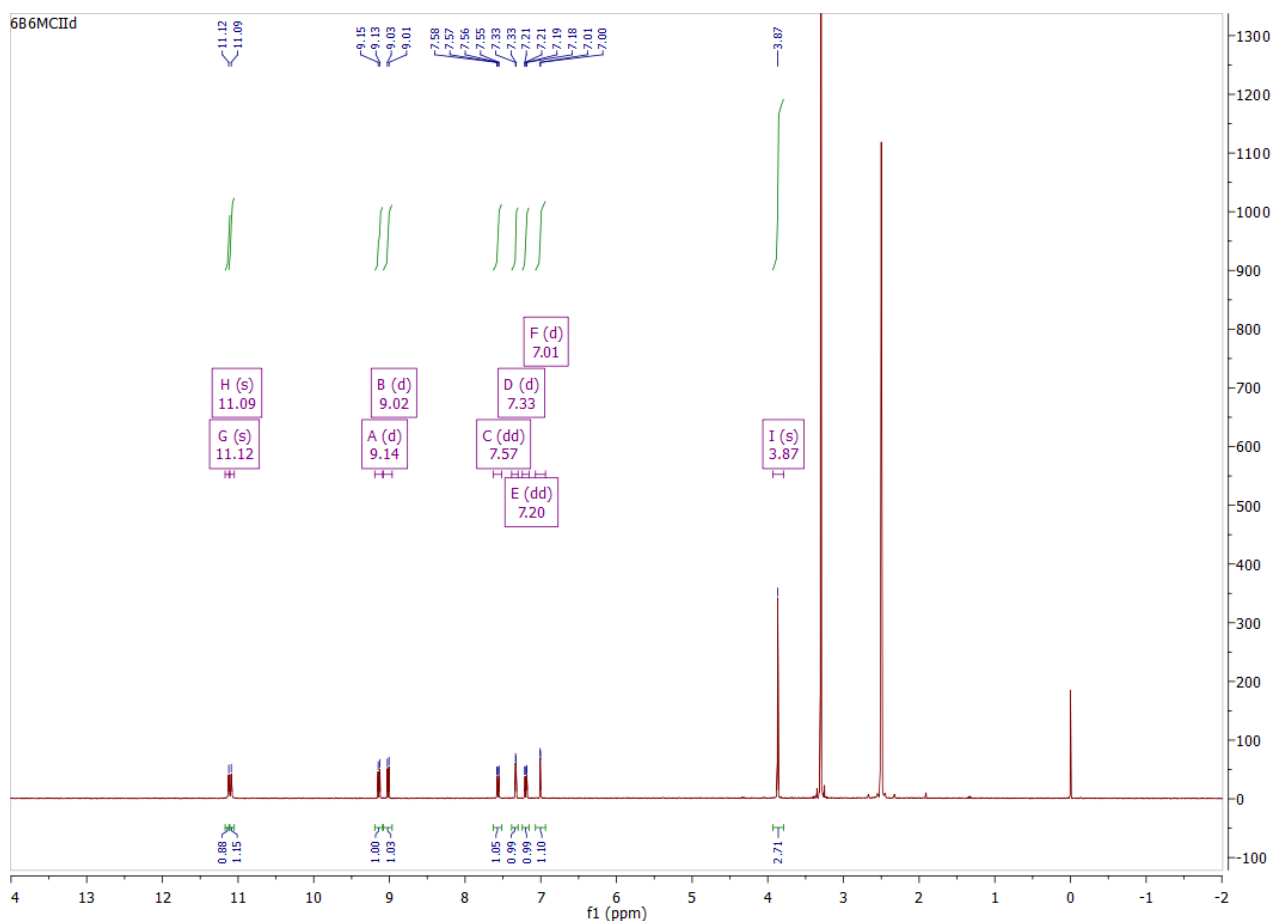
**Supplementary Fig. 64 |**  $^{13}\text{C}$  NMR spectra of 6MCIIId.

**Methyl 6-bromoisoindigo-6'-carboxylate (6B6MCIId):**

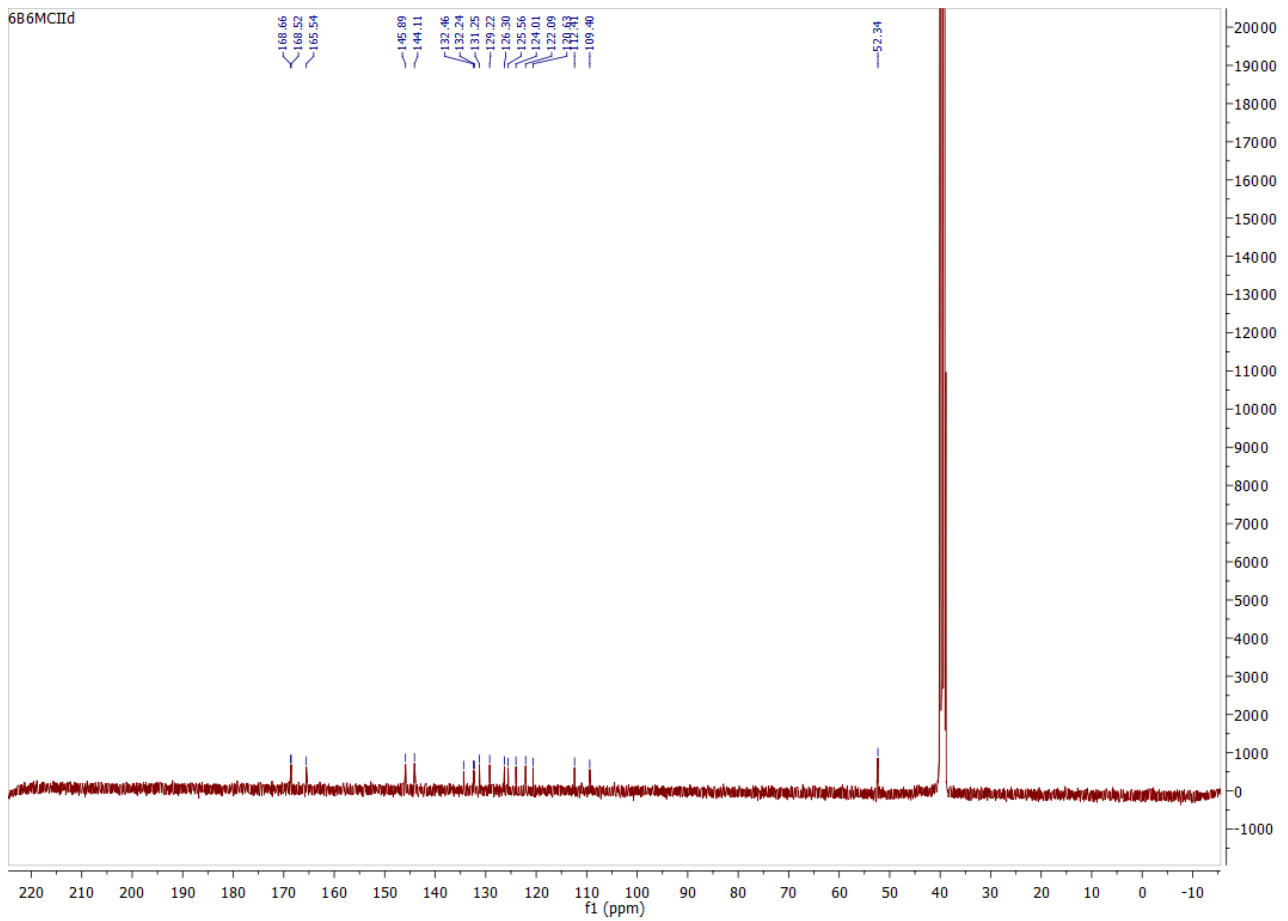


**Supplementary Fig. 65 |** Chemical structure of 6B6MCIId.

The target was synthesised by the general procedure starting with 6-bromoisoindigo (1.13 g, 5 mmol) and methyl 2-oxindole-6-carboxylate (956 mg, 5 mmol) in a day to afford the desired product (1.74 g, 87%).  $^1\text{H}$  NMR (400 MHz, DMSO)  $\delta$  11.12 (s, 1H), 11.09 (s, 1H), 9.14 (d,  $J$  = 8.4 Hz, 1H), 9.02 (d,  $J$  = 8.7 Hz, 1H), 7.57 (dd,  $J$  = 8.4, 1.7 Hz, 1H), 7.33 (d,  $J$  = 1.6 Hz, 1H), 7.20 (dd,  $J$  = 8.7, 2.0 Hz, 1H), 7.01 (d,  $J$  = 2.0 Hz, 1H), 3.87 (s, 3H).  $^{13}\text{C}$  NMR (101 MHz, DMSO)  $\delta$  168.66, 168.52, 165.54, 145.89, 144.11, 134.37, 132.46, 132.24, 131.25, 129.22, 126.30, 125.56, 124.01, 122.09, 120.63, 112.41, 109.40, 52.34. Low-res ESI-MS ( $m/z$ ): [M-H] $^-$  calcd. for  $\text{C}_{18}\text{H}_{10}\text{BrN}_2\text{O}_4$ , 397; found, 397.

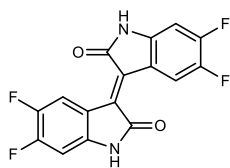


**Supplementary Fig. 66 |**  $^1\text{H}$  NMR spectra of 6B6MCIId.



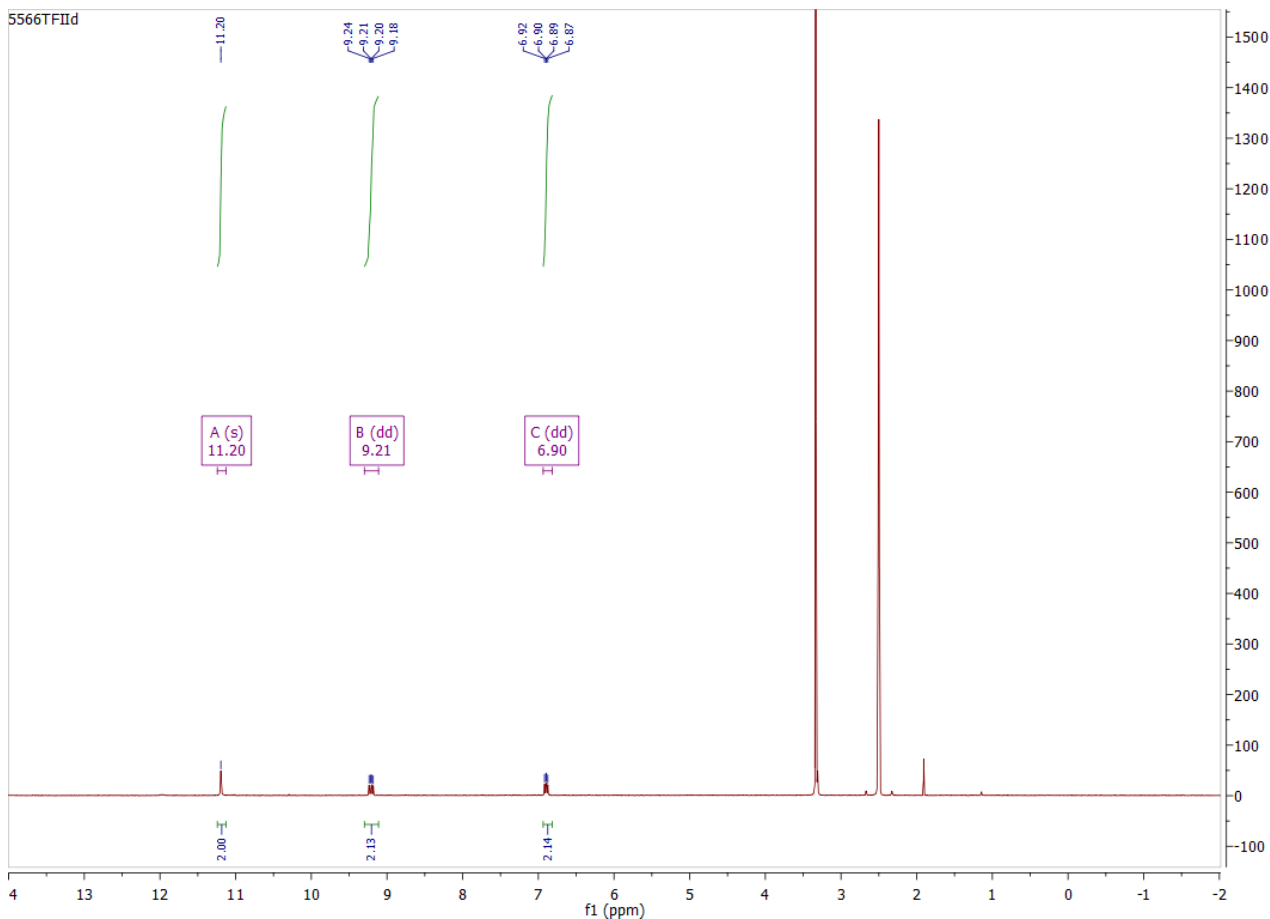
**Supplementary Fig. 67 |**  $^{13}\text{C}$  NMR spectra of 6B6MCIId.

**5,5',6,6'-Tetrafluoroisoindigo (5566TFIId):**



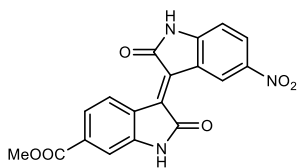
**Supplementary Fig. 68 |** Chemical structure of 5566TFIId.

The target was synthesised by the general procedure starting with 5,6-difluoroindoline-2,3-dione (366.2 mg, 2 mmol) and 5,6-difluoroindolin-2-one (338.3 mg, 2 mmol) in three days to afford the desired product (345 mg, 52%).  $^1\text{H}$  NMR (400 MHz, DMSO)  $\delta$  11.20 (s, 2H), 9.21 (dd,  $J$  = 13.3, 8.7 Hz, 2H), 6.90 (dd,  $J$  = 10.2, 7.1 Hz, 2H). HRMS (m/z): [M-H]<sup>-</sup> calcd. for C<sub>16</sub>H<sub>5</sub>F<sub>4</sub>N<sub>2</sub>O<sub>2</sub>, 333.0293; found, 333.0291.



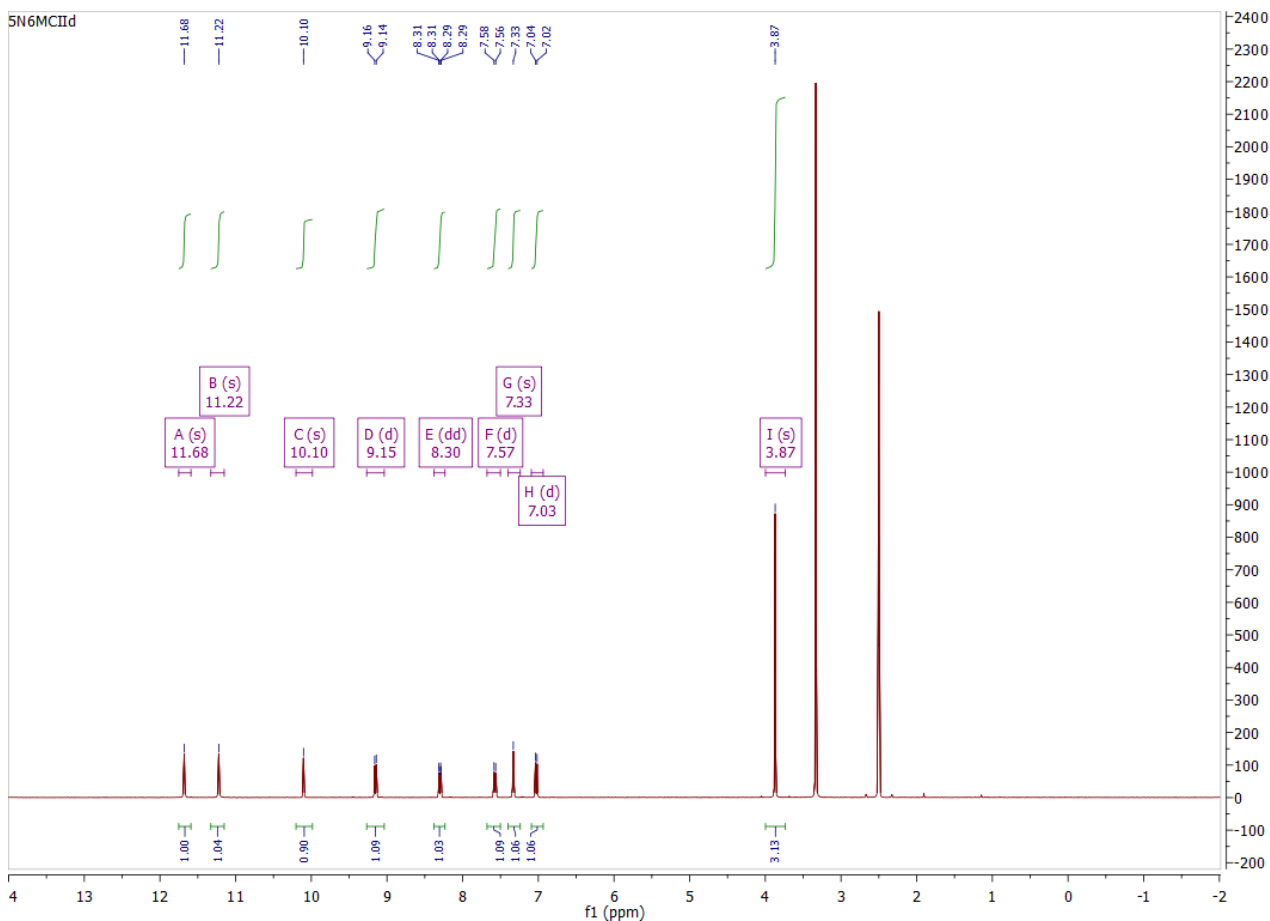
**Supplementary Fig. 69 |**  $^1\text{H}$  NMR spectra of 5566TFIId.

**Methyl-5-nitroisoindigo-6-carboxylate (5N6MCIIId):**



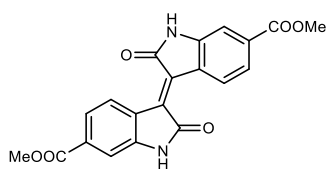
**Supplementary Fig. 70 |** Chemical structure of 5N6MCIIId.

The target was synthesised by the general procedure starting with 5-nitroisatin (960.7 mg, 5 mmol) and methyl 2-oxindole-6-carboxylate (956 mg, 5 mmol) in three days to afford the desired product (1.77 g, 97%).  $^1\text{H}$  NMR (400 MHz, DMSO)  $\delta$  11.68 (s, 1H), 11.22 (s, 1H), 10.10 (s, 1H), 9.15 (d,  $J$  = 8.4 Hz, 1H), 8.30 (dd,  $J$  = 8.7, 2.1 Hz, 1H), 7.57 (d,  $J$  = 8.5 Hz, 1H), 7.33 (s, 1H), 7.03 (d,  $J$  = 8.7 Hz, 1H), 3.87 (s, 3H). HRMS (m/z): [M-H] $^-$  calcd. for  $\text{C}_{18}\text{H}_{10}\text{N}_3\text{O}_6$ , 364.0575; found, 364.0574.



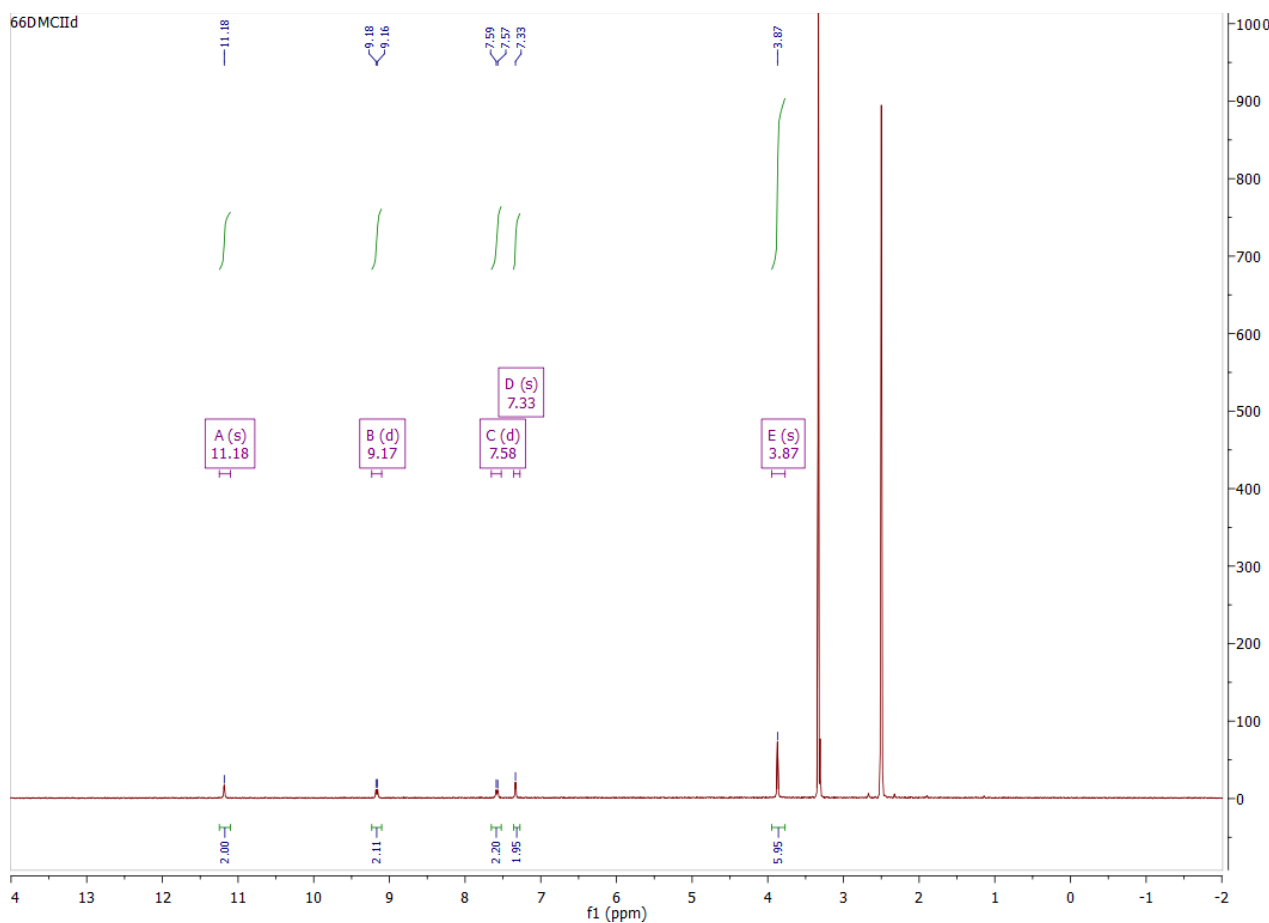
**Supplementary Fig. 71 |**  $^1\text{H}$  NMR spectra of 5N6MCIIId.

**Dimethyl isoindigo-6,6'-dicarboxylate (66DMCIId):**



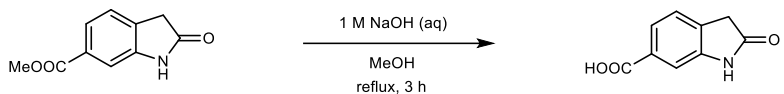
**Supplementary Fig. 72 |** Chemical structure of 66DMCIId.

The target was synthesised by the general procedure starting with methyl isatin-6-carboxylate (615.5 mg, 3 mmol) and methyl 2-oxindole-6-carboxylate (573.6 mg, 3 mmol) in three days to afford the desired product (1.1 g, 97%).  $^1\text{H}$  NMR (400 MHz, DMSO)  $\delta$  11.18 (s, 2H), 9.17 (d,  $J$  = 8.2 Hz, 2H), 7.58 (d,  $J$  = 7.9 Hz, 2H), 7.33 (s, 2H), 3.87 (s, 6H). HRMS (m/z): [M-H] $^-$  calcd. for C<sub>20</sub>H<sub>13</sub>N<sub>2</sub>O<sub>6</sub>, 377.0779; found, 377.0785.



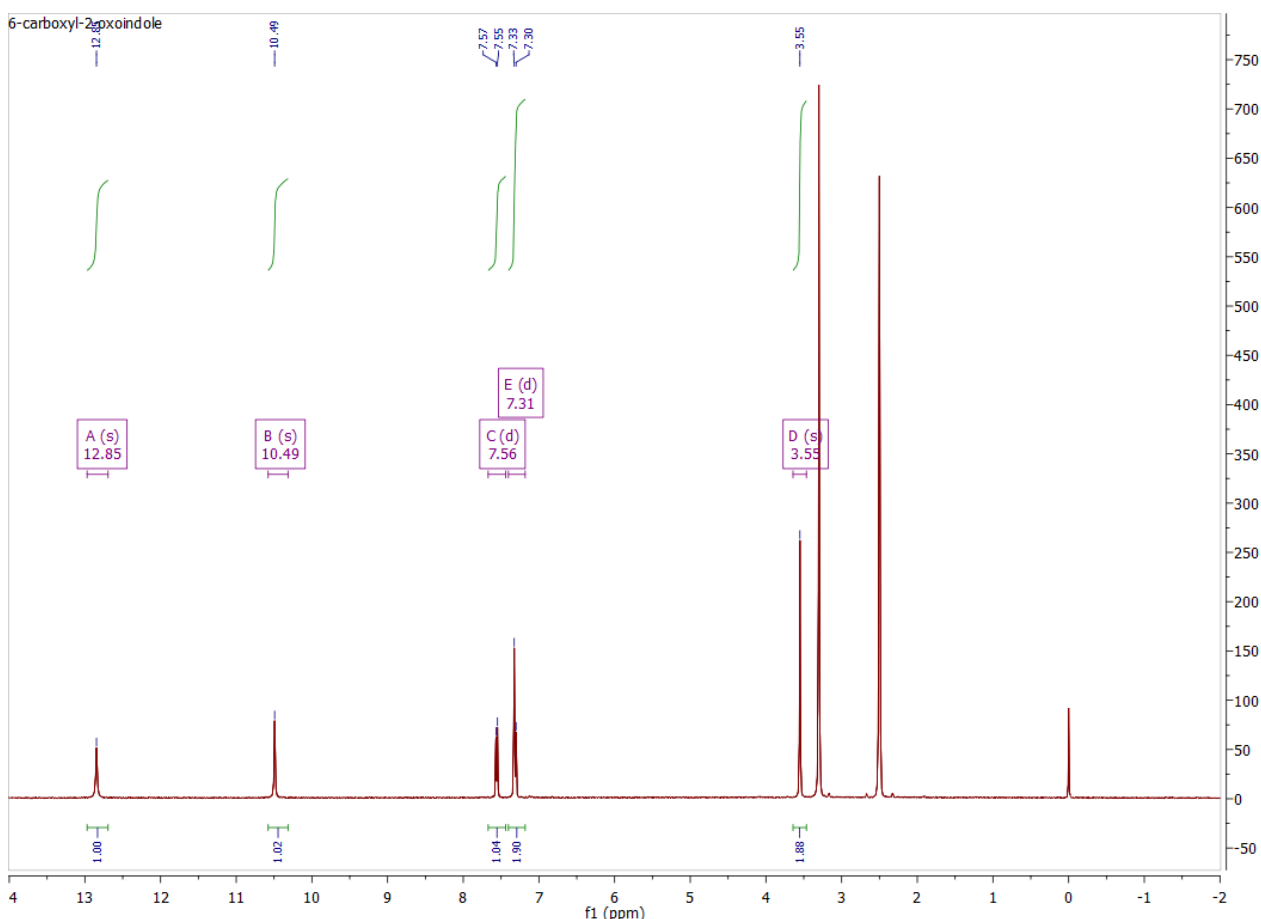
**Supplementary Fig. 73 |**  $^1\text{H}$  NMR spectra of 66DMCIId.

**2-Oxoindoline-6-carboxylic acid:**



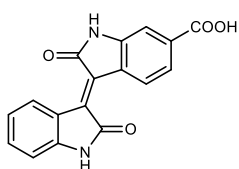
**Supplementary Fig. 74 |** Synthesis of 2-oxoindoline-6-carboxylic acid.

Methyl 2-oxindole-6-carboxylate (2 g, 10.4 mmol) was suspended in a mixture of methanol (20 ml) and 1 M NaOH (aq, 21 ml). The mixture was heated at reflux for 3 hours and allowed to cool down to room temperature. The solution was neutralised with 1 M HCl (aq) at 0 °C and a beige colour precipitate was formed. The precipitate was collected by filtration and washed with water and methanol. The crude product was dried in vacuo at 60 °C to give a beige solid (1.8 g, 97%), which was used in the next step without further purification.  $^1\text{H}$  NMR (400 MHz, DMSO)  $\delta$  12.85 (s, 1H), 10.49 (s, 1H), 7.56 (d,  $J$  = 7.6 Hz, 1H), 7.33-7.30 (2H), 3.55 (s, 2H).



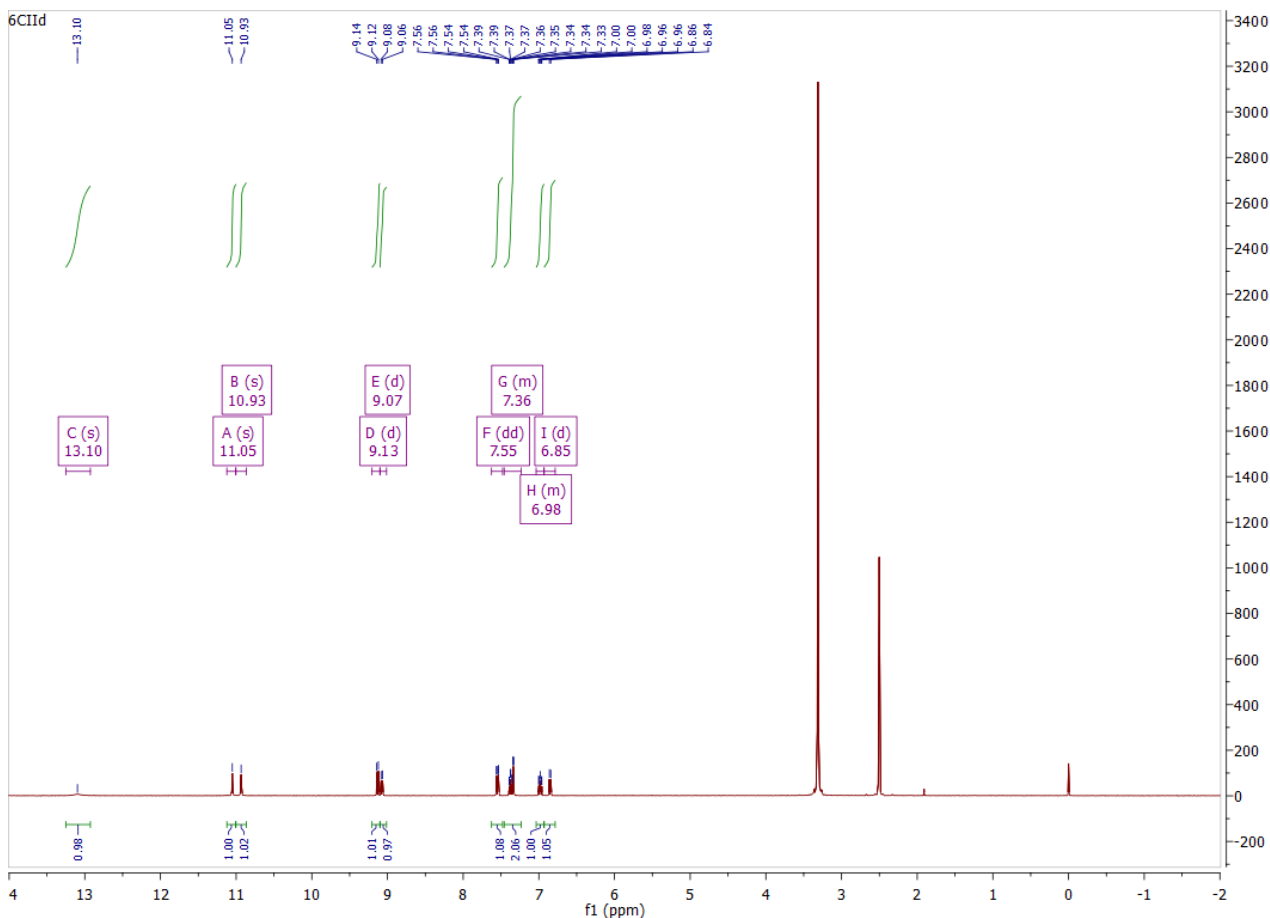
**Supplementary Fig. 75 |**  $^1\text{H}$  NMR spectra of 2-oxoindoline-6-carboxylic acid.

**Isoindigo-6-carboxylic acid (6CIId):**

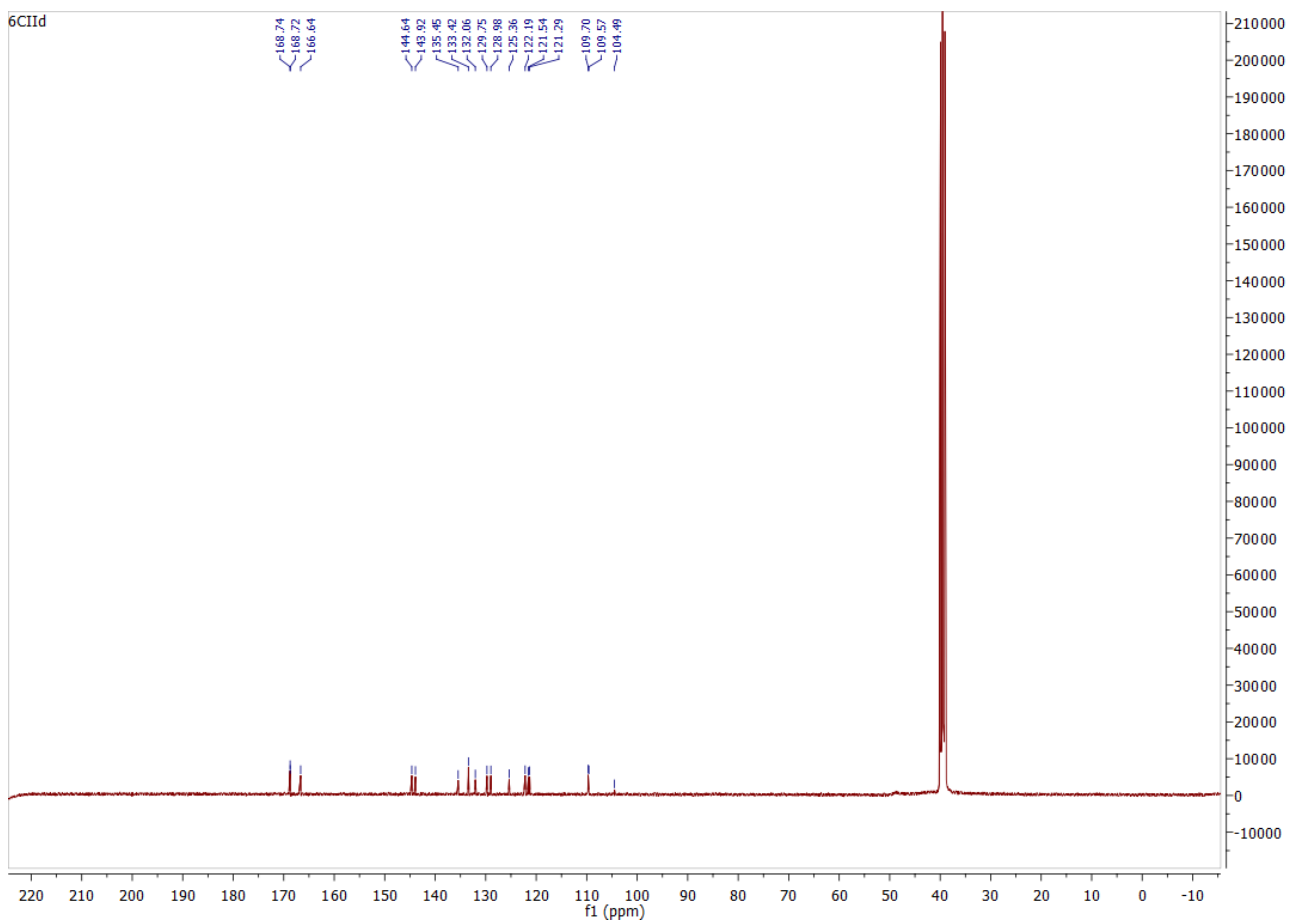


**Supplementary Fig. 76 |** Chemical structure of 6CIId.

The target was synthesised by the general procedure starting with isatin (1.47 g, 10 mmol) and 2-oxindoline-6-carboxylic acid (1.77 g, 10 mmol) in a day to afford the desired product (2.55 g, 83%).  $^1\text{H}$  NMR (400 MHz, DMSO)  $\delta$  13.10 (s, 1H), 11.05 (s, 1H), 10.93 (s, 1H), 9.13 (d,  $J$  = 8.4 Hz, 1H), 9.07 (d,  $J$  = 8.1 Hz, 1H), 7.55 (dd,  $J$  = 8.4, 1.7 Hz, 1H), 7.46 – 7.23 (m, 2H), 7.04 – 6.93 (m, 1H), 6.85 (d,  $J$  = 7.2 Hz, 1H).  $^{13}\text{C}$  NMR (101 MHz, DMSO)  $\delta$  168.74, 168.72, 166.64, 144.64, 143.92, 135.45, 133.42, 132.06, 129.75, 128.98, 125.36, 122.19, 121.54, 121.29, 109.70, 109.57, 104.49. Low-res ESI-MS ( $m/z$ ): [M-H]<sup>-</sup> calcd. for C<sub>17</sub>H<sub>9</sub>N<sub>2</sub>O<sub>4</sub>, 305; found, 305.

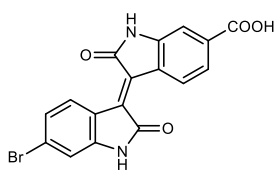


**Supplementary Fig. 77 |**  $^1\text{H}$  NMR spectra of 6CIId.



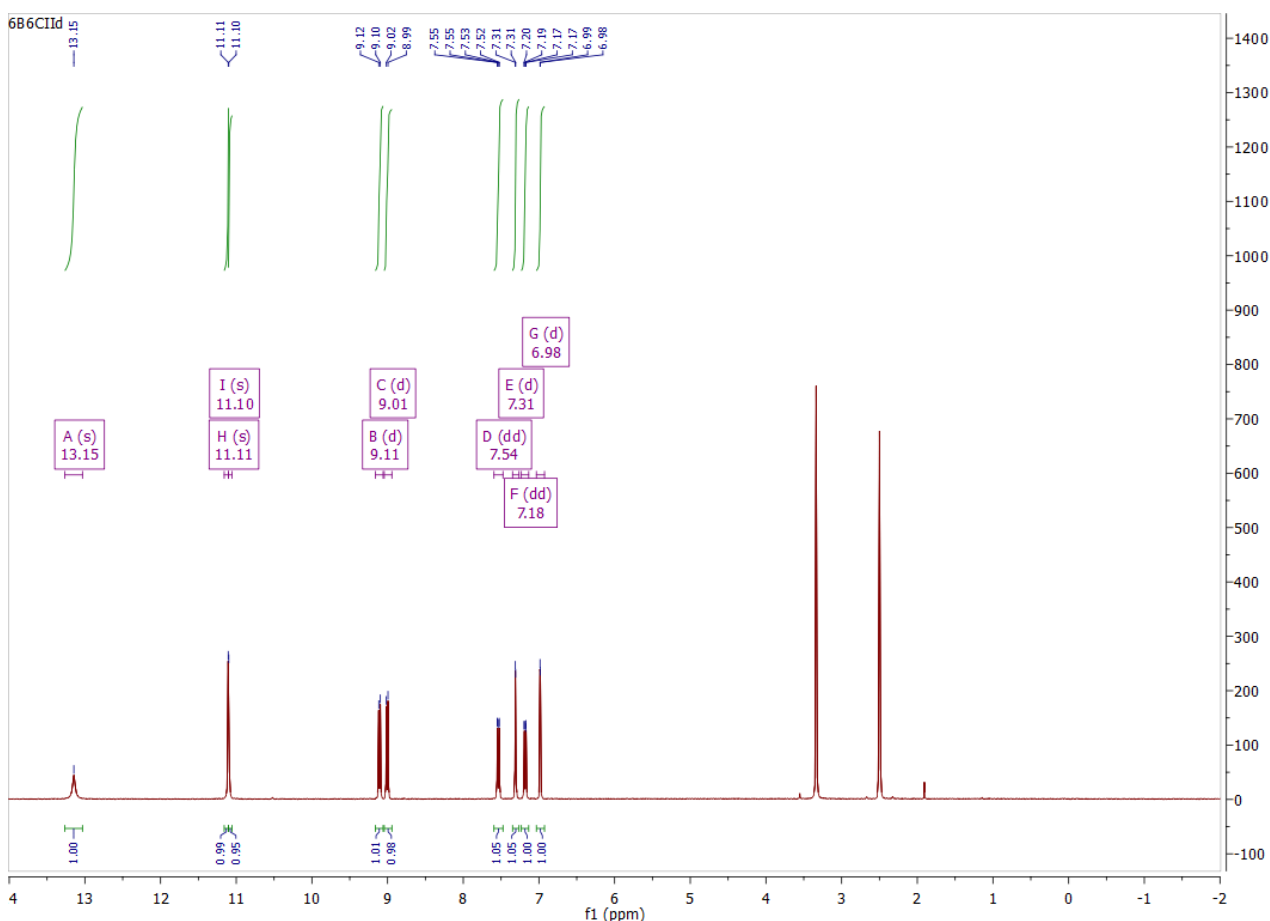
**Supplementary Fig. 78 |**  $^{13}\text{C}$  NMR spectra of 6CIId.

**6-Bromoisoindigo-6'-carboxylic acid (6B6CIId):**



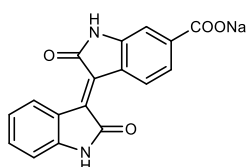
**Supplementary Fig. 79 |** Chemical structure of 6B6CIId.

The target was synthesised by the general procedure starting with 6-bromoisatin (2.26 g, 10 mmol) and 2-oxindoline-6-carboxylic acid (1.77 g, 10 mmol) in a day to afford the desired product (3.52 g, 91%).  $^1\text{H}$  NMR (400 MHz, DMSO)  $\delta$  13.15 (s, 1H), 11.11 (s, 1H), 11.10 (s, 1H), 9.11 (d,  $J$  = 8.4 Hz, 1H), 9.01 (d,  $J$  = 8.7 Hz, 1H), 7.54 (dd,  $J$  = 8.4, 1.6 Hz, 1H), 7.31 (d,  $J$  = 1.3 Hz, 1H), 7.18 (dd,  $J$  = 8.7, 2.0 Hz, 1H), 6.98 (d,  $J$  = 1.9 Hz, 1H). Low-res ESI-MS ( $m/z$ ): [M-H] $^-$  calcd. for  $\text{C}_{17}\text{H}_8\text{BrN}_2\text{O}_4$ , 383; found, 383.



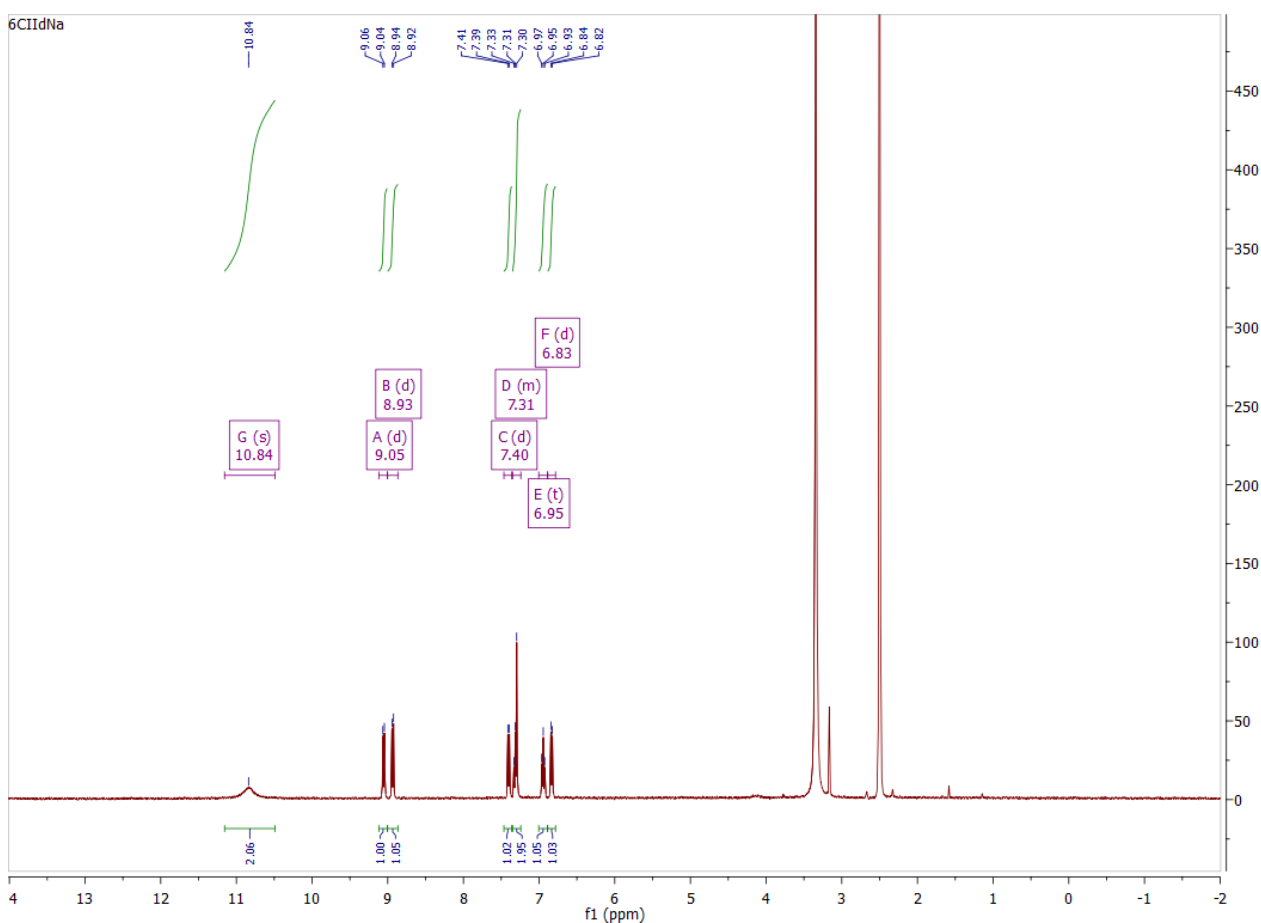
**Supplementary Fig. 80 |**  $^1\text{H}$  NMR spectra of 6B6CIId.

**Sodium isoindigo-6-carboxylate (6CIIdNa):**



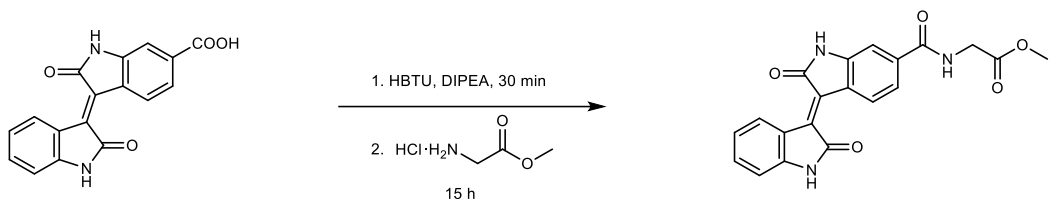
**Supplementary Fig. 81 |** Chemical structure of 6CIIdNa.

6CIId (306.3 mg, 1 mmol) was added portionwise to a solution of NaOH (0.2 M, 5 ml) in methanol at 0 °C. The mixture was stirred for another 15 min at 0 °C before it was concentrated in vacuo to dryness to afford a brown solid (328 mg, >99%).  $^1\text{H}$  NMR (400 MHz, DMSO)  $\delta$  10.84 (s, 2H), 9.05 (d,  $J$  = 8.1 Hz, 1H), 8.93 (d,  $J$  = 8.3 Hz, 1H), 7.40 (d,  $J$  = 8.3 Hz, 1H), 7.35 – 7.24 (m, 2H), 6.95 (t,  $J$  = 7.9 Hz, 1H), 6.83 (d,  $J$  = 7.8 Hz, 1H). Low-res ESI-MS ( $m/z$ ): [M–H] $^-$  calcd. for  $\text{C}_{17}\text{H}_9\text{N}_2\text{O}_4$ , 305; found, 305.



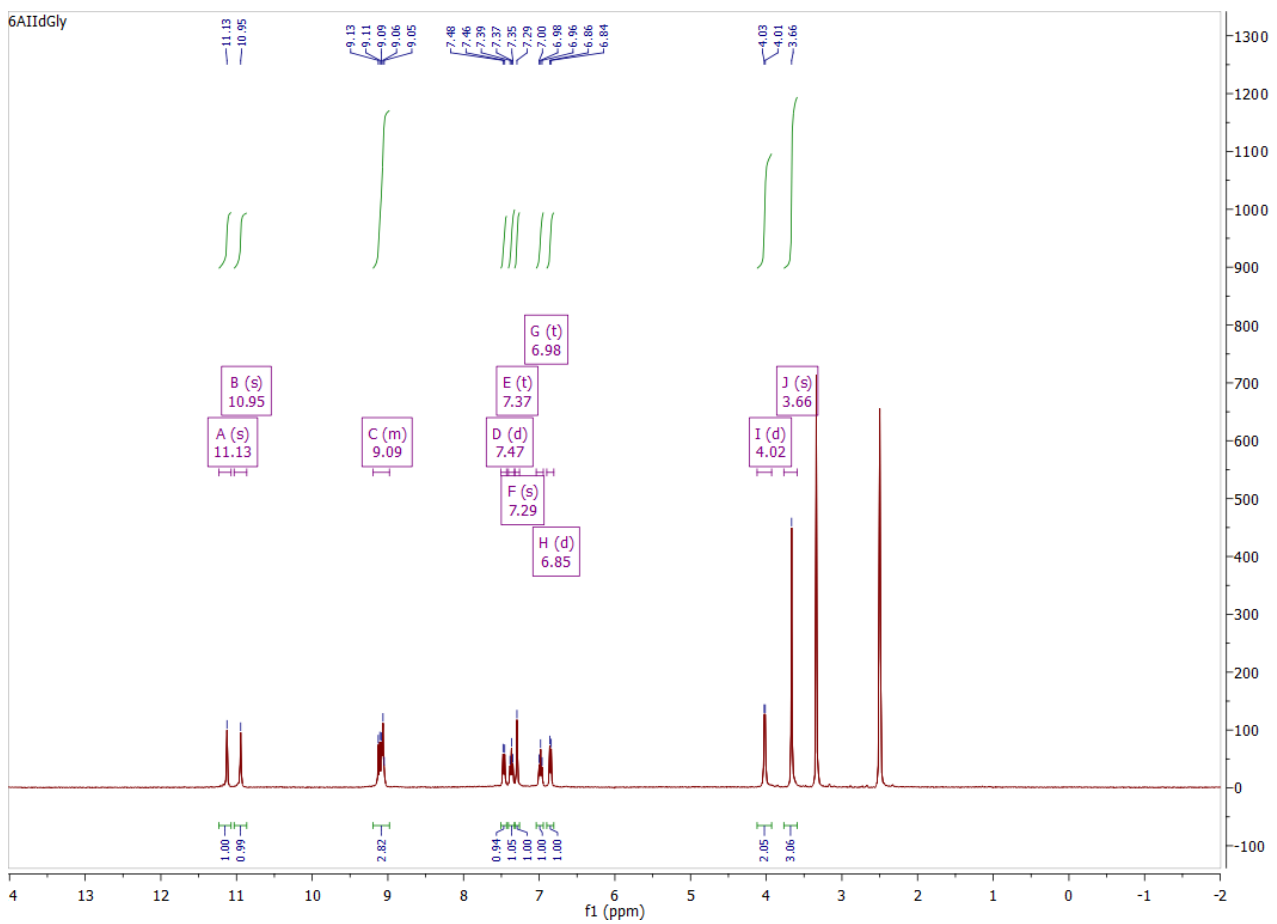
**Supplementary Fig. 82 |**  $^1\text{H}$  NMR spectra of 6CIIdNa.

**Methyl isoindigo-6-carbonylglycinate (6AIIdGly):**

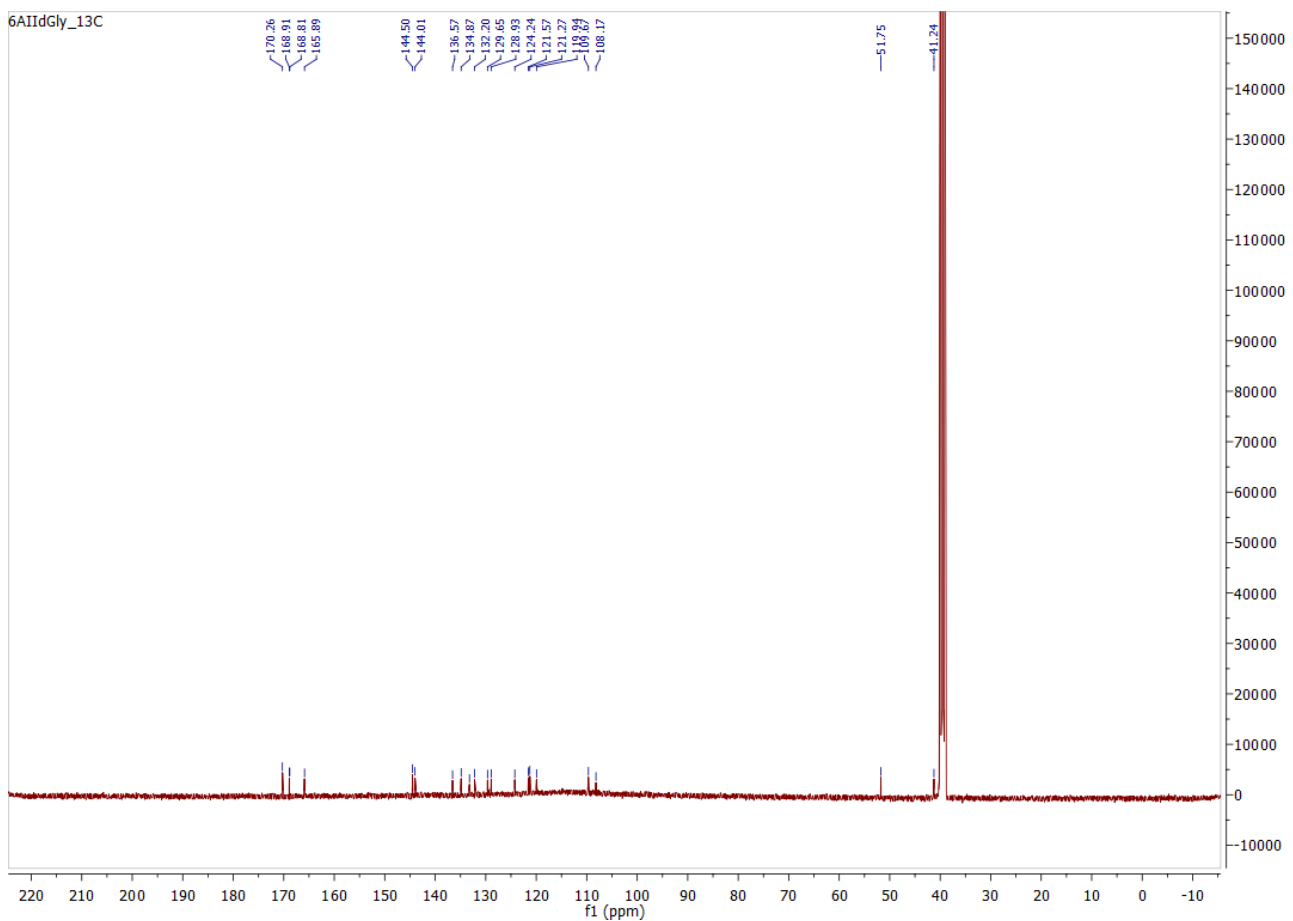


**Supplementary Fig. 83 | Synthesis of 6AIIdGly.**

To a mixture of 6CIId (1.23 g, 4 mmol) and 2-(1*H*-benzotriazol-1-yl)-1,1,3,3-tetramethyluronium hexafluorophosphate (HBTU) (1.64 g, 4.32 mmol) in anhydrous DMF (25 ml) was added *N,N*-diisopropylethylamine (DIPEA) (12 mmol, 2.1 ml) dropwisely. The mixture was stirred in Ar for 30 min before glycine methyl ester hydrochloride (540 mg, 4.32 mmol) in DMF (5 ml) was added. The reaction was monitored by TLC and stirred for another 15 h at room temperature. Upon completion of the reaction, the dark solution was poured onto a saturated NaHCO<sub>3</sub> aqueous solution (300 ml). The precipitate was collected by filtration, washed repeatedly with saturated NaHCO<sub>3</sub> (aq), water, 0.2 M HCl (aq), cold methanol and dichloromethane, and dried in vacuo to give a dark red solid. The crude product was recrystallised from ethanol to afford a dark red powder (1.284 g, 85%). <sup>1</sup>H NMR (400 MHz, DMSO) δ 11.12 (s, 1H), 10.94 (s, 1H), 9.18 – 8.98 (m, 3H), 7.47 (dd, *J* = 8.4, 1.6 Hz, 1H), 7.37 (td, *J* = 7.7, 0.9 Hz, 1H), 7.29 (d, *J* = 1.4 Hz, 1H), 7.03 – 6.94 (m, 1H), 6.85 (d, *J* = 7.6 Hz, 1H), 4.02 (d, *J* = 5.8 Hz, 2H), 3.67 (s, 3H). <sup>13</sup>C NMR (101 MHz, DMSO) δ 170.26, 168.91, 168.81, 165.89, 144.50, 144.01, 136.57, 134.87, 133.22, 132.20, 129.65, 128.93, 124.24, 121.57, 121.27, 119.94, 109.67, 108.17, 51.75, 41.24. Low-res ESI-MS (m/z): [M-H]<sup>-</sup> calcd. for C<sub>20</sub>H<sub>14</sub>N<sub>3</sub>O<sub>5</sub>, 376; found, 376.

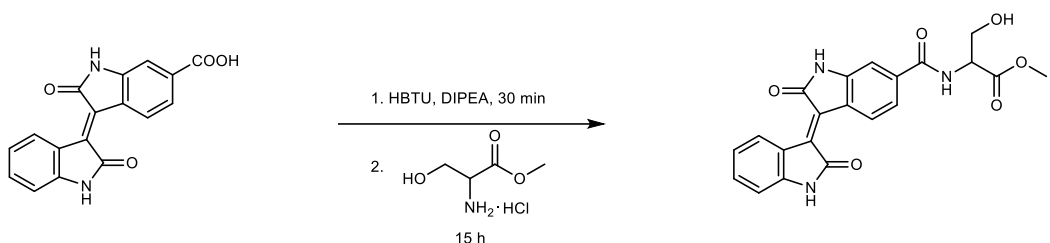


**Supplementary Fig. 84 |** <sup>1</sup>H NMR spectra of 6AIIdGly.



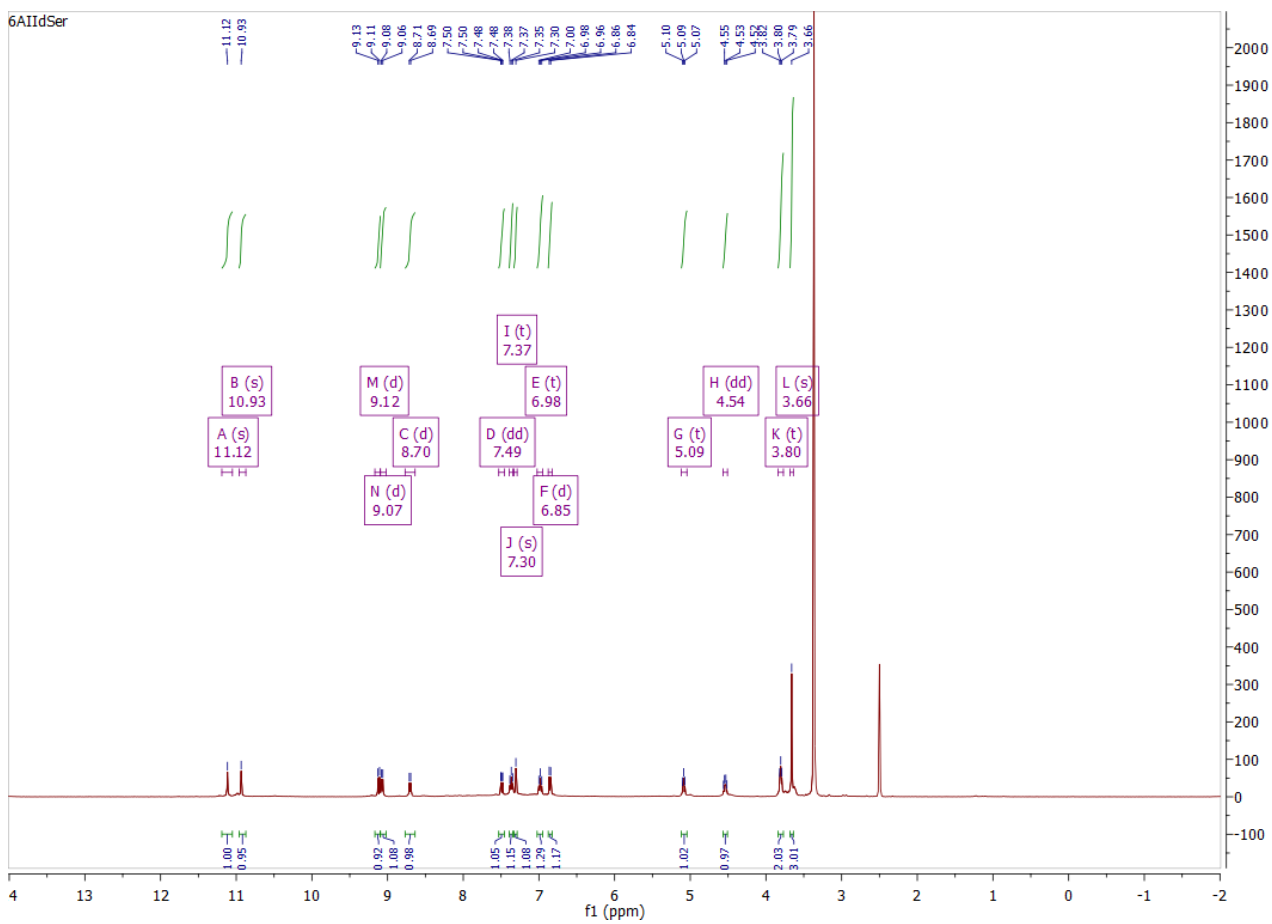
**Supplementary Fig. 85 |**  $^{13}\text{C}$  NMR spectra of 6AIIdGly.

**Methyl isoindigo-6-carbonylserinate (6AIIdSer):**

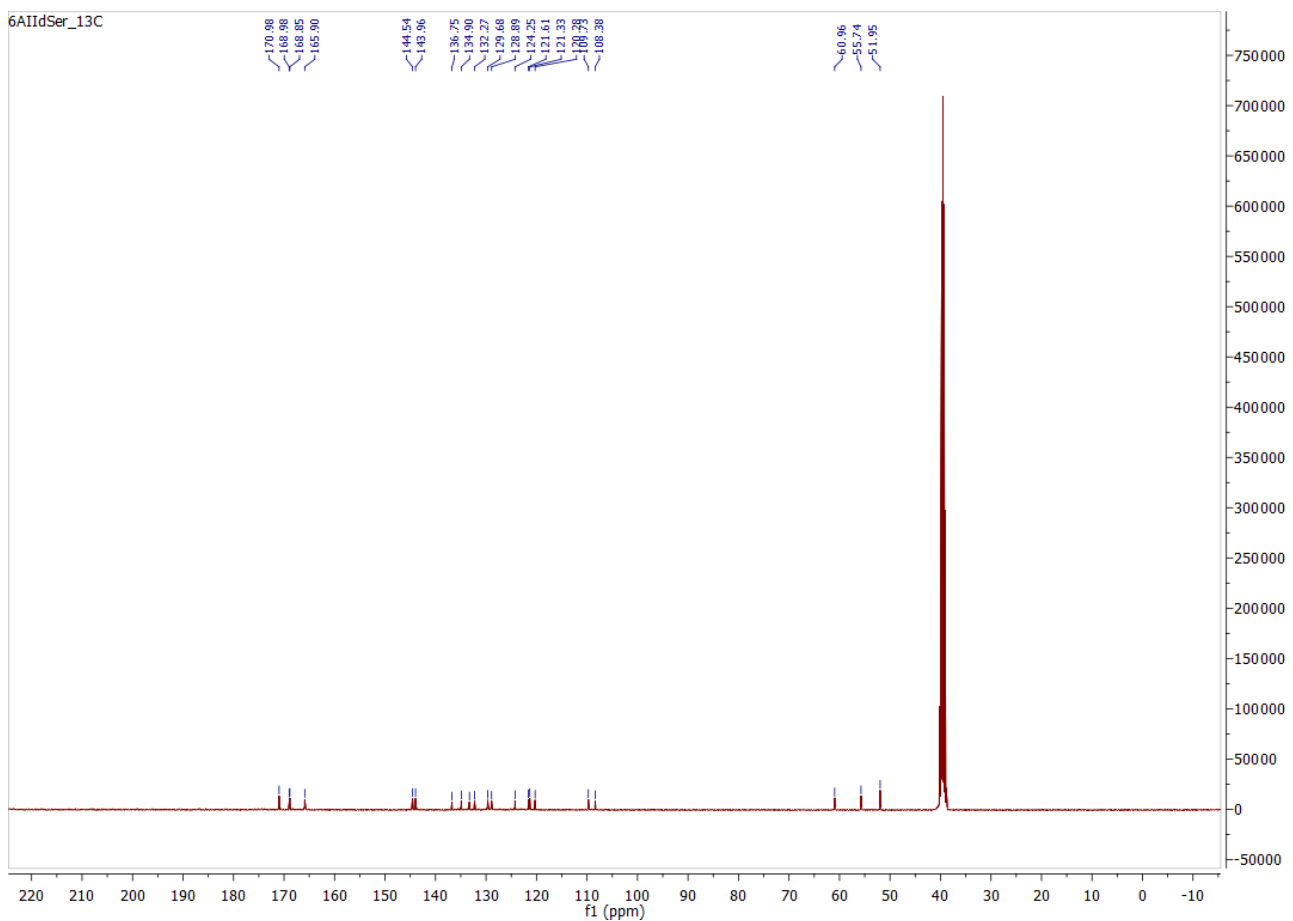


**Supplementary Fig. 86 | Synthesis of 6AIIdSer.**

To a mixture of 6CIId (1.85 g, 6 mmol) and 2-(1*H*-benzotriazol-1-yl)-1,1,3,3-tetramethyluronium hexafluorophosphate (HBTU) (2.46 g, 6.48 mmol) in anhydrous DMF (30 ml) was added *N,N*-diisopropylethylamine (DIPEA) (3.15 ml, 18 mmol) dropwisely. The mixture was stirred in Ar for 30 min before L-serine methyl ester hydrochloride (1.16 g, 6.48 mmol) in DMF (5 ml) was added. The reaction was monitored by TLC and stirred for another 15 h at room temperature. Upon completion of the reaction, the dark solution was poured onto a saturated NaHCO<sub>3</sub> aqueous solution (300 ml). The precipitate was collected by filtration, washed repeatedly with saturated NaHCO<sub>3</sub> (aq), water, 0.2 M HCl (aq), cold methanol and dichloromethane, and dried in vacuo to give a dark red solid. The crude product was recrystallised from ethanol to afford a dark red powder (1.39 g, 57%). <sup>1</sup>H NMR (400 MHz, DMSO) δ 11.12 (s, 1H), 10.93 (s, 1H), 9.12 (d, *J* = 8.4 Hz, 1H), 9.07 (d, *J* = 7.9 Hz, 1H), 8.70 (d, *J* = 7.3 Hz, 1H), 7.49 (dd, *J* = 8.5, 1.4 Hz, 1H), 7.37 (t, *J* = 7.2 Hz, 1H), 7.30 (s, 1H), 6.98 (t, *J* = 7.6 Hz, 1H), 6.85 (d, *J* = 7.6 Hz, 1H), 5.09 (t, *J* = 6.1 Hz, 1H), 4.54 (dd, *J* = 12.6, 5.5 Hz, 1H), 3.80 (t, *J* = 5.7 Hz, 2H), 3.66 (s, 3H). <sup>13</sup>C NMR (101 MHz, DMSO) δ 170.98, 168.98, 168.85, 165.90, 144.54, 143.96, 136.75, 134.90, 133.29, 132.27, 129.68, 128.89, 124.25, 121.61, 121.33, 120.28, 109.73, 108.38, 60.96, 55.74, 51.95. Low-res ESI-MS (m/z): [M-H]<sup>-</sup> calcd. for C<sub>21</sub>H<sub>16</sub>N<sub>3</sub>O<sub>6</sub>, 406; found, 406.

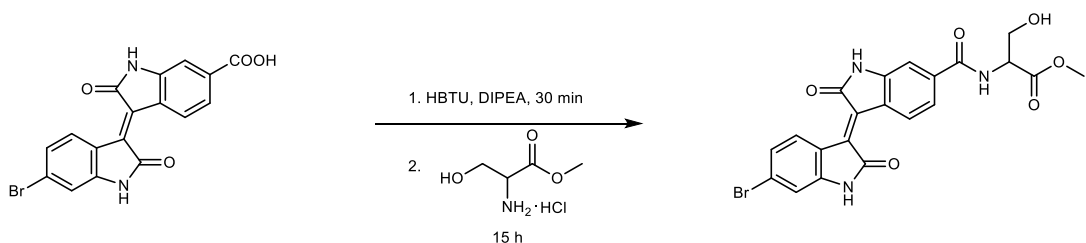


**Supplementary Fig. 87 |**  $^1\text{H}$  NMR spectra of 6AIIdSer.



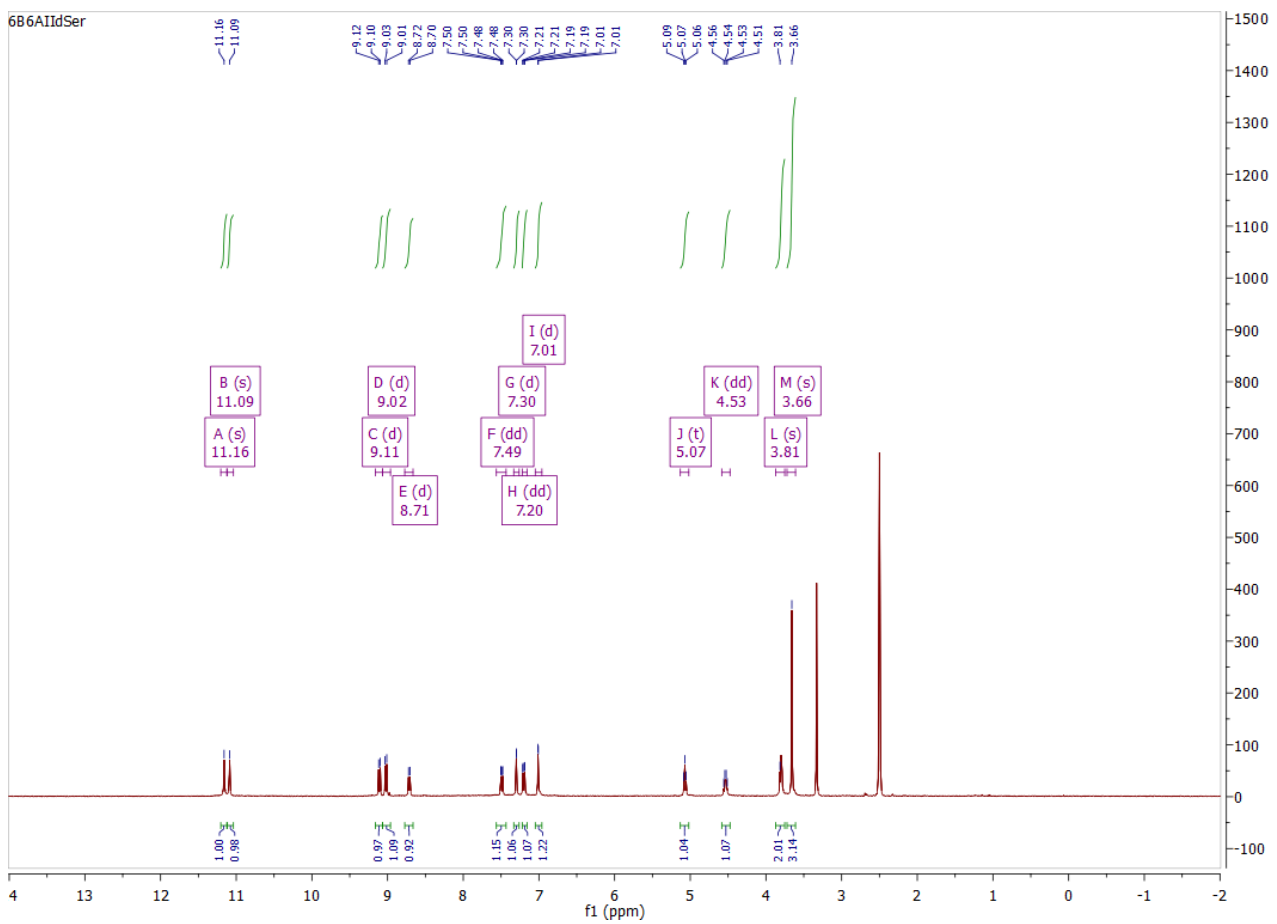
**Supplementary Fig. 88 |**  $^{13}\text{C}$  NMR spectra of 6AIIdSer.

**Methyl 6-bromoisoindigo-6'-carbonylserinate (6B6AIIdSer):**

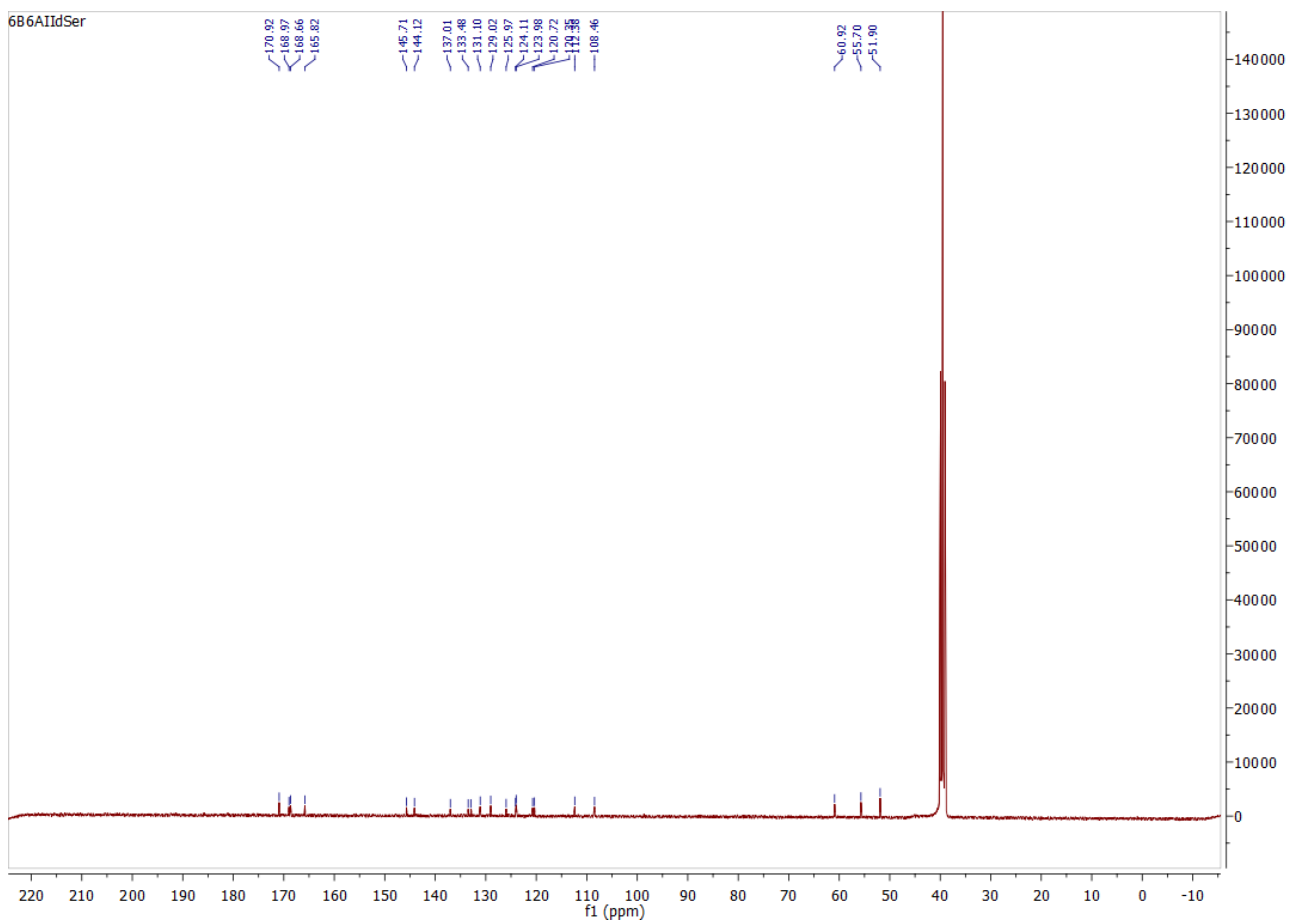


**Supplementary Fig. 89 | Synthesis of 6B6AIIdSer.**

To a mixture of 6B6CIId (2.31 g, 6 mmol) and 2-(1*H*-benzotriazol-1-yl)-1,1,3,3-tetramethyluronium hexafluorophosphate (HBTU) (2.46 g, 6.48 mmol) in anhydrous DMF (30 ml) was added *N,N*-diisopropylethylamine (DIPEA) (3.15 ml, 18 mmol) dropwisely. The mixture was stirred in Ar for 30 min before L-serine methyl ester hydrochloride (1.16 g, 6.48 mmol) in DMF (5 ml) was added. The reaction was monitored by TLC and stirred for another 15 h at room temperature. Upon completion of the reaction, the dark solution was poured onto a saturated NaHCO<sub>3</sub> aqueous solution (300 ml). The precipitate was collected by filtration, washed repeatedly with saturated NaHCO<sub>3</sub> (aq), water, 0.2 M HCl (aq), cold methanol and dichloromethane, and dried in vacuo to give the pure solid product in dark red (2.14 g, 73%). <sup>1</sup>H NMR (400 MHz, DMSO) δ 11.16 (s, 1H), 11.09 (s, 1H), 9.11 (d, *J* = 8.4 Hz, 1H), 9.02 (d, *J* = 8.7 Hz, 1H), 8.71 (d, *J* = 7.4 Hz, 1H), 7.49 (dd, *J* = 8.4, 1.6 Hz, 1H), 7.30 (d, *J* = 1.4 Hz, 1H), 7.20 (dd, *J* = 8.6, 2.0 Hz, 1H), 7.01 (d, *J* = 1.9 Hz, 1H), 5.07 (t, *J* = 6.1 Hz, 1H), 4.53 (dd, *J* = 12.7, 5.5 Hz, 1H), 3.81 (s, 2H), 3.66 (s, 3H). <sup>13</sup>C NMR (101 MHz, DMSO) δ 170.92, 168.97, 168.66, 165.82, 145.71, 144.12, 137.01, 133.48, 132.90, 131.10, 129.02, 125.97, 124.11, 123.98, 120.72, 120.35, 112.38, 108.46, 60.92, 55.70, 51.90. Low-res ESI-MS (m/z): [M-H]<sup>-</sup> calcd. for C<sub>21</sub>H<sub>16</sub>N<sub>3</sub>O<sub>6</sub>, 484; found, 484.

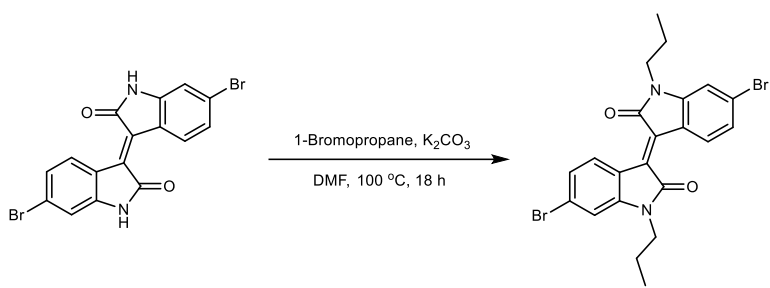


**Supplementary Fig. 90 |**  $^1\text{H}$  NMR spectra of 6B6AIIdSer.



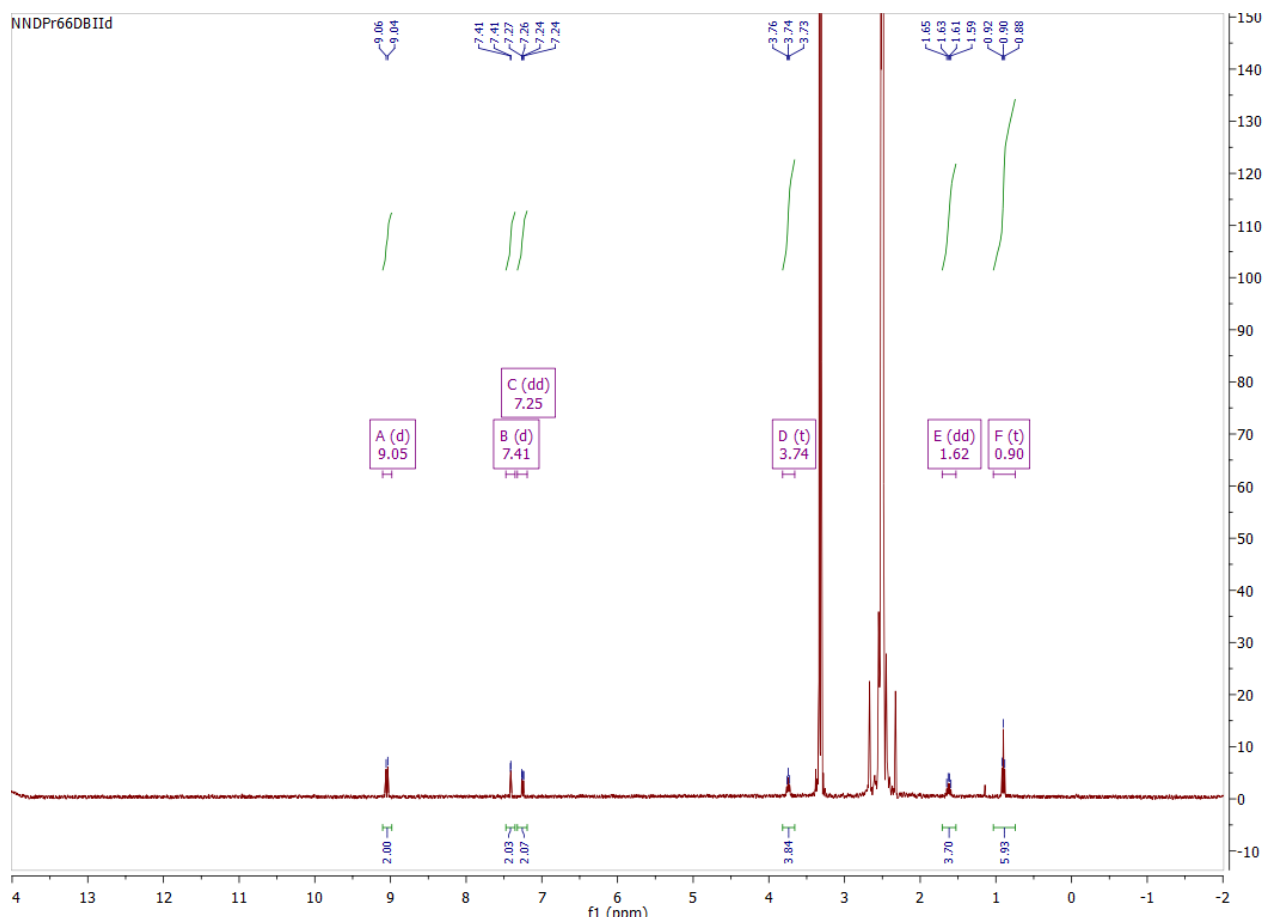
Supplementary Fig. 91 |  $^{13}\text{C}$  NMR spectra of 6B6AIIdSer.

***N,N'*-Dipropyl-6,6'-dibromoisoindigo (NNDPr66DBIId):**



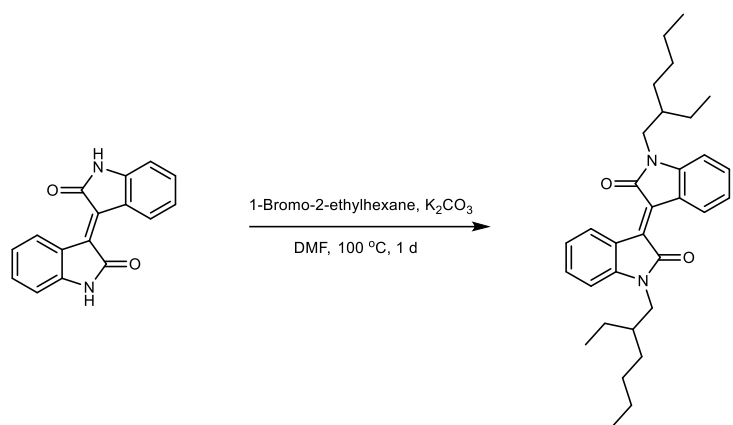
**Supplementary Fig. 92 | Synthesis of NNDPr66DBIId.**

To a mixture of 66DBIId (158 mg, 0.377 mmol) and  $\text{K}_2\text{CO}_3$  (261 mg, 1.89 mmol) in DMF (5 ml) under Ar was added propyl bromide (0.2 ml). The mixture was heated at 100 °C under Ar for 18 h. The reaction mixture was cooled and evaporated to dryness in vacuo. The crude solid was partition between dichloromethane and water. The organic phase was dried over  $\text{Na}_2\text{SO}_4$ , filtered, and dried in vacuo. The crude product was then purified by column chromatography on silica gel (230 ~ 400 mesh, hexane/ $\text{CH}_2\text{Cl}_2$  = 1:3) to give a red colour solid (104 mg, 55%).  $^1\text{H}$  NMR (400 MHz, DMSO)  $\delta$  9.05 (d,  $J$  = 8.6 Hz, 2H), 7.41 (d,  $J$  = 1.9 Hz, 2H), 7.25 (dd,  $J$  = 8.6, 1.9 Hz, 2H), 3.74 (t,  $J$  = 7.0 Hz, 4H), 1.62 (dd,  $J$  = 14.6, 7.6 Hz, 4H), 0.90 (t,  $J$  = 7.4 Hz, 6H).



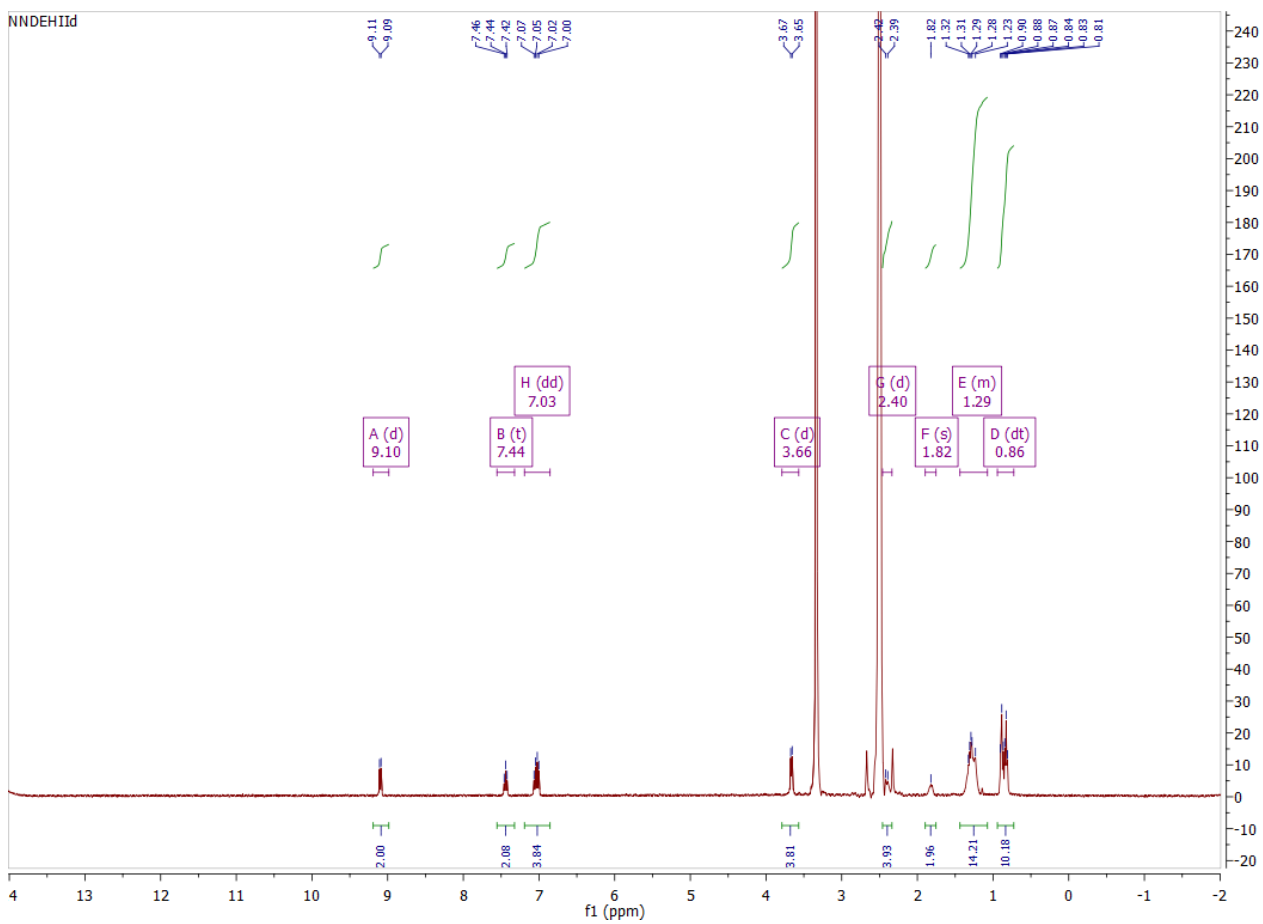
**Supplementary Fig. 93 |  $^1\text{H}$  NMR spectra of NNDPr66DBIId.**

***N,N'*-Di-(2-ethylhexyl)-isoindigo (NNDEHIIId):**



**Supplementary Fig. 94 |** Synthesis of NNDEHIIId.

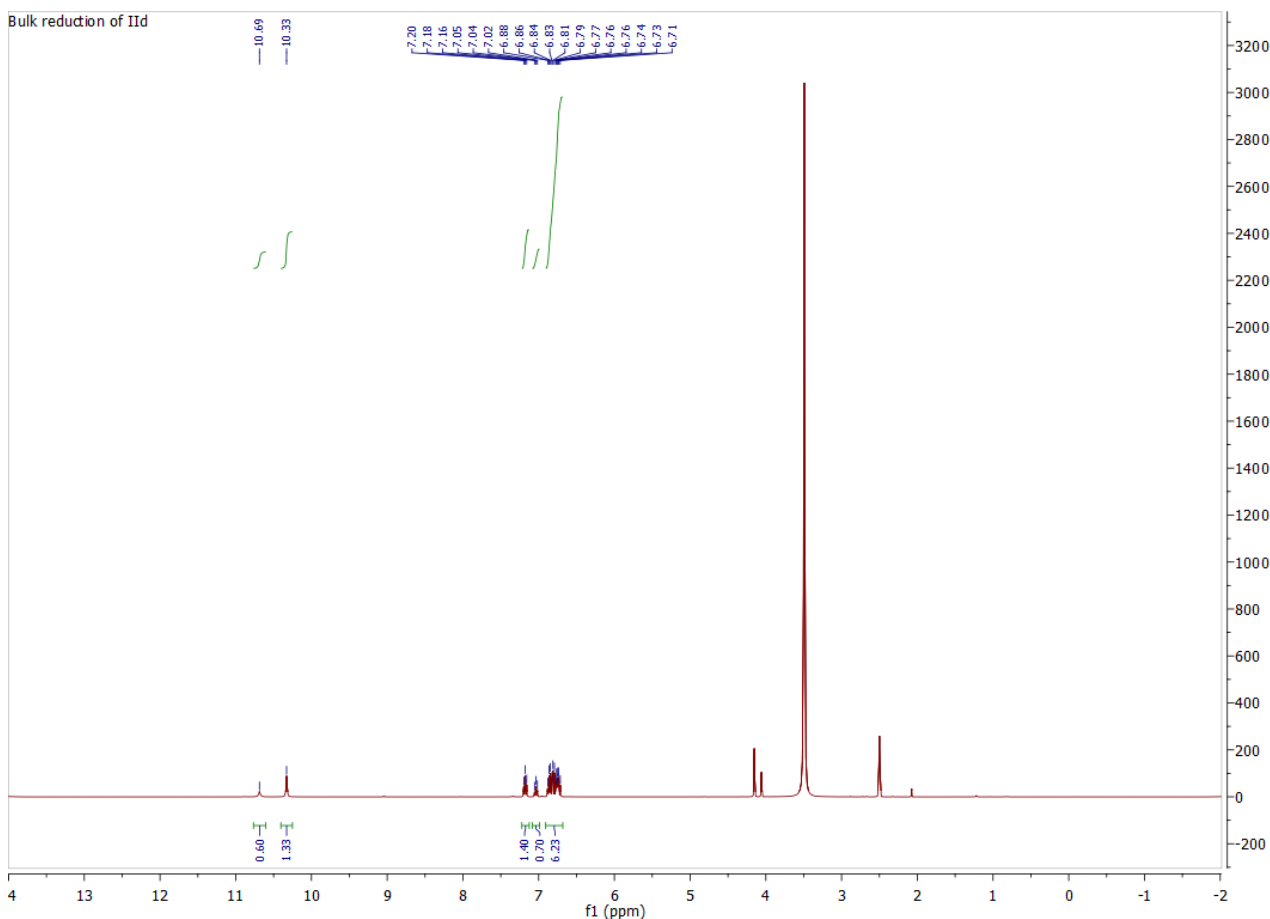
To a mixture of isoindigo (2.62 g, 10 mmol) and  $K_2CO_3$  (6.9 g, 50 mmol) in DMF (100 ml) was added 1-bromo-2-ethylhexane (3.8 ml, 22 mmol) under Ar atmosphere. The mixture was heated at 100 °C for 1 day. After the reaction was cooled to room temperature, the mixture was poured onto 1 l of water and a dark red precipitate was formed. The solid was filtered, washed with a copious amount of water and cold methanol, and dried in vacuo. The crude product was purified by column chromatography on silica gel (230~400 mesh, hexane/ $CH_2Cl_2$  = 1:1) to give a dark red solid (1.58 g, 32%).  $^1H$  NMR (400 MHz, DMSO)  $\delta$  9.10 (d,  $J$  = 7.6 Hz, 2H), 7.44 (t,  $J$  = 7.7 Hz, 2H), 7.03 (dd,  $J$  = 17.1, 8.0 Hz, 4H), 3.66 (d,  $J$  = 7.6 Hz, 4H), 2.40 (d,  $J$  = 10.6 Hz, 4H), 1.82 (s, 2H), 1.44 – 1.07 (m, 14H), 0.86 (dt,  $J$  = 13.8, 7.2 Hz, 10H).



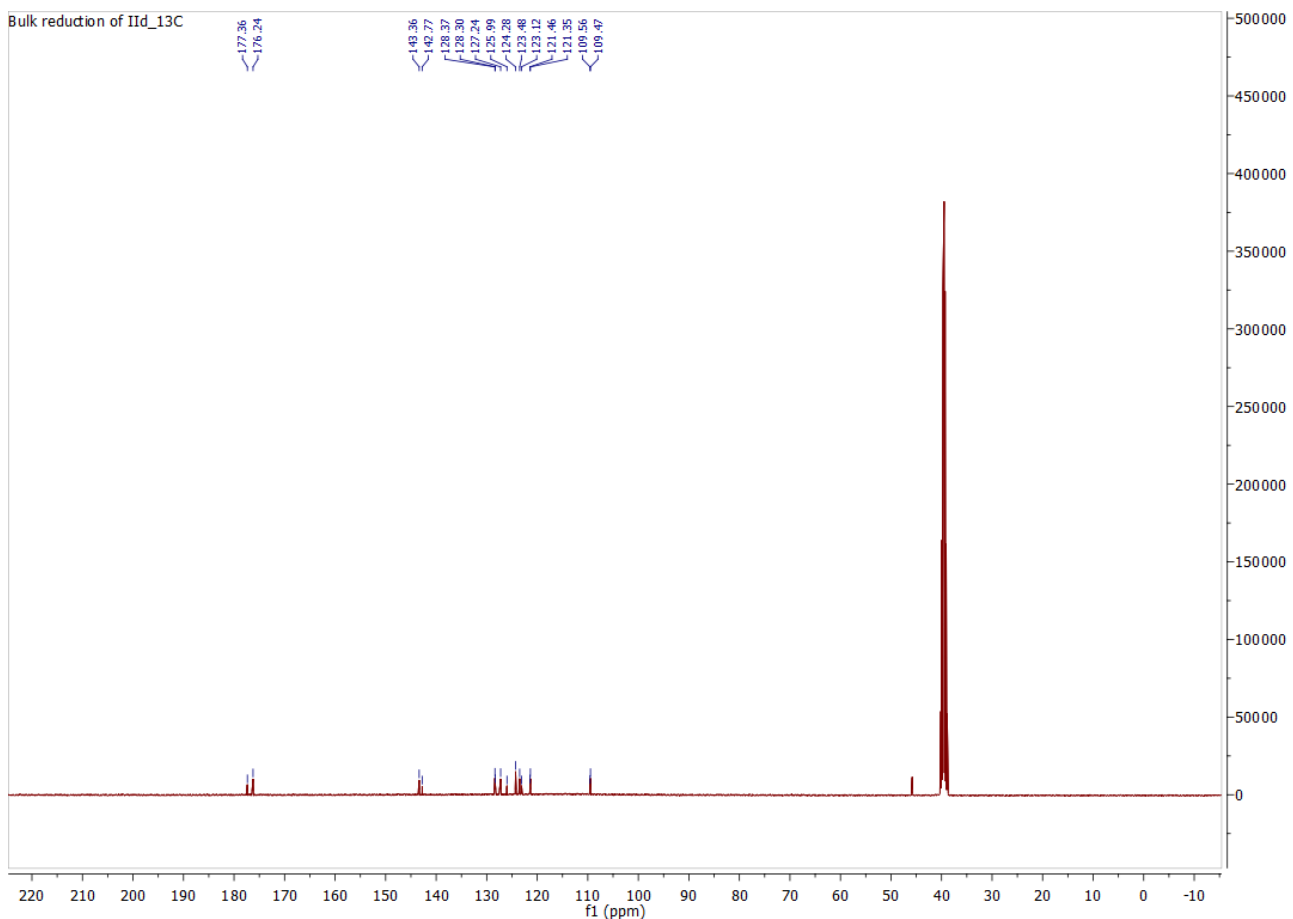
**Supplementary Fig. 95 |** <sup>1</sup>H NMR spectra of NNDEHIId.

### Bulk electrolysis

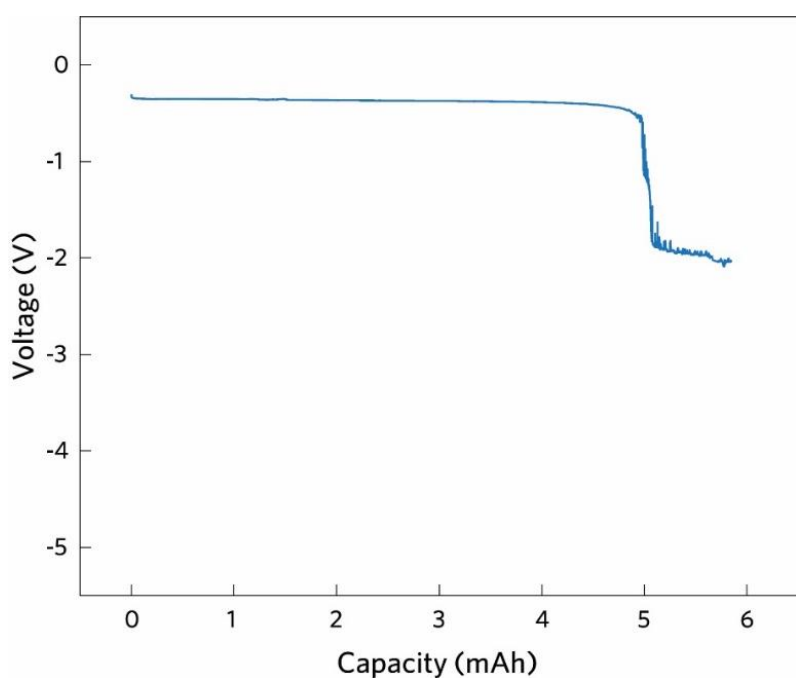
$\text{IId}^{2-}$  and  $\text{IId}\text{-CO}_2$  adduct were synthesised by constant current bulk electrolysis of  $\text{IId}$  in  $\text{DMSO-d}_6$  under  $\text{N}_2$  or  $\text{CO}_2$  atmosphere. The setup consisted of a three-neck round-bottom flask for the working, counter, and reference electrodes, respectively. Carbon felt (CT GF030; Fuel Cell Store) was used as the working electrode and a silver wire was used as the reference electrode. The counter electrode was separated from the isoindigo solution with a fritted electrode chamber (MR-1196; Bioanalytical Systems). A piece of carbon felt coated with  $\text{LiFePO}_4$  (50 mg) was used as the counter electrode, which was immersed in a neat electrolyte (1 ml) without isoindigo.  $\text{LiClO}_4$  (250 mM) in  $\text{DMSO-d}_6$  was used as the electrolyte. In a standard condition,  $\text{IId}$  (26.2 mg, 0.1 mmol) was stirred and reduced at a constant current of 1.5 mA in  $\text{DMSO-d}_6$  (2.5 ml, 250 mM  $\text{LiClO}_4$ ) under continuous  $\text{N}_2$  or  $\text{CO}_2$  bubbling. The product was used for NMR analysis without further purification.



**Supplementary Fig. 96 |**  $^1\text{H}$  NMR spectra of the crude solution after bulk reduction of  $\text{IId}$ .



**Supplementary Fig. 97 |**  $^{13}\text{C}$  NMR spectra of the crude solution after bulk reduction of II<sub>d</sub>.



**Supplementary Fig. 98 |** Potential-capacity curve of the bulk electrolytic reduction of II<sub>d</sub>.

### Nafion membrane pretreatment

The Nafion membranes (Nafion 115; Ionpower) were pretreated using the following method<sup>2</sup>. The membrane was boiled in 3% hydrogen peroxide for 1 h. The membranes were then boiled in 0.25 M sulfuric acid solution for 1 h and cleaned in boiling deionised water for 30 min (twice). Subsequently, the membranes were boiled in 0.25 M sodium hydroxide solution for 1 h and cleaned in boiling deionised water for 30 min (twice). Finally, the membranes were dried under vacuum at 80 °C for at least 1 d and stored in anhydrous DMF.

### DFT calculations

The Gaussian16 code<sup>3</sup> was used in the DFT calculations with the B3LYP functional<sup>4,5</sup> and the 6-31++g(d,p) basis set<sup>6-8</sup>. The conductor-like polarizable continuum model (CPCM) was used to simulate the solvation effect of DMF solvent at room temperature<sup>9</sup>. In order to simulate the processes in solvated environment, free energies excluding translational contributions at 298 K are calculated. Benchmark of calculated redox potentials of the first and second electron transfer steps against measured potentials and comparison of functionals can be found in our previous work<sup>2</sup>. Vibrational frequencies were calculated for optimized structures by determining the second derivative of the energy with respect to the nuclear coordinates and then transforming to mass-weighted coordinates.

The equilibrium redox potential of the Lewis base sorbents (abbreviated as B) was calculated as  $(G(B_{\text{red}}) - G(B_{\text{ox}})) / (-|e|)$ , where  $G(B_{\text{red}})$  and  $G(B_{\text{ox}})$  are the Gibbs free energies of the oxidised and reduced base, respectively. The CO<sub>2</sub> binding energy ( $E_b$ ) was calculated as  $E_b = G_{\text{CO}_2@B} - G_B - G_{\text{CO}_2}$ , where the first term on the right side of the equation is the Gibbs free energy of CO<sub>2</sub> adsorbed on the sorbent molecule, the second and third terms are the Gibbs energies of the isolated B (any charge state) and CO<sub>2</sub>, respectively.

### Cell culture

NIH3T3/GFP fibroblast cell line was kindly provided by Dr. Yun Chen at Johns Hopkins University and cultured in Dulbecco's Modified Eagle's Medium (DMEM; Gibco) supplemented with 10% fetal bovine serum (FBS; Hyclone) and 1% penicillin/streptomycin (Pen/Strep; Gibco). U2OS.EGFP cells were kindly provided by Dr. J Keith Joung at Massachusetts General Hospital and cultured in DMEM supplemented with 10% FBS, 2 mM GlutaMAX (Gibco), and 1% Pen/Strep. MCF10A epithelial cell line was kindly provided by Dr. Konstantinos Konstantopoulos at Johns Hopkins University and cultured in DMEM/F-12 (1:1) supplemented with 5% New Zealand horse serum (Gibco), 20 ng ml<sup>-1</sup> EGF (PeproTech), 0.5 µg ml<sup>-1</sup> hydrocortisone (Sigma Aldrich), 100 ng ml<sup>-1</sup> cholera toxin (Sigma Aldrich), 10 µg ml<sup>-1</sup> insulin (Gibco), and 1% Pen/Strep. All cells were cultured in a humidified incubator at 5% CO<sub>2</sub> and 37 °C. All cell lines were tested negative for mycoplasma.

### Cytotoxicity assay and cell morphology

Cell cytotoxicity was examined by alamarBlue HS Cell Viability Reagent (Invitrogen) according to manufacturer's protocol<sup>10,11</sup>. Briefly, cells were plated in 96 wellplates (Falcon) at a density of 20,000 per well for overnight. Testing chemicals dissolved in DMF were sterilised by passing through 0.2 µm DMSO-safe Acrodisc syringe filters (Pall Laboratory) and then added into culture medium at predetermined concentrations. All testing conditions contained 1% DMF as the solvent background. The cells were incubated with the chemicals for 48 hours, washed once with Dulbecco's Phosphate Buffered Saline (DPBS; Gibco), and then incubated with fresh culture medium containing alamarBlue reagent for 4 hours in a humidified incubator at 37 °C and 5% CO<sub>2</sub>. Absorbance was measured at 570

nm by a SpectraMax microplate reader, with 600 nm as a reference wavelength. The cell viability was calculated by relative absorbance to control groups. Data were presented as mean  $\pm$  standard deviation (SD). The dose-response curves were fitted using a four-parameter logistic function to calculate the cytotoxic median lethal concentration ( $LC_{50}$ ). Cell morphology was monitored throughout the assay and images were acquired with an EVOS cell imaging system (Thermo Fisher).

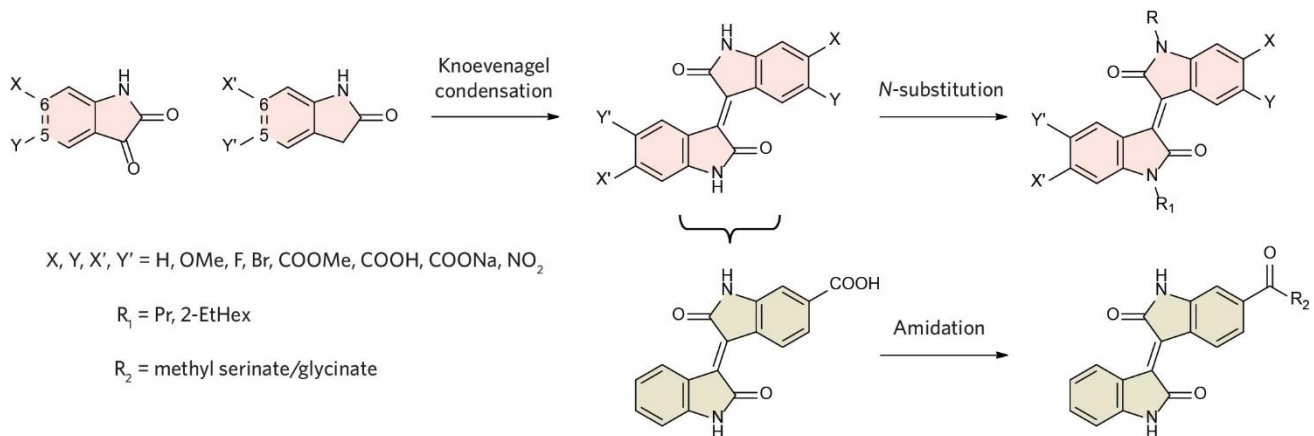
## Supplementary Notes

### Supplementary Note 1 | Characterisations of the intramolecular hydrogen bonding

To confirm the formation of intramolecular hydrogen bonding, we conducted Variable-Temperature (VT)  $^1\text{H}$  NMR experiments by heating the crude solution of **IIId** after bulk electrolysis from 20 to 90 °C (**Supplementary Fig. 3**). As the temperature increases, the characteristic peaks at 10.33 and 10.69 ppm broaden and shift upfield, which is consistent with the fact that hydrogen bonding weakens at elevated temperatures. At 90 °C, the peaks almost vanish due to the fast proton exchange, suggesting the breaking of intramolecular hydrogen bonding. Interestingly, when the temperature is cooled back to 30 °C, the NMR spectrum shows the intact **IIId-CO<sub>2</sub>** adduct, indicating that our structural design, by harnessing intramolecular hydrogen bonding, can effectively stabilise the EMCC intermediate. Besides, the reversible variation of peak integration at 7.18 and 7.04 ppm at different temperatures suggest the presence of rotational isomers. Furthermore, 2D  $^1\text{H}$ - $^{13}\text{C}$  Heteronuclear Single Quantum Coherence (HSQC) NMR was performed to fully understand the assignment of each NMR peak (**Supplementary Fig. 4**). The disappearance of peaks at 10.69 and 10.33 ppm in the 1D spectrum confirms their origination from the amide protons. The aromatic protons and carbons are resolved by the cross peaks in the 2D spectrum. Based on these results, a full assignment of the NMR peaks is given in **Supplementary Fig. 2**.

In addition to NMR, we recorded the Fourier transform infrared (FT-IR) spectra of the crude solution after bulk electrolysis (**Supplementary Fig. 5**). Compared to **IIId**, the IR band assigned to C=O stretching (1699 cm<sup>-1</sup>) vanished, and a new band appeared at 1716 cm<sup>-1</sup> in **IIId-CO<sub>2</sub>**, supporting the formation of the carbonate bond. Moreover, the IR band of free carboxylate ion should be more red-shifted (~1600 cm<sup>-1</sup>) than 1716 cm<sup>-1</sup> due to the resonance effect. Therefore, the band at 1716 cm<sup>-1</sup> suggests the formation of carboxylic acid-like species, corroborating the presence of intramolecular hydrogen bonding between the carbonate oxygen and amide hydrogen. Although the structures of rotational isomers are not fully confirmed due to the lack of single crystal structures, our NMR and FT-IR results strongly support the existence of the proposed intramolecular hydrogen bonding.

## Supplementary Note 2 | Modular synthesis of isoindigos



Isatin	Oxindole	Non-exhaustive library of isoindigos
(>10 + 21 <sup>n</sup> )	×	(>10 + 21 <sup>n</sup> )
↓	↓	↓
proteinogenic amino acids	5 or 6-substituent	<i>N</i> -substituent
		>> 1000

**Supplementary Fig. 99 | Modular design and synthesis of isoindigo-based redox-active CO<sub>2</sub> carriers.**

Through Knoevenagel condensation between 2-oxindoles and isatins, electron-donating or withdrawing groups (EDGs or EWGs) can be easily encoded into the aromatic systems of isoindigos at 5 or 6-position (Supplementary Fig. 99). The *N*-substituent groups can be introduced subsequently via S<sub>N</sub>2 reactions. This ease in the synthesis and modification of isoindigo moieties allows us to quickly build a vast library of EMCC sorbent candidates with 21 examples in total, where the redox potential, CO<sub>2</sub> binding constant, and solubility can be easily tuned via molecular engineering. Specifically, we explored a variety of substituents including electron-donating methoxy and electron-withdrawing fluoro, bromo, carboxyl, methyl carboxylate, amide, and nitro groups at 5 or 6-position of isoindigo to study the electronic and steric impact on their redox potentials and CO<sub>2</sub> affinities. Besides, *N*-substituents with aliphatic chains have also been probed to verify the role of intramolecular hydrogen bonding in CO<sub>2</sub> complexation. This design gives rise to a non-exhaustive library of isoindigos.

### Supplementary Note 3 | CO<sub>2</sub> binding constant and reaction rate constant

The CO<sub>2</sub> binding constant ( $K_{\text{CO}_2}$ ) was calculated by Eq 1:

$$K_{\text{CO}_2} = \frac{\exp\left(\frac{F}{RT} \Delta E_{\text{peak}(2)}\right) - 1}{[\text{CO}_2]} \quad (\text{Eq } 1)$$

where  $F$  is the Faraday constant,  $R$  is the ideal gas constant,  $T$  is the temperature,  $\Delta E_{\text{peak}(2)}$  is the difference between the second reduction CV peak potentials (IId<sup>•-</sup>/IId<sup>2-</sup>) in CO<sub>2</sub> and N<sub>2</sub> atmospheres (**Supplementary Fig. 7** and **8**), and [CO<sub>2</sub>] is the concentration of dissolved CO<sub>2</sub> (0.198 M in DMF under 100% CO<sub>2</sub> headspace at 298 K).

In electrochemistry, the *Cottrell equation* describes the current response ( $i$ ) when the potential is a step function in time ( $t$ ):

$$i = nAF C_0^* \left(\frac{D}{\pi t}\right)^{\frac{1}{2}} \quad (\text{Eq } 2)$$

where  $i$  is current,  $n$  is the number of electrons transferred per molecule,  $A$  is the area of the electrode,  $C_0^*$  is the bulk concentration of the redox-active isoindigo molecule,  $D$  is the diffusion coefficient, and  $t$  is time. The expected current for a diffusion limited electrochemical process following an ECE (electron transfer, chemical reaction, electron transfer) mechanism at a plane electrode under diffusion-controlled conditions is:

$$i = AFC_0^* \left(\frac{D}{\pi t}\right)^{\frac{1}{2}} [n_1 + n_2(1 - e^{-k_f t})] \quad (\text{Eq } 3)$$

where  $n_1$  and  $n_2$  are the number of electrons transferred in the first and second step, respectively, and  $k_f$  is the forward reaction rate constant of the chemical reaction. Here, to calculate  $k_f$  after the first electron transfer,  $n_2$  and  $n_1$  are set to 1. Eq 3 then becomes:

$$i = AFC_0^* \left(\frac{D}{\pi t}\right)^{\frac{1}{2}} (2 - e^{-k_f t}) \quad (\text{Eq } 4)$$

The integrated Cottrell equation relates total charge  $Q$  with time for chronoamperometry:

$$Q = 2nAF D^{\frac{1}{2}} C_0^* \pi^{-\frac{1}{2}} t^{\frac{1}{2}} \quad (\text{Eq } 5)$$

Then, the constant  $k$  can be calculated, here  $k$  is assumed constant:

$$k = nAF D^{\frac{1}{2}} C_0^* \pi^{-\frac{1}{2}} \quad (\text{Eq } 6)$$

where  $n$  is the number of electrons reduced per molecule.

To calculate  $k_f$ , the constant  $k$  is calculated using Eq 5 using potentiostatic measurements. Plugging in Eq 6, and rearranging Eq 4 gives:

$$k_f t = -\ln\left(2 - \frac{it^{\frac{1}{2}}}{k}\right) \quad (\text{Eq } 7)$$

The data for determining  $k_f$  is shown in **Supplementary Figs. 16 to 19** using 5 mM sorbent molecules in 0.1 M NBu<sub>4</sub>PF<sub>6</sub> DMF electrolyte. The value  $k$  was determined using data under N<sub>2</sub>;  $k_f$  was obtained under 1 bar 20% CO<sub>2</sub> (0.0396 M CO<sub>2</sub> in solution). The bimolecular reaction rate constant  $k_{bimolecular}$  was determined using Eq 8 and summarised in **Supplementary Table 2**.

$$k_{bimolecular} = k_f / [\text{CO}_2] \quad (\text{Eq 8})$$

where [CO<sub>2</sub>] = 0.0396 M.

#### Supplementary Note 4 | CO<sub>2</sub> binding behaviours of 5N6MCIIId and 6CIIdNa

We further designed an isoindigo with extremely strong EWG substituents to test the tolerance of the intramolecular hydrogen bonding (*b*) for promoting CO<sub>2</sub> binding. 5N6MCIIId, with a nitro substitution at 5-position in one ring and a methyl carboxylate substitution at 6'-position in the other ring, exhibits the most anodically shifted reduction potential under N<sub>2</sub> (-0.93 V vs. Fc<sup>+</sup>/Fc) among all isoindigos in this work. Due to the non-symmetrical structure in 5N6MCIIId, the strong electron-withdrawing carboxylate and nitro group can work synergistically to frustrate the CO<sub>2</sub> binding in one oxindole ring. The carboxylate group withdraws the electron density from the O atom within the ring connecting it, while the nitro group in the adjacent ring creates steric hindrance and dipole-dipole repulsion to inhibit CO<sub>2</sub> binding (**Supplementary Fig. 21**). In addition, the methyl carboxylate group is also a hydrogen bonding acceptor which may disrupt the intermolecular hydrogen bonding (*b*) between the amide hydrogen and the CO<sub>2</sub> complexed. As a result, the molecule displays a weaker binding with CO<sub>2</sub> compared to the other *N*-unsubstituted isoindigos with a log  $K_{\text{CO}_2}$  of 4.62. Nevertheless, this value is qualified for CO<sub>2</sub> capture from flue gas, and the reductive potential required for completing two-electron transfer is -1.15 V vs. Fc<sup>+</sup>/Fc, meaning it still can circumvent the oxygen-related side reactions during the EMCC process.

In addition to EDG and EWG substituents, we also study the effect of ionic substituents on the isoindigo moiety. We synthesised an isoindigo (6CIIdNa) bearing sodium carboxylate group at 6-position (Fig. 3). Despite the electron-withdrawing effect of the substituent, 6CIIdNa displays a reduction potential at -1.33 V vs. Fc<sup>+</sup>/Fc under N<sub>2</sub> and a CO<sub>2</sub> binding constant of 5.79. The cathodically shifted potential can be explained by the electrostatic repulsion between the negatively charged electrode surface and the anionic 6CIIdNa which creates an energy barrier to reduce the molecule to species with more negative charges. The decreased CO<sub>2</sub> binding affinity is probably caused by the disruption of the intermolecular hydrogen bonding (*b*) between the amide hydrogen and the CO<sub>2</sub> complexed, since the carboxylate anion is a strong hydrogen bonding acceptor.

## Supplementary Note 5 | Degradation rate of EMCC prototype based on 6B6AIIdSer

To mitigate the crossover problem, the CO<sub>2</sub> adduct was not fully oxidised back to the neutral sorbent in each CO<sub>2</sub> capture-release cycle on purpose, causing a major loss of the electrochemical capacity. Other sources of decay may originate from many different factors, such as crossover of the redox-active electrode molecules, decomposition of the electrolyte or carbon paper, or degradation of the CO<sub>2</sub> carrier. For 6B6AIIdSer (**Supplementary Fig. 34**), we utilise the energy capacity of the sorbent tank as a reference to estimate the degradation rate using the following equation,

$$r_d = \left( \frac{Q_0 - Q_n}{n \cdot Q_0} \right) * 100\% \quad (\text{Eq 9})$$

where  $r_d$  is the degradation rate,  $Q_0$  is the initial energy capacity of the sorbent tank,  $Q_n$  is the last-cycle energy capacity of the sorbent tank, and  $n$  is the cycle number.

Using -1.3 V as the cut-off potential, the energy capacity of the flow cell decreased to 7 mAh in the last cycle tested. The initial energy capacity of 6B6AIIdSer (0.2 M, 5 ml) is 53.6 mAh. Therefore, the estimated degradation rate is ~2%. Noticeably, the actual degradation rate should be much less if the CO<sub>2</sub> adduct was fully oxidised in each CO<sub>2</sub> capture-release cycle.

## Supplementary Note 6 | An alternative method to estimate the CO<sub>2</sub> binding constant

As an alternative method, we also performed CV measurements of isoindigos at different CO<sub>2</sub> concentrations (**Supplementary Fig. 39**). The relationship between  $\Delta E_{\text{peak}}(2)$  and CO<sub>2</sub> concentration is fitted according to the following equation to determine the CO<sub>2</sub> binding constant:

$$\Delta E_{\text{peak}}(2) = \frac{RT}{zF} \ln (1 + K[\text{CO}_2]^n) \quad (\text{Eq 10})$$

where  $F$  is the Faraday constant,  $R$  is the ideal gas constant,  $T$  is the temperature,  $z$  is the number of electron transferred,  $\Delta E_{\text{peak}}(2)$  is the difference between the second reduction peak potentials (IId<sup>•-</sup>/IId<sup>2-</sup>) in CO<sub>2</sub> and N<sub>2</sub> atmospheres, [CO<sub>2</sub>] is the concentration of dissolved CO<sub>2</sub> (0.198 M in DMF under 100% CO<sub>2</sub> headspace at 298 K),  $n$  is the number of binding sites, and  $K$  is the CO<sub>2</sub> binding constant.

As shown in **Supplementary Fig. 40**, curve fitting gives rise to similar  $K$  values on the order of 10<sup>12</sup> for IId and 6MCIId. However, the fitting quality was unsatisfactory (relatively low  $R^2$  values and unreasonable number of binding sites >2), likely due to the limited CO<sub>2</sub> complexation kinetics under low CO<sub>2</sub> concentrations that complicated the thermodynamic analysis.

## Supplementary References

1. Simeon, F. *et al.* Electrochemical and molecular assessment of quinones as CO<sub>2</sub>-binding redox molecules for carbon capture. *J. Phys. Chem. C* **126**, 1389-1399 (2022).
2. Li, X., Zhao, X., Liu, Y., Hatton, T. A. & Liu, Y. Redox-tunable Lewis bases for electrochemical carbon dioxide capture. *Nat. Energy* **7**, 1065-1075 (2022).
3. Gaussian 16 Rev. C.01 (Wallingford, CT, 2016).
4. Becke, A. D. Density-functional thermochemistry. III. The role of exact exchange. *J. Chem. Phys.* **98**, 5648-5652 (1993).
5. Lee, C., Yang, W. & Parr, R. G. Development of the Colle-Salvetti correlation-energy formula into a functional of the electron density. *Phys. Rev. B* **37**, 785-789 (1988).
6. Clark, T., Chandrasekhar, J., Spitznagel, G. W. & Schleyer, P. V. R. Efficient diffuse function-augmented basis sets for anion calculations. III. The 3-21+G basis set for first-row elements, Li-F. *J. Comput. Chem.* **4**, 294-301 (1983).
7. Hariharan, P. C. & Pople, J. A. The influence of polarization functions on molecular orbital hydrogenation energies. *Theor. Chim. Acta* **28**, 213-222 (1973).
8. Hehre, W. J., Ditchfield, R. & Pople, J. A. Self-consistent molecular orbital methods. XII. Further extensions of gaussian-type basis sets for use in molecular orbital studies of organic molecules. *J. Chem. Phys.* **56**, 2257-2261 (1972).
9. Barone, V. & Cossi, M. Quantum calculation of molecular energies and energy gradients in solution by a conductor solvent model. *J. Phys. Chem. A* **102**, 1995-2001 (1998).
10. Rampersad, S. N. Multiple applications of alamar blue as an indicator of metabolic function and cellular health in cell viability bioassays. *Sensors* **12**, 12347-12360 (2012).
11. Kumar, P., Nagarajan, A. & Uchil, P. D. Analysis of cell viability by the alamarBlue assay. *Cold Spring Harb. Protoc.* **6**, 462-464 (2018).